CHARACTERIZATION OF EPIGENETIC REGULATORS IN UROTHELIAL CARCINOMA

by

Hannah C. Wise

A Dissertation

Presented to the Faculty of the Louis V. Gerstner, Jr.

Graduate School of Biomedical Sciences,

Memorial Sloan Kettering Cancer Center

in Partial Fulfillment of the Requirements for the Degree of

Doctor of Philosophy

New York, NY

January 2020

_____ _____

David B. Solit, MD
Dissertation Mentor

Date

Dedication

To my family and friends for their unending support and love, especially my husband Colby. Your faith in me inspires me to be so much more.

Abstract

With the completion of large-scale sequencing efforts, including the Cancer Genome Atlas (TCGA) studies in several diseases, the oncology field has become inundated with genomic data, making it challenging to prioritize functional studies of the growing list of mutational variants of unknown significance. At the same time, these studies allow for comparisons between genetic variants across cancer types that could not be previously made. Here, we set out to utilize insights from large-scale sequencing studies to characterize alterations in several genes with careful regard to tissue-specific context, genetic background and timing of alterations, in an effort to better inform patient outcomes.

Driven by the observation that *ERBB2* kinase domain mutations are frequent in breast cancer, while extracellular domain mutations are more common in bladder cancer, we first compared activating potential of *ERBB2* mutants. We found that kinase domain mutations have more tumorigenic qualities, and a strong response to HER2-targeted inhibition. While mutations in *ERBB2* and other members of Ras/MAPK pathway have been relatively well characterized in the literature, mutations in *MAP2K1* (MEK1) remain understudied. Using a 3D clustering algorithm to predict oncogenic mutations, we were able to identify novel oncogenic *MAP2K1* mutations and confirm their activating potential in cell lines. We further identified differential sensitivity to MEK1 inhibition between variants.

We next turned to a disease-driven approach to characterize common alterations in bladder cancer, where despite its prevalence and high morbidity and mortality, few

new treatments have been FDA-approved in the last 20 years for this disease. With the TCGA muscle invasive bladder cancer study, several potentially targetable alterations were identified. Strikingly, epigenetic modifiers, including *KDM6A, ARID1A*, *KMT2D*, and *EP300*, were altered in approximately 75% of cases. To explore KDM6A loss in a bladder context, we used a CRISPR/Cas9 approach to generate an isogenic KDM6A knockout model in bladder cancer cell lines. KDM6A knockout resulted in accelerated cell growth and colony formation compared to parental cells. KDM6A loss also disrupted placement of histone marks, leading to a significantly altered RNA expression profile.

Bladder cancer also lacks well-developed mouse models, which are essential to investigate therapeutic opportunities. Although mouse models of bladder cancer remain technically challenging, we were able to combine bladder specific knockout of KDM6A and P53 with the carcinogenic BBN model to study tumor development and progression *in vivo*, and show that mutations in these tumors do reflect the human disease.

Lastly, we examined the evolution of epigenetic alterations in bladder cancer by assessing mutational frequencies in low grade, high grade, and metastatic disease, and comparing alterations between matched primary and metastatic patient samples. *KDM6A* alterations were more frequently altered in low grade disease and highly concordant in matched pairs, while *ARID1A* mutation exclusive to the metastatic samples was observed in four patients.

In the future, we hope that a deeper understanding of the functional consequences of epigenetic alterations in bladder cancer will provide viable targets for new therapeutics, ultimately leading to improved quality of life and outcomes for bladder cancer patients.

Vitae

Hannah C. Wise grew up in Phoenix, Arizona. Her love for science can be attributed to membership in her elementary school's Garden Science Club at an early age. Although she wasn't keen on the gardening, the science continued to fascinate her through high school, where she discovered her love for the complexities of life, or rather the study of life. Upon deciding that she would major in biological engineering, Hannah made the bold move to trade in Arizona's sunshine and warmth for the harsh east coast weather at the Massachusetts Institute of Technology. While at MIT, Hannah had the opportunity to complete an internship with the Louis V. Gerstner, Jr. Graduate School of Biomedical Sciences at Memorial Sloan Kettering Cancer Center. Inspired by the strong connection between bench and bedside at MSKCC, she decided to pursue her graduate studies there after graduating with her Bachelor's degree in biological engineering from MIT in 2013. She spent her thesis work in the laboratory of Dr. David B. Solit.

Acknowledgements

First of all, I would like to thank my thesis mentor, Dr. David Solit, for your infinite support throughout my graduate studies. It has been an honor to work with you and to absorb at least a small portion of your knowledge and insight. I would like to thank the current and former members of the Solit lab, including Aphrothiti Hanrahan, Gopa Iyer, Alexis Jones, Brooke Sylvester, Moriah Nissan, Ricardo Ramirez, Byron Lee, Amber Ahmad, Hikmat Al-Ahmadie, Wenhuo Hu, Kwanghee Kim, Naresh Vasani, James Rodriguez, Nima Almassi, and Tim Clinton. Thank you for making the Solit lab a collaborative and fun environment, and making sure I graduated!

I would also like to thank our many collaborators, without whom this work would not have been possible. Thank you JJ Gao and Matt Chang for your 3D mutation analysis, Cory Abate-Shen and Michael Shen, for your expertise and mouse models, and Shweta Chavan, for your help making sense of a large and complicated sequencing cohort. I would also like to thank my committee members, Mary Baylies, Sarat Chandarlapaty, and Barry Taylor, for your support and guidance over the years. Thank you to my committee chair, Yu Chen and external committee member, Bishoy Faltas.

Thank you to all of the Gerstner Sloan Kettering Graduate School. I am so glad I chose to attend GSK. Thank you to Ken Marians, former GSK dean, and Mike Overholtzer, current dean, for leading this fantastic program. Thank you to Linda Burnley and Tom Magaldi, associate deans, for all of your support. Thank you to the GSK administrative staff past and present who keep the school running: Ivan Gerena, Katherine Gentile, Iwona Abramek, Maria Torres, Stacy De La Cruz, Julie Masen, and David McDonagh. Thank you all my fellow GSK students, especially my classmates. It's

been a time, but we survived, and I look forward to seeing all your accomplishments in the future.

Table of Contents

List of Figures

List of Abbreviations

NMIBC	Non-muscle invasive bladder cancer
MIBC	Muscle invasive bladder cancer
CIS	Carcinoma in situ
PUNLMP	Papillary urothelial neoplasms of low malignant potential
LG pTa	Low grade non-invasive papillary carcinoma
HG pTa	High grade non-invasive papillary carcinoma
TURBT	Transurethreal resection of bladder tumor
CT	Computerized tomography
MRI	Magnetic resonance imaging
UTUC	Upper tract urothelial carcinoma
BCG	Bacillus Calmette-Guérin
BRM	Brahma homologue
BRG1	BRM/SW12-related gene 1
BAF	BRG1-associated factor
SWI/SNF	Switch/sucrose nonfermentable
OIS	Oncogene induced senescence
HDAC	Histone deacetylases
MSK-IMPACT	Memorial Sloan Kettering - integrated mutation profiling of actionable cancer targets
RNA-seq	RNA sequencing
VUS	Variant of unknown significance
TERT-NHUC	TERT immortalized normal human urothelial cell

H&E	Hematoxylin and eosin
PCA	Principle component analysis
GSEA	Gene set enrichment analysis
TSS	Transcriptional start site
GEMM	Genetically engineered mouse models
JAX	The Jackson Laboratory
Adeno-Cre	Adenoviral-Cre recombinase
Cre-ER	Cre recombinase – estrogen receptor
NGS	Next generation sequencing
mT	Membrane-targeted tandem dimer Tomato
mG	Membrane-targeted green fluorescent protein
EpCAM	Epithelial cell adhesion and activating molecule
IHC	Immunohistochemmistry
UPK3	Urokplakin 3
TrxG	Trithorax group proteins
PcG	Polycomb group proteins
HMT	Histone methyltransferase
FBS	Fetal bovine serum
PBS	Phosphate buffered saline
DME	Dulbecco's Modified Eagle medium
MEM	Minimal essential medium
TPR	Tetratricopeptide repeats
JmjC	Jumanji C domain

PRC	Polycomb repressive complex
T-ALL	T-cell acute lymphoblastic leukemia
CCF	Cancer cell fraction
IP	Intraperitoneal

Introduction

Bladder Cancer

Bladder cancer is the fourth most common cancer type among men in the United States, with an expected 61,700 cases diagnosed in 2019[1]. Women make up about one fourth of all bladder patients, with an expected 18,770 cases diagnosed in 2019. While overall five-year survival rates for bladder cancer are relatively high (77% for all stages), the estimated deaths in the United States alone attributable to bladder cancer total 17,670 each year. While patients with early stage disease fare well, five-year survival rates drop to 35% for patients with regional disease, defined as local and regional lymph node disease, and 5% for those with distant metastasis.

Bladder cancers arise from the epithelial cells lining the lumen of the bladder, known as the urothelium, and are subdivided into non-muscle invasive bladder cancer (NMIBC) or muscle invasive bladder cancer (MIBC) based on how deeply cancerous cells have invaded into the various tissue layers of the bladder. These layers consist of the urothelium, the lamina propria, the bladder muscle and the surrounding perivesical fat. NMIBC is defined as urothelial carcinoma that has not invaded beyond the lamina propria into the muscle layer. MIBC is urothelial carcinoma that has invaded into or beyond the muscle layer.

NMIBC includes tumors that are designated as stages Ta, Tis, also referred to as carcinoma *in situ* (CIS), and T1 according to the TNM staging classification. Ta lesions are papillary carcinomas that often grow into the hollow lumen of the bladder, but do not invade into the connective tissue or muscle of the bladder. CIS (Tis) is a flat lesion of the

urothelium with atypia that does not invade into the connective tissue. Although non-invasive, CIS is considered a high grade lesion and is thought to be the most common precursor lesion for high grade muscle invasive urothelial carcinomas[2]. T1 staged tumors are defined as those that have grown into the lamina propria but have not invaded the muscle layer.

Once the tumor has invaded the muscle layer, the cancer is classified as a MIBC. MIBC includes those that are stage T2, T3, and T4 cancers. T2 is defined as a tumor that has invaded partially or completely through the muscle layer but has not grown into the fatty tissue surrounding the muscle layer. Once the tumor has invaded into this fatty tissue layer surrounding the muscle, it is classified as T3. T4 is defined as a tumor that has invaded a nearby organ, such as the prostate, seminal vesicles, uterus, or vagina[3].

In addition to staging, bladder cancers are also classified according to their histologic grade as either low or high grade disease. Histological and morphological features of the cancer cells and their invasiveness determine the grading of bladder cancer, and correct assignment of grade largely relies on the experience of the pathologist. In 2016, the World Health Organization introduced a new classification system for urothelial tumors. Expanding upon earlier revisions from 1998 and 2004, the most recent classification now includes papillary urothelial neoplasms of low malignant potential (PUNLMP), non-invasive papillary low grade carcinoma, and non-invasive papillary high grade carcinoma.

As the name suggests, PUNLMP is a subset of tumors of low malignant potential that are not considered invasive cancers. While the abnormal cells in a PUNLMP grow in finger-like papillary structures, they remain discreet and slender with mostly normal

urothelial cells surrounding them. There may be a slight increase in the number of atypical appearing cells, but cytological atypia is limited[4]. Recurrence is common for patients with PUNLMP, but progression rates in various studies are low, ranging from 8-14%[5–9].

Non-invasive papillary low grade carcinoma (LG pTa, where p denotes pathological staging) can be difficult to distinguish from PUNLMP, and there is some dispute in the field as to whether PUNLMP should be its own distinct entity or rather included within LG pTa. However, LG pTa is characterized by the presence of cytological disorder that is not found in PUNLMP, and ordered papillae. Mitoses are not frequently observed in PUNLMP and when present are localized to the lower half of the urothelium. LG pTa can present with a component of high grade disease within the same lesion, in which case the sample is graded according to the highest grade observed[4]. Low grade T1 disease is also observed, although cancers that invade the lamina propria are generally observed to be more aggressive and thus typically classified as high grade.

Non-invasive papillary high grade carcinoma (HG pTa) differs from PUNLMP and LG pTa in that these lesions are highly disordered with cytological and architectural irregularities. High grade lesions show high level nuclear atypia with prominent nucleoli and frequent mitosis. Papillae are unstructured and fused, and thickening of the urothelium and necrosis may be observed[4]. While patients with non-invasive disease generally have a better outcome than those with MIBC, HG pTa is considered an aggressive bladder cancer subtype. High grade lesions can also be staged from pT1-4 in addition to pTa, and any tumor that has invaded the muscle layer (pT2-4) is considered high grade irrespective of morphologic features by the 2016 WHO classifications[10].

Treatment options for bladder cancer vary depending on the stage and grade of the tumor at diagnosis. Upon suspicion of bladder cancer often due to a finding of gross or microscopic hematuria, the initial staging evaluation includes cystoscopy, abdominal and pelvic CT or MRI, and imaging of the upper tract. Further examination is often performed under anesthesia, at which time the tumor can be partially or fully removed via a transurethral resection of bladder tumor (TURBT) procedure. Based on the pathologic review of the TURBT specimen, the tumor is assigned a stage and grade with further treatment options varying depending on the stage and co-morbidities of the patient.

Low grade Ta tumors do not require additional surgical treatment but depending on risk stratification, patients often receive intravesical chemotherapy (mitomycin or gemcitabine) followed by observation, or observation alone[11,12]. High grade Ta tumors require a repeat TURBT if the initial resection was incomplete or did not include muscle in the specimen to confirm that there was no invasive disease. Once confirmed to be NMIBC, patients with high grade Ta tumors are typically treated with several courses of Bacillus Calmette-Guérin (BCG), a mycobacteria that has been shown to reduce the risk of subsequent recurrence and progression to invasive disease[13–18]. Patients with HG Ta tumors may also receive intravesical chemotherapy, but BCG has been associated with better outcomes compared to chemotherapy[19,20].

Subsequent follow-up of low grade T1 tumors requires a repeat TURBT to determine if any residual disease is present. In the absence of residual disease, LG T1 tumors may be further treated with intravesical chemotherapy or BCG. In the presence of residual disease, BCG can be given with the goal of avoiding more radical surgery. Cystectomy is also an option for patients with T1 tumors, though this is usually reserved

for those patients with high grade residual T1 disease and those with muscle invasive disease. Following treatment, patients with high grade T1 disease also require a repeat TURBT to determine if residual disease is present. Like low grade T1 tumors, patients with HG T1 tumors are typically treated with BCG or intravesical chemotherapy in the absence of residual disease. However, cystectomy is strongly considered in place of a repeat TURBT because of the higher risk of progression associated with high grade disease.

Muscle invasive disease is treated more aggressively from the outset compared to NMIBC. In addition to abdominal and pelvic CT or MRI, patients with T2 or T3 tumors require chest and bone imaging to exclude the presence of metastatic disease. Patients who are cystectomy candidates including those with region lymph node metastases often receive neoadjuvant cisplatin-based combination chemotherapy, which has been shown to have a survival benefit in patients with MIBC[21–23]. Following neoadjuvant chemotherapy, patients may be eligible for a curative intent radical cystectomy. For patients who are not a candidate for cystectomy due to co-morbid medical issues, curative intent concurrent chemoradiotherapy or radiotherapy alone are alternative approaches.

While most muscle invasive bladder cancers are urothelial carcinomas, pathology review will reveal that a subset have a different variant histologic appearance such as small cell, adenocarcinoma, plasmacytoid, micropapillary or squamous histology. Bladder cancers often exhibit morphologic heterogeneity with one or more histologic variants present within individual tumors. Tumors with variant histology are typically more aggressive and such patients have a greater risk of recurrence following cystectomy and higher cancer specific mortality.

The treatment approach for patients with T4 tumors who lack distant metastasis involves systemic therapy with the goal of downstaging the tumor. Patients with T4 disease without metastatic disease may be candidates for radical cystectomy following systemic therapy, but many patients with T4 disease have an inadequate response to systemic therapy to allow for surgical resection. Select T4 patients with metastatic disease may also be considered for cystectomy if there is significant response to systemic treatment.

Radical cystectomy remains the primary treatment option for bladder cancer patients with muscle invasive disease and those with non-muscle invasive tumors who are refractory to BCG. While effective, complete removal of the bladder significantly impacts a patients' quality of life. For this reason, ongoing studies are testing whether a subset of genomically defined patients can be treated with TURBT and chemotherapy alone, without the need for radical cystectomy. Furthermore, while neoadjuvant chemotherapy is a standard of care, a large fraction of patients do not receive neoadjuvant chemotherapy prior to cystectomy due to concerns over the toxicity of chemotherapy and the recognition that it has only modest clinical benefit. For patients with metastatic disease, platinum-based chemotherapy, most commonly cisplatin and gemcitabine, is the first-line standard-of-care.

With the advent of immunotherapy in the early 2000's, checkpoint inhibitors became of high interest in variety of tumor types including bladder cancer. Anti-PD1 and anti-PD-L1 antibodies have clinical activity in a number of different cancer types, and are now FDA approved for use in patients with melanoma, kidney, and head and neck cancers, bladder cancer, and an increasing number of other cancer types[24–30].

Atezolizumab and pembrolizumab were first anti-PD1/PD-L1 antibodies approved for use in patients with urothelial carcinoma who were refractory to or ineligible for platinum-based chemotherapy[31]. However, chemotherapy remains the preferred first line of treatment for patient with metastatic disease. Immune checkpoint inhibitors can induce dramatic and durable response but only a subset of patients with urothelial cancer benefit. The biologic basis for the variable response of bladder cancer patient to immunotherapy and the mechanisms of acquired resistance to immune checkpoint blockade remain largely unknown.

Despite dramatic results in other cancer types, targeted therapies have demonstrated only limited anti-tumor effects in bladder cancer over the past 20 years. The FGFR inhibitor erdafitinib was approved by the FDA in April 2019 for the treatment of locally advanced and metastatic bladder cancer[32,33]. This approval was based upon an overall response rate of 32.2% of patients with FGFR2/FGFR3-positive locally advanced metastatic bladder cancer. Despite the recent FDA approvals of PD-1/PD-L1 and FGFR3 inhibitors for bladder cancer, novel therapies are urgently needed for patients with metastatic disease. A lack of targeted therapies impacts patient care, as severe off-target side effects can prevent patients from receiving chemotherapy and immunotherapies. However, to develop novel targeted therapies, the genetic drivers of bladder cancer pathogenesis and progression must be further elucidated.

Several large-scale efforts have sought to define the genomic landscape of invasive bladder cancers with the goal of identifying novel therapeutic targets[34,35]. The most notable finding of these efforts was the identification of mutations in genes that regulate chromatin state in the vast majority of urothelial cancers. Alterations in *KDM6A*,

ARID1A, *KMT2D*, and *KMT2C* are most commonly observed and are present in approximately 75% of cases. Other frequently mutated genes included *TP53* (50%), *PIK3CA* (25%), *RB1* (24%), *FGFR3* (17%), and *ERBB2* (17%) (Figure 1). These genes represent multiple targetable drivers in bladder cancer, including *ERBB2* as discussed in depth below.

Genetics vs. Epigenetics

The concept of inherited traits was first proposed in the nineteenth century, when Gregor Mendel working with pea plants found that characteristics could be passed on from one generation to the next. Although Mendel's work was largely overlooked during his lifetime, it was later re-discovered at which time it helped advance the field of genetics with contributions from Thomas Hunt Morgan and others[36]. While the idea that genes held hereditary information, later found to be encoded by and passed on in DNA, was well accepted by the mid-twentieth century, the concept of epigenesis was just beginning to be formed. In the developmental biology field, a theory supported by Conrad Waddington and other scientists proposed that genetics and developmental biology were closely related. Waddington selected the Greek term epigenesis creating the field of epigenetics, which he broadly defined as "the unfolding of the genetic program for development"[37].

In the developmental biology field, epigenetic mechanisms were developed to explain the differentiated state of cells. While the genetic DNA of all cells in an embryo of a higher organism is largely identical, during development, different cell types acquire different phenotypes that are maintained through cell division. These observations led to

the proposal of hereditary mechanisms beyond the genetic sequence of a cell's DNA. The first mechanism of epigenetic regulation proposed by several scientists was DNA methylation[38–40]. Studies suggested that DNA methylation could impact gene expression at specific sequences, turning some genes off in certain settings, and other genes on in other settings. It was observed that methylation patterns could be inherited if enzymes placing methyl marks recognized hemi-methylated DNA that would be present immediately after replication. In 1990, Maynard Smith termed the phrase "dual inheritance," describing the idea that classical inheritance is determined by both genetic inheritance and epigenetic inheritance, the latter information that is not based on sequence changes in DNA[41].

More recently, epigenetic mechanisms have been of increasing interest in a broad range of scientific fields, with numerous laboratories focused on understanding how chromatin structure impacts gene expression. In addition to DNA methylation, two other mechanisms of epigenetic regulation of gene expression have been identified. One group of epigenetic regulators includes the chromatin remodelers. These proteins are involved in rearranging DNA around histones, thus regulating the ability of the transcription machinery to access specific sequences of DNA, thereby regulating gene expression. The other group consists of histone modifiers. These proteins influence transcriptional regulation by post-translationally modifying histones by placing marks at different regulatory sites via methylation, acetylation, phosphorylation and ubiquitylation[42]. Both chromatin remodelers and histone modifiers have been shown to play important roles in cell homeostasis and disease.

Ras/MAPK Signaling

HER2 is a transmembrane receptor tyrosine kinase in the epidermal growth factor receptor (Erbb) family. Erbb family receptors regulate cell growth and proliferation, among other cellular processes. The four Erbb family members are the epidermal growth factor receptor (*EGFR*), HER2/*ERBB2*, HER3/*ERBB3* and HER4/*ERBB4*. Each receptor consists of an extracellular domain with four sub-domains, including the ligand binding domain and dimerization domain. The intracellular domain includes a tyrosine kinase domain, though HER3 is kinase dead. Erbb receptors are typically activated following binding of ligand to the extracellular domain of the receptor, which results in a conformational change that promotes the formation of receptor homo- or heterodimers.

Several ligands have been identified that bind to and activate Erbb family receptors, adding to the complexity of the signaling system. While some ligands show specificity for a single receptor, such as the epidermal growth factor (EGF) and transforming growth factor- α (TGF α), both of which bind to EGFR, other ligands have dual specificity, like heparin-binding EGF and epiregulin, which bind to EGFR as well as HER4[43]. HER2 is unique in that it lacks a known ligand, and is instead always locked in the open state, with the dimerization domain available to form dimers with other HER family members. While ligands show specificity for certain receptors, overexpression of HER2, a common finding in breast cancer but also observed in a minority of bladder cancers, can expand this specificity, resulting in aberrant signaling[44].

Upon dimerization, the tyrosine kinase domain is trans-phosphorylated, resulting in activation of specific effector pathways depending on the dimer pair[45]. HER2 can dimerize with EGFR, which leads preferentially to MAPK activation. In this dimer pair,

HER2 acts as the activator, binding to EGFR, the receiver, and stabilizing and activating the kinase domain of EGFR[46]. The C-terminal tail of HER2 is then phosphorylated by EGFR, and adaptor proteins, such as GRB2 and Shc, are then able to bind the receptor, which results in the recruitment of Ras GTPases. Ras cycles between an inactive GDP-bound state and an active GTP-bound state. When in the active state, Ras is able to bind to and active Raf proteins (ARAF, BRAF, CRAF), which are serine/threonine kinases. Activated Raf in turn activates MEK1 and MEK2, which in turn activate extracellular signal-regulated kinase/mitogen-activated protein kinases 1 and 2 (ERK1/2)[47–50].

Activated ERK has many downstream targets, including membrane proteins, nuclear substrates, and ribosomal S6 kinases (RSKs). While ERK activation can directly affect transcriptional regulation through its nuclear targets, such as the c-Myc and Ets transcription factors, activation of the RSKs also gives MAPK signaling a broad downstream affect. RSK substrates are involved in transcriptional regulation, cell proliferation, and cell survival[51,52]. HER2 activation also results in decreased levels of p27kip1, a cyclin-dependent kinase inhibitor, which regulates cell cycle progression by inhibiting G1 cyclin-dependent kinases[53].

HER2 dimerizes with HER3, which can result in strong induction of PI3K/AKT signaling[54]. In this dimer pair, HER3 is the activator and HER2 acts as the receiver, since HER3 lacks intrinsic kinase activity[46]. Once the C-terminal tail of HER3 is phosphorylated by HER2, phosphotidylinositol-3 kinase (PI3K) is able to bind to HER3 through its SH2 domain. Binding activates PI3K, which then phosphorylates phosphatidylinositol-4,5-bisphosphate (PIP2), generating phosphatidylinositol-3,4,5-trisphosphate (PIP3). The presence of PIP3 results in localization of AKT to the cell

membrane, where it is phosphorylated and activated. AKT requires two phosphorylation sites for activation: Threonine 308 and Serine 473. Activated AKT regulates downstream effectors that promote cell survival and growth and proliferation[55,56]. The PI3k/AKT pathway is negatively regulated by PTEN, a phosphatase that converts PIP3 to PIP2[57].

Role of ERBB2 in development

Each of the Erbb family receptors play an important role in development, as shown by the observation that EGFR-/-, HER2-/-, HER3-/- and HER4-/- mice are all embryonic or perinatal lethal. More specifically, HER2, HER3, and HER4 are involved in cardiovascular and nervous system development, with HER2-/-, HER3-/- and HER4-/- mice not viable due to irregular cardiac development[58].

In addition, the Erbb family also plays a significant role throughout various stages of mammary development. During ductal morphogenesis, both EGFR and HER2 can be found in all major cell types. However, in the differentiated gland, EGFR, HER2, HER3 and HER4 are constrained to the epithelium[59]. During puberty, high levels of EGFR and HER2 can be detected in mammary glands, while HER3 and HER4 levels are very low[60]. The roles appear to reverse during pregnancy and lactation, with high levels of HER3 and HER4, and low levels of EGFR and HER2[61]. Although HER2-/- mice are embryonic lethal, the role of HER2 has been further studied using a dominant negative HER2 under the control of the mouse mammary tumor virus (MMTV) promoter. These mice are defective in alveolar expansion during gestation and lactation[62]. Mammary development also relies on different HER2 pathways. The formation of branched tubules depends on the PI3K/AKT pathway, while alveolar morphogenesis relies on Ras/MAPK signaling[63].

Role of Ras/MAPK in cancer

HER2 amplification has been shown to drive oncogenesis, and is a common occurrence in breast and esophageal cancers, among other tumor types[64,65]. While overexpression of HER2 can lead to enhanced and prolonged signaling of both the Ras/MAPK and PI3K/AKT signaling pathways and other downstream signaling cascades, HER2 has been shown to signal mainly through HER3 and the PI3K/AKT pathway in breast cancer. HER3 is constitutively phosphorylated in a number of breast cancer cell lines[66], and both HER2 and HER3 are required for proliferation in HER2 amplified breast cancer cell lines[67]. In contrast, knockdown of EGFR had no effect on proliferation of HER2 amplified breast cancer cells[68]. In addition, HER3 is strongly expressed in 17.5% of breast carcinomas and co-expressed with HER2 in 11.8%, while EGFR is strongly expressed in only 2.7% and co-expressed with HER2 in 5.5% of tumors[69].

In contrast to breast cancer, the consequences of aberrant HER2 signaling in bladder cancer has not been well established, but levels of Erbb family receptors have been examined. EGFR is expressed at some level in 72.2% of bladder cancers, and 33.9% of bladder cancers co-express EGFR and HER2. HER3 is expressed in 56.3% of bladder cancers, and is co-expressed with HER2 in 27.3% of tumors[70]. The *EGFR* gene is amplified in 9% of bladder urothelial carcinomas, but *EGFR* amplification is mutually exclusive of *ERBB2* mutations[35].

Genetically engineered mouse models of HER2 driven breast cancer have been developed. Overexpression of the activated rat HER2 homologue, *neu*, has been shown to

be sufficient for breast tumor development in a transgenic MMTV/*neu* mouse model. A single amino acid substitution in the *neu* transmembrane domain, V664E, has strong transforming activity[71]. This substitution corresponds to V659E in human HER2, but the mutation is not found in nature[72]. In this model, activated *neu* is under the control of the MMTV long terminal repeat, which is expressed primarily in the mammary, parotid, and Harderian-lacrimal glands and the epididymis.

While MMTV/*neu* mice originally appear normal, sexually mature females are unable to nurse their young. Virgin female mice begin to show hyperplastic and dysplastic nodules of the mammary epithelium at eight weeks. After three months, all female mice develop mammary tumors and completely lack normal mammary epithelium, suggesting a single-step transformation model[71]. In addition to activated *neu*, wild-type *neu* has also been show to drive tumorigenesis in mouse models, though tumor development in mice with wild-type *neu* have a longer latency period and do not begin to appear until approximately seven months at the earliest[73].

Activation of the other MAPK members is also common in human cancer. The RAS genes (*KRAS*, *NRAS*, *HRAS*), *BRAF* and *NFI* are frequently mutated in a wide variety of cancers including melanoma, non-small cell lung, colorectal, ovarian, pancreas and thyroid cancers. While RAS pathway alterations are less common in bladder cancer, a subset of urothelial cancers have *HRAS* mutations whereas *KRAS* mutations are common in bladder adenocarcinomas. While less common, mutations in *MAP2K1*, the gene that encodes MEK1, are present in histiocytosis, melanoma, colorectal cancers, squamous cell skin cancers, and more rarely in bladder cancers. A small number of *MAP2K1* mutations have been shown to induce constitutive kinase activation[74–76].

ERBB2 and MEK1 targeted therapies

HER2 targeted therapies are now a component of standard therapy for *ERBB2* amplified breast and gastric cancers[77,78]. One commonly used therapy is the monoclonal antibody trastuzumab (Herceptin). Trastuzumab targets domain IV of the extracellular region of HER2, and does not block dimerization[79]. Binding of trastuzuamb to this juxtamembrane portion of HER2 prevents activation of the kinase domain. Trastuzumab is also thought to have anti-tumor effects in part through its ability to block cleavage of HER2, which prevents downstream signaling, and by inducing an immune response through natural killer (NK) cell recognition of the Fc domain on the drug[80–82].

Other HER2 targeted therapies available for clinical use include tyrosine kinase inhibitors, including lapatinib and neratinib. Lapatinib is an ATP-competitive, small molecule reversible inhibitor of EGFR and HER2, which is more effective against the truncated p95 HER2 as it targets the intracellular kinase domain instead of the extracellular domain.[83] Neratinib is a pan-Erbb tyrosine kinase inhibitor that binds to HER2 irreversibly, preventing phosphorylation of the receptor and thus downstream signaling[54]. Neratinib has been shown to have anti-tumor activity in combination with capecitabine in patients who have experience disease progression on trastuzumab-based therapy[84].

Anti-tumor responses have also been observed with selective inhibitors of MEK in patients with activating *MAP2K1* mutations. Histiocytosis patients with *MAP2K1* mutations, including F53L, Q56P and K57N, have had durable responses to the MEK inhibitors trametinib and cobimetinib[76,85]. Trametinib was originally approved for use in

patients with BRAF mutant metastatic melanoma and is now often used in combination with RAF inhibitors. Trametinib functions as an allosteric inhibitor, binding adjacent to the ATP-binding site of MEK1/2. Selumetinib functions similarly[86]. In contrast, the inhibitor CH5126766 (Chugai), while still an allosteric MEK1/2 inhibitor, has been shown to induce a conformational change in MEK1, causing MEK1 to bind to BRAF and act in a dominant negative manner to prevent downstream signaling[87].

Epigenetic Regulators

The Trithorax group proteins (TrxG), responsible for transcriptional activation, and the Polycomb group proteins (PcG), responsible for transcriptional repression, are involved in the epigenetic regulation of many cellular processes. The balance of activity between these two groups helps control transcriptional activity of genes targeted and regulated by these proteins.

PcG proteins were originally identified in Drosophila as mutations that led to expression changes in Hox genes, a set of genes responsible for coding orientation of an embryo during development. Shortly after, a member of the TrxG proteins was identified as a positive regulator of the clustered homeotic (Hox) genes[88–90]. Through these discoveries, TrxG proteins were defined as antagonists of PcG-dependent silencing. TrxG proteins can be divided into three categories based on their function. These are ATP-dependent chromatin remodeling factors that read histone marks, SET-domain containing proteins that modify histone tails, and TrxG proteins that can bind directly with specific DNA sequences.

Chromatin Remodelers: The SWI/SNF Complex

One of the first and best-characterized chromatin remodeling complexes is the yeast switch/sucrose nonfermentable (SWI/SNF) complex. The genes in the SWI/SNF complex were originally identified as transcriptional regulators of switching genes for mating and growth on sucrose media[91,92]. These genes were later shown to form a complex involved in transcriptional regulation of many genes with the ability to move nucleosomes and facilitate binding of transcription factors to their target[93–95]. Homologous genes were identified in mammals, and purification of these complexes revealed the BRM/SWI2-related gene 1 (BRG1)-associated factor (BAF) complex[96–98].

The BAF complex consists of an ATPase enzymatic subunit, either brahma homologue (BRM) or BRG1, highly conserved "core" subunits, including SNF5 (also known as SMARCB1), BAF155 and BAF170, and a combination of multiple other subunits that provide the BAF complex with variations in targeting, assembly and lineage-specific functions. These variable subunits include either AT-rich interactive domain-containing protein 1A (ARID1A, also known as BAF250a and SMARCF1) or ARID1B; BAF53 A or B; BAF45 A, B, C, or D; BAF60 A, B, or C; BAF57 and β-actin[99–101].

The exact makeup of the BAF complexes can vary depending on developmental and lineage-specific factors. For example, BAF60c has been shown to be necessary in heart development, while ARID1B is required to maintain undifferentiated embryonic stem cells in mice[102,103]. In neural stem and progenitor cells, BAF45a and BAF53a are necessary for proliferation. Upon differentiation, BAF45c and BAF53b replace these subunits[104]. Because these subunits are largely regulated by lineage-specific expression,

many different BAF complexes exist in mammals and play a role in lineage-specific gene regulation.

Based on the variations in proteins that can make up the BAF complexes, the downstream function of the complex can also vary. Although the SWI/SNF complex was originally identified as an activator of transcriptional regulation, more recent studies suggest that the BAF complexes play a role in both gene activation and repression. In mammalian thymic development, BRG1 and BAF57 are involved in CD4 silencing, as well as CD8 activation[105]. BRG1 has also been shown to repress differentiation programs in embryonic stem cells, while also co-localizing with transcriptional regulators to facilitate expression of the core pluripotency network[105]. The BAF complex can also promote repression by attracting histone deacetylases (HDACs) to remove activating histone marks. SNF5 has been shown to repress cyclin D1 (*CCND1*) in an HDAC1-dependent manner.

The ARID1A subunit of the BAF complex is named for the 100 amino acid AT-rich interaction domain (ARID), which interacts with DNA in a nonspecific manner[106]. ARID1A has been shown to play a role in transcriptional coactivation induced by hormonal receptors, including glucocorticoid, androgen and estrogen receptors[107–110]. ARID1A has also been shown to play a role in embryonic development. It is expressed widely and ablation leads to developmental arrest and compromised stem cell pluripotency in mice[107,111,112]. While SWI/SNF complexes are thought to have some specificity depending on the specific ARID subunit, complexes containing ARID1A, ARID1B and ARID2 have been identified in individual cells. Binding overlap was

observed between all the complexes, suggesting that the homologous subunits may interact with each other to further regulate transcription[113].

Histone Modifiers: COMPASS-like complexes and PRC2

Histone-modifying complexes were first discovered in yeast, after the SET domain-containing 1 (Set1) protein was identified as a histone methyltransferase (HMT), responsible for catalyzing mono-, di-, and trimethylation of H3K4 within a larger protein complex. This complex is known as COMPASS (complex proteins associated with Set1)[114]. In mammals, Set1 homologues were identified, including *KMT2A* (MLL1), *KMT2D* (MLL2), and *KMT2C* (MLL3), proteins originally discovered based upon their involvement in mixed-lineage leukemias. These histone methyltransferases interact with a combination of other proteins, including ASH2L, WDR5, RBBP5, NCOA6 and KDM6A (also known as UTX), to form COMPASS-like complexes.

KDM6A is a histone demethylase that has been shown to complex with KMT2D and KMT2C, and is associated with regulation of *HOX* genes during development[115]. KDM6A has two paralogs in mammals, UTY and KDM6B (JMJD3). While all three proteins have overlapping targets, unique functions of each have been identified at various stages of development. UTY also has considerably lower demethylase activity, and is therefore unable to compensate for KDM6A activity throughout development[116]. Germline *KDM6A* mutations, along with *KMT2D* mutations, have been described in Kabuki syndrome, which is characterized by defects in craniofacial, heart and brain development[117]. Structurally, the KDM6A protein is characterized by homonymous tetratricopeptide repeats (TPR) at the N-terminal end and the Jumanji C (JmjC) domain at

the C-terminal end of the protein. The JmjC domain is responsible for the catalytic demethylase activity of protein[118].

Like the TrxG proteins, the Polycomb group proteins form two major complexes, polycomb repressive complex 1 and 2 (PRC1 and PRC2). PRC2 is responsible for H3K27 methylation, the mark of transcriptional repression, and is thought to directly oppose the activity of COMPASS-like complexes. The histone methyltransferase EZH2 is the catalytic subunit of the PRC2 complex, but requires additional proteins including SUZ12 and EED for methyltransferase activity and specificity[119]. Loss of KDM6A activity is thus predicted to result in unopposed EZH2 activity, increased H3K27 methylation, and therefore repression of genes regulated by KDM6A.

The Role of Epigenetic Regulators in Cancer Development

It has become evident that epigenetic regulators play a significant role in cancer development. Alterations in DNA methylating proteins and histone modifiers are common in leukemia and other hematologic malignancies, while mutations in histone readers are frequently found in solid tumors, including melanoma, thyroid and breast cancers. The mechanisms whereby alterations in these regulators promote tumor formation and/or progression have been elucidated in several cancer types. However, cellular context remains of utmost importance for studying epigenetic alterations. EZH2 has been identified as having both oncogenic and tumor suppressor functions, with differential roles associated with distinct cancer types[119].

KDM6A function has been studies in several settings, including lymphoma, breast, prostate and cervical cancers, with the exact role dependent on tumor type and

genetic background. Although defined as a tumor suppressor in T-cell acute lymphoblastic leukemia (T-ALL), further studies have demonstrated its role as coactivator in a subset of T-ALL. In breast cancer, KDM6A was also shown to support the oncogenic role of the estrogen receptor. In prostate cancer, KDM6A is necessary to maintain androgen signaling. Introduction of wild-type KDM6A into KDM6A null esophageal cancer cell lines results in a significant decrease in H3K27me3 and an increase in cell doubling time, suggesting a tumor suppressor role for KDM6A, in that cell lineage[120].

Epigenetic-targeted therapies

The recent clinical success of selective inhibitors of the methyltransferase EZH2 in patients with lymphomas suggests that epigenetic dysregulation is a crucial step in the formation of some tumor lineages and may be required for tumor maintenance. Thus, inhibitors of EZH2 may represent a novel therapeutic approach for bladder and other cancer types. Interestingly, clinical activity in bladder cancer was observed in a phase I study of the histone deacetylase (HDAC) inhibitor vorinostat[121]. In bladder cancer, *KDM6A* mutations frequently co-occur with oncogenic driver alterations in *FGFR3* and *ERBB2*. KDM6A loss may thus modulate response to targeted therapies directed against these alterations, which could have implications for the development of rational therapeutic combinations. Therefore, an improved understanding of the biologic role of KDM6A loss in promoting bladder cancer development and metastatic progression has the potential to significantly advance the field.

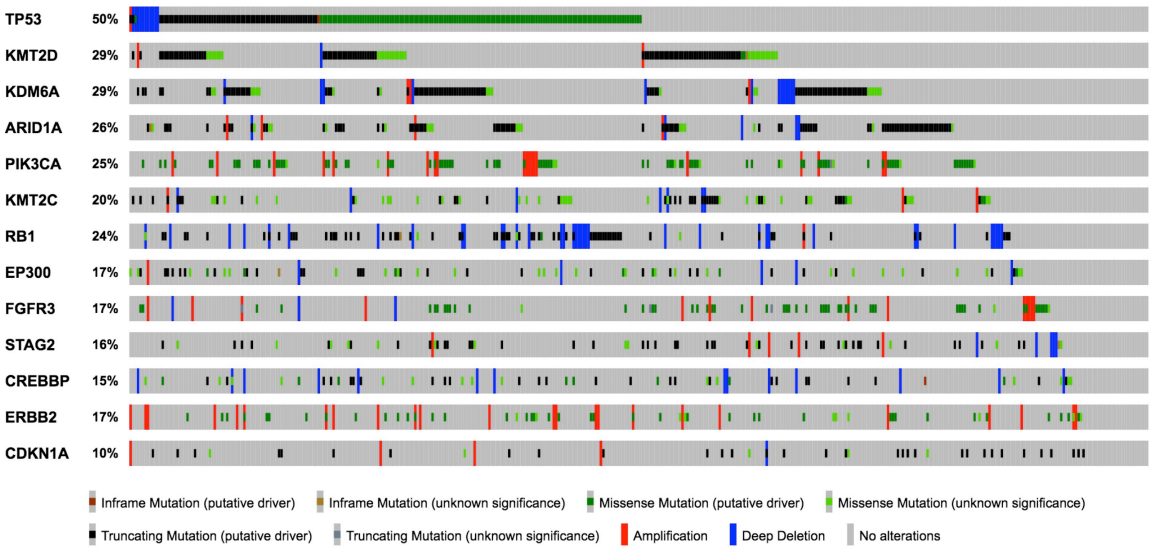

Figure 1: TCGA-identified mutations in muscle invasive urothelial carcinoma.

Each column represents an individual tumor sample, and each row represents the mutational status of the gene listed on the left. Grey box denotes no alteration in a gene, red denotes amplification, blue denotes deep deletion, black line denotes truncating mutation, and green line denotes missense mutation.

Materials and Methods

Cell lines and culture conditions

The bladder cancer cells MGHU4 and VMCUB2 were maintained in minimum essential medium (MEM) supplemented with 10% fetal bovine serum (FBS), penicillin/streptomycin, L-glutamine, 10mM NEAA and 10mM sodium pyruvate. RT4 bladder cancer cells were maintained in McCoy's medium supplemented with 10% FBS, penicillin/streptomycin and L-glutamine. Human embryonic kidney (HEK)-293H cells (Invitrogen) were maintained in Dulbecco's Modified Eagle's (DME)-HG medium with 10% FBS, supplemented with 2 mM glutamine, and 50 units/ml each of penicillin and streptomycin.

Cell line assays

Proliferation assays

Cells were plated in duplicates in 6-well plates at 25,000 cells per well. Cells were trypsinized and counted by ViCell at the corresponding collection day outlined in each figure. For drug proliferation assays, cells were plated in duplicates in 6-well plates at 100,000 cells per well. Drug was added 24 hours after initial plating. Cells were collected every 3-4 days, counted, and replated at 100,000 cells per well with new drug.

Transfections

MAP2K1 (MEK) mutant constructs were generated from the MEK1-GFP plasmid (#14746, Addgene, Cambridge, MA, USA) using the QuikChange II XL Site-Directed

Mutagenesis Kit (Stratagene) as recommended. Sanger sequencing was performed to verify all mutant plasmids. HEK-293H cells were seeded for 70–90% confluency at the time of transfection, then transiently transfected with wild-type or mutant MEK1-GFP plasmids using Lipofectamine® 2000 Transfection Reagent (Invitrogen). Plasmid transfection levels were standardized according to green fluorescent protein (GFP) expression. Cells were collected 24 hours post-transfection.

Western Blotting

Cells were lysed in 1% NP-40 buffer with protease and phosphatase inhibitors. Lysates were centrifuged at 13,200 rpm for 10 minutes to pellet debris, and the protein concentration of the supernatant was determined by bicinchoninic acid protein assay (Pierce). Equal amounts of total protein were resolved by SDS-PAGE and transferred onto nitrocellulose membranes by electroblotting. Membranes were blocked for one hour in 5% nonfat milk in TBS-T [0.1% Tween-20 TBS, 10 mM Tris (pH 7.4) and 150 mM NaCl] at room temperature, and subsequently probed overnight at 4°C with antibody against the protein of interest. Anti p42/44 MAPK, phosphorylated p42/44 MAPK, Akt, phosphorylated Akt (ser473), phosphorylated STAT3 and GAPDH antibodies were obtained from Cell Signaling Technology. KDM6A antibodies were obtained from Sigma. Trimethylated H3K27 was obtained from Millipore. After incubation with horseradish peroxidase-conjugated secondary antibody, proteins were detected by chemiluminescence (SuperSignal West Dura Chemiluminescent Substrate, Thermo Scientific) and visualized using the Fuji LAS-4000 imager (GE Life Sciences).

Boyden Chamber

Cells were plated in the upper chamber of a transwell insert (8um) in a 24-well plate at 50,000 cells per well with no FBS. Media containing 10% FBS and 1μg/mL EGF was added to the bottom well. After 24 hours, cells were fixed and stained in 4% PFA with crystal violet. Cells were washed with phosphate buffered saline (PBS) three times, and inner well was cleaned using a Q-tip to remove cells that did not migrate. Stained cells were counted via microscope.

Wound Healing

Cells were plated using a 4-well silicone insert (Ibidi). Cells were plated at 10,000 cells per well. After cells were seeded and greater than 90% confluent, the silicone insert was removed with sterile forceps, creating a gap of 500um. After 10-24 hours, depending on the growth rate of the cell line, cells were imaged, and distance of the gap was calculated. Gap distance was calculated in Adobe Photoshop. Percent change was calculated by subtracting the distance at endpoint from the distance at 0 hours and dividing by the distance at 0 hours.

RNA-sequencing

Total RNA from frozen tissue was isolated using Trizol (Thermo Fisher Scientific) and the quantity and quality of the resulting RNA was measured using an Agilent 2100 Bioanalyzer. RNA sequencing was performed by the Integrated Genomics Core (MSKCC). The TruSeq RNA Library Prep Kit v2 (Illumina) was used for library preparation, followed by sequencing (60 million paired-end reads) on an Illumina HiSeq

2500. Read numbers for genes were extracted by RSEM (using the STAR alignment program)[122]. Mean reads per sample was 25 million. Differentially expressed genes were identified by DESeq2[123]. Principal component analysis was performed using the top 1000 differentially expressed genes. Gene Set Enrichment Analysis was applied to identify significantly different pathways[124].

ChIP-sequencing

Cells were plated at 5 million cells per plate in 15cm plates and collected at 24 hours at approximately 90% confluency. Cells were fixed in 1% formaldehyde for 10 minutes, quenched with glycine and collected in PBS with protease inhibitor (Sigma 1:100). After spinning down, cells were lysed in lysis buffer 1 (50mM Hepes-KOH, pH 7.5, 140mM NaCl, 1mM EDTA, 10% Glycerol, 0.5% NP-40, 0.25% Triton x-100), pelleted and re-suspended in lysis buffer 2 (10mM Tris-HCl pH 8, 200mM NaCl, 1mM EDTA, 0.5mM EGTA), pelleted again and re-suspended in lysis buffer 3 (10mM Tris-HCl, pH 8, 100nM NaCl, 0.5mM EDTA, 0.5mM EGTA, 0.1% Na-Deoxycholate, 0.5% N-lauroylsarcosine). Lysate was sonicated to generate DNA shards between 180 and 500 base pairs. H3K27me3 antibody (Millipore) was incubated with secondary magnetic beads and added to sonicated DNA for immunoprecipitation overnight. Beads were then washed with TE wash buffer (10mM Tris-HCl, pH 8, 1mM EDTA, 50mM NaCl) and eluted in elution buffer (50mM Tri-HCl, pH 8, 10mM ETA, 1% SDS) for 30 minutes at 65 degrees Celsius. DNA was decrosslinked overnight at 65 degrees Celsius, purified using Qiagen PCR purification kit and sequenced by the Integrated Genomics Core (MSKCC).

The fastq files were trimmed to remove adapter and low quality sequences using trim_galore and then aligned to the UCSC genome assembly hg19 using Bowtie (version 2.1.0)[125]. Duplicate reads were removed using Picard MarkDuplicates. To detect peaks, the software MACS (version 1.4)[126] was applied using default parameters unless otherwise stated. Peaks were annotated to genomic features (Promoter, Gene body, Intergenic) using HOMER program[127]. IGV was used to finally present the peaks for each sample[128].

Mouse models

Adeno-Cre surgical instillation in the bladder

Animals were bred to the desired genotype and then treated once with an adenovirus expressing Cre-recombinase (Adeno-Cre) or a control vector (Adeno-empty) obtained from the University of Iowa Vector Core Facility (Ad5CMVCre). Concentrated virus (25ul; 4 $X10^{11}$ PFU/ml) was mixed with 20ul of Dulbecco's Modified Eagle Medium (DMEM) and 5µl of hexadimethrine bromide (polybrene, a cationic polymer used to increase the efficiency of virus infection, 80 ug/ml), and 5µl of diluted virus was surgically injected into the bladder lumen of adult mice (2-4 months of age) as explained below. An injection of 0.01 mg/kg of buprenorphine by subcutaneous injection route was given for pre-emptive systemic analgesia immediately after the animal was anesthetized, and fur was removed with a depilatory agent (NAIR). The animal was placed in dorsal recumbency position on a warming pad and secured.

Briefly, for Adeno-Cre injection, the surgical field was prepped and sterilized for surgery. All surgical instruments were sterilized. The animal was covered with a sterile

drape with a hole that is large enough to allow for access to the incision, but not to exceed the size of the prepared surgical site. The bladder was surgically visualized through a 1-cm incision in the lower abdomen and evacuated of urine using an empty Hamilton syringe. Adeno-Cre was then administered through the same hole used to evacuate urine. The surgical site was closed in a two-step process. The muscle layer was closed with suture in a simple interrupted pattern. Skin edges were opposed and closed with sterile wound clips.

Following the procedure, the mouse's overall health was monitored for 2 hours post-surgery for signs of pain or difficult or shallow breathing until the mouse was fully ambulatory. Since this is a major surgery, NSAID, meloxicam (2mg/kg) and buprenorphine (0.06mg/kg) were given to the animals to limit surgical pain during the first 24 hours post surgery, for at least 48hr post surgery. After 48 hours, surveillance included monitoring of general condition, water and food consumption, fecal output and consistency, condition of the surgical wound, and signs of pain or discomfort which could include unusual restlessness, inability to relax, huddling, a hunched posture, soiling of the perineal region, reduced food and water intake. Animals were weighed daily to monitor for weight loss from reduced oral intake and monitored daily for the above signs of distress.

Orthotopic cell line injection

Preparation for orthotopic cell line injections followed the same procedure as surgical instillation of Adeno-Cre into the bladder. Instead of Adeno-Cre viral solution, a cell suspension of two million cells in 50 μl phosphate buffered solution (PBS)) was

slowly injected into the wall of the bladder dome using a 30-gauge needle with the bevel of the needle facing upwards. Then the needle was then withdrawn, and a Q-tip placed over the injection site for 30 seconds to prevent bleeding. Follow up post surgery followed the same procedure as the Adeno-Cre post-surgery procedure.

Ultrasound-guided intra-bladder tamoxifen injection

Under isoflurane anesthesia, mice were prepared for imaging by applying 70% alcohol followed by 1% betadine to the lower abdomen. A 30G Hamilton syringe (100 μL) was mounted onto a micromanipulator that was part of the Vevo ultrasound imaging station (VisualSonic). This allowed precise delivery of the needle tip under direct ultrasounds imaging guidance. Fifty microliters of solution was then delivered into the bladder lumen. Mice were monitored throughout the procedure for any evidence of distress and also monitored until it they were awake and it was confirmed that they were not in distress post-anesthesia.

BBN

N-butyl-N-(4-hydroxybutyl)-nitrosamine (BBN) (TCI) was diluted in distilled water to 0.5% or 1%. Mice were provided the BBN solution as drinking water, and water was replaced once or twice weekly. Mice were euthanized at specific time points and bladders were weighed and frozen for WES analysis. For combination of GEMM with BBN, mice were injected with tamoxifen via intraperitoneal (IP) injections once daily for four days. One month after IP injections, mice were started on BBN drinking regimen.

Bladders were collected at death, half of it frozen for Western blot analysis, and the other half fixed for H&E staining.

Genomic studies

Pathology and Cohort Classification

Histologic subtypes of bladder cancer were determined based on clinical pathology reports of the samples. Similarly, grade was determined by clinical pathology reports and classified as low grade, high grade, or metastatic.

Identification of unmatched cohort

Patients were identified in the MSKCC clinical sequencing bladder cohort. Patients in the matched cohort were not included in the unmatched cohort. For patients with multiple bladder samples, only one sample was used in the unmatched cohort with the most recent sample being used, except for patients with a low grade tumors. Because the low grade cohort was significantly smaller compared to the high grade and metastatic cohorts, low grade sample were prioritized over the most recent sample to increase cohort numbers.

Identification of matched cohort

Patients were identified retrospectively and prospectively. For patients identified retrospectively, a metastatic bladder specimen was first identified in the MSKCC clinical sequencing cohort. For each patient with a metastatic sample, we determined if the primary tumor samples had been previously banked by pathology and had not been

sequenced. For patient samples identified prospectively, patients from the MSKCC clinical sequencing cohort with at least one primary and at least one metastatic sample were included. All samples were reviewed by a genitourinary pathologist to confirm that they were of urothelial origin.

After excluding samples with insufficient tumor tissue, insufficient data quality due to low total DNA quantity and purity, or failed library preparation, a total of 66 patients had matched primary and metastatic tumor samples, and matched normal control specimens available for analysis. For these samples, we performed either MSK-IMPACT and/or whole-exome sequencing (WES) analysis. Of these, 23 patients had sufficient tumor tissue for both whole-exome and high-depth coverage MSK-IMPACT. Of the remaining patients, 39 had tumor tissue sufficient for only MSK-IMPACT, whereas 4 patients were sequenced using WES only.

Prospective Sequencing and Analysis

For all patient samples, tumor and patient-matched normal DNA was extracted, respectively, from formalin-fixed paraffin embedded (FFPE) tumor biopsy samples or from mononuclear cells from peripheral blood. For each tumor, a pathologist reviewed a hematoxylin and eosin–stained section to ensure adequate tumor content for analysis. When indicated, tumors were macrodissected to maximize tumor content. All specimens underwent next-generation sequencing using MSK-IMPACT assay, a hybridization capture-based next-generation sequencing assay, which analyzes all protein-coding exons of between 341 and 468 cancer-associated genes depending upon the assay version, all as

previously described[129,130]. Somatic mutations, DNA copy number alterations, and structural rearrangements were identified as previously described[129].

Whole exome sequencing

We used a comprehensive in-house WES pipeline TEMPO - Time efficient mutational profiling in oncology (https://github.com/mskcc/tempo) that performs alignment using BWA-mem algorithm followed by mutation calling using Strekla2 and Mutect2 variant callers. The combined, annotated and filtered variant calls were used for downstream analysis. Details of the variant call processing are described at https://ccstempo.netlify.com/variant-annotation-and-filtering.html#somatic-snvs-and-indels. Copy-number analysis was performed with FACETS (https://github.com/mskcc/facets) and processed using facets-suite (https://github.com/mskcc/facets-suite).

In order to delineate mutational processes driving acquisition of somatic alterations, mutational signature decomposition[131] was performed for all the tumor samples with a minimum of five single nucleotide somatic mutations using an R package mutation-signatures (https://github.com/mskcc/mutation-signatures). For cases where more than one signature was present, a weighted combination of signatures was calculated reflecting the proportion of mutations in the sample attributed to that signature.

Chapter 1: Characterization of Ras/MAPK mutational variants

Over the past two decades, several dozen cancer therapies have been developed that selectively inhibit molecular alterations that promote cancer initiation and/or progression. In large part, these drugs are effective only in patients whose tumors harbor specific molecular alterations. The need for clinicians to be able to identify the subset of patients most likely to respond to targeted therapies has necessitated the development of diagnostic assays that can rapidly and accurately identify those patients whose tumors harbor the predictive biomarkers of interest.

Initial diagnostic platforms were based on polymerase chain reaction, immunohistochemistry (IHC) or fluorescence *in situ* hybridization and thus capable of identifying alterations in only one or a few cancer-associated genes. More recently, next generation sequencing (NGS) methods have been developed and deployed clinically that can rapidly and at significantly lower cost analyze hundreds or thousands of cancer-associated genes using small quantities of DNA derived from both frozen and formalin fixed paraffin embedded tumor tissues[129]. The rapid adoption of clinical NGS-based diagnostic tests has thus led to hope that a significantly larger proportion of cancer patients will soon benefit from personalized treatment regimens.

While systemic therapies, including cytotoxic chemotherapies, targeted therapies such as kinase inhibitors and immunotherapies, can have profound and durable clinical activity, only a fraction of cancer patients currently benefit from each of these approaches. This can be attributed to several factors. First, current tumor profiling

methods identify genomic alterations that predict for drug response in only a minority of cancer patients. Second, not all patients who receive a matched targeted therapy based on their individual tumor genomic profile respond. Variability of treatment response may be the result of additional genomic complexity, for example the presence of *PTEN* mutations in patients with EGFR mutant tumors[132], that can abrogate dependence of the patients tumor on the mutated/dysregulated drug target. In such instances, broader molecular profiling may identify additional co-alterations that could suggest potential combinatorial approaches.

As targeted therapies and NGS are adopted as a component of the routine clinical management of an increasing number of cancer types, more data will be generated that will require novel ways to assess the tumorigenicity of individual genetic variants. Analysis of this data will require computational approaches that can prioritize variants of unknown biologic and clinical significance for biologic and clinical study. As an example, a statistical method developed by the Taylor laboratory at Memorial Sloan Kettering Cancer Center has identified hundreds of hotspot mutations that recurrently arise across various cancer types[130]. However, the vast majority of somatic mutations identified in tumors occur infrequently and most of these rare variants are likely non-functional passenger events. Functional studies performed to date indicate that a small subset of these rare mutations (long-tail driver mutations) will be functional drivers critical to the development and or progression of individual cancers. These rare somatic and germline variants would be overlooked by methods that rely exclusively on mutation frequency at individual amino acid positions. It is therefore important to develop more refined methods that can at the genome scale identify rare mutations that are likely

functional. Though individually rare, these long-tail driver mutations are likely present in a significant fraction of tumors and thus represent recurrent molecular alterations that could be potential drug targets.

Results

Characterizing ERBB2 mutations in breast versus bladder cancer

Mutations in the *ERBB2* gene have been identified in a number of cancer types, including cancers of the bladder, breast, stomach, colon and lung. Many of these *ERBB2* mutations have been confirmed to be oncogenic in laboratory models, including the S310Y, D769H, V777L and V842I hotspot mutations (Figure 2A). These mutations have been shown to increase auto-phosphorylation of HER2[133]. The prevalence of individual mutations has been shown to vary as a function of cancer type. For example, the extracellular domain mutation S310F has been found to be more commonly associated with bladder cancer, whereas the kinase domain mutations L755S and V777L are more frequent in breast cancers (Figure 2B).

Notably, preliminary studies show that the sensitivity of *ERBB2* mutations to ATP competitive inhibitors of the kinase varies as a function of the individual mutant allele with some mutations showing sensitivity to specific kinase inhibitors, whereas others are resistant[133,134]. These data suggest that the response of patients with *ERBB2* mutant tumors to selective HER kinase inhibitors may vary as a function of the specific mutant allele present in that patient's tumor. While some of the most common mutations in *ERBB2* had been previously characterized, the functionality of most mutations in this gene remains unknown.

In order to determine whether neratinib had activity in a broad range of cancer types, a basket trial was initiated in which patients with mutations in HER2 and/or HER3 were eligible for study participation regardless of cancer type (MSKCC IRB Protocol 13-140, Clinicaltrials.gov NCT01953926). While there were competing trials of neratinib in lung and breast cancer, this trial design was unique in that it provided patients with both common and rare cancers the opportunity to participate in a trial of neratinib, presuming their tumor harbored a HER2 or HER3 mutation (Figure 3A). Clinical activity was observed in many patients. Figure 3B shows representative PET scans from a patient with breast cancer whose tumor harbored a V777L *ERBB2* mutation. As shown, this patient achieved a complete response by PET imaging within 2 months of starting neratinib, which was further confirmed at 4 months. While promising, not all patients with *ERBB2* mutant tumors responded to neratinib. Notably, while a significant fraction of breast cancer patients responded, only stable disease as best response was observed in patients with bladder cancer. Four out of first five bladder cancer patients had the same extracellular hotspot S310F mutation, whereas the breast tumors typically harbored kinase domain mutations (Figure 3C).

In order to generate the *ERBB2* vectors to be expressed in various cell lines, we used site-directed mutagenesis to create each *ERBB2* mutant allele. Briefly, the mutated *ERBB2* gene was subcloned into the lentiviral destination vector. Once the lentiviral vector was sequenced to confirm the presence of the *ERBB2* gene with the correct mutation, cell lines were infected with the virus. Cells expressing the vector were then selected with the goal of generating a stable cell line for functional studies. The mouse fibroblast cell line, NIH3T3, was initially chosen for these experiments because of the

ease with which this cell line can be genetically manipulated, as well as its low expression of endogenous Erbb family kinases. Because of the low levels of endogenous HER2 expression in NIH3T3 cells, changes in downstream signaling effects could be attributed to the expression of the exogenous HER2 mutant allele[135].

Once stable cell lines expressing the desired *ERBB2* mutation were generated, we examined the effect of the mutation on HER kinase signaling. Western blot analysis was used to determine activation of HER2 by comparing levels of phosphorylated HER2 in HER2 mutants to a HER2 wild-type control cells. Activation of downstream signaling was also determined by comparing levels of phosphorylated MEK, ERK, AKT and S6 protein among the mutant cell lines with cells expressing either wild-type HER2 or empty vector controls. Western blot analysis showed that expression of HER2 S310F and HER2 V777L in NIH3T3 cells resulted in high levels of auto-phosphorylated HER2 as well as a slight increase in phosphorylation of downstream signaling proteins, such as phospho-AKT, compared to expression of wild-type HER2 (Figure 4A).

To quantitate the transforming ability of each mutation, cell lines expressing three of the *ERBB2* mutants, S310F, L755S, and V777L, were grown in soft agar to assess the ability of the cells to grow without attachment to a solid surface. Because anchorage-independent growth is a characteristic of transformation, colony formation would suggest that a mutation is transforming[136]. The cells were also grown in the presence of neratinib to determine the sensitivity of each mutation to the drug.

While cells expressing all three mutants exhibited increased HER2 phosphorylation versus wild type on the Western blots, we observed differences in the ability of specific mutant alleles to promote growth in soft agar in the presence and

absence of neratinib. We also found that all three mutants formed more colonies as compared to cells expressing wild-type HER2, with the V777L mutation inducing the largest number of colonies. In addition, treatment with neratinib abrogated colony formation in all three mutant lines (Figure 4B). Although the S310F allele, which is the most frequent mutation found in bladder cancer, was sensitive to neratinib, it appeared to be a weaker driver of colony formation. Therefore, the limited activity of neratinib noted in the basket trial may have been attributable, at least in part, to reduced dependence of cells expressing this mutant on HER2 for transformation.

Characterizing MEK1 mutants identified by 3D hotspot analysis

Identifying mutations in genes for which targeted therapies exist or are being developed, regardless of their individual frequency in the population, is critical for the effective practice of precision oncology. Our analysis performed with Drs. JJ Gao, Matthew Chang, Niki Schultz and Chris Sanders identified 3D clusters in several genes for which selective inhibitors are either used as part of standard clinical management or are being actively tested in clinical trials, including *EGFR*, *KIT*, *MTOR*, *PIK3CA*, *MAPK1*, and *FGFR3*. The 3D clusters within these genes contained known activating single-residue hotspot mutations as well as rare candidate driver mutations.

More specifically, we identified a 3D cluster ($p = 0.03$) in *MAP2K1*, the gene encoding MEK1, that included seven mutated residues (R49, A52, F53, Q56, K57, G128, and Y130) (Figure 5A). Two of these residues (F53 and K57) had previously been shown to be recurrent hotspots[130] and to induce constitutive ERK pathway activation[137]. The other five have only rarely been identified in tumors (mutation frequency of 0.01–0.03%

individually). All seven of these mutated residues reside in the shared interface between helix A and the kinase domain (Figure 5B). As helix A has previously been shown to negatively regulate MEK1 kinase activity by interacting with the kinase domain[138], mutations that disrupt this interaction may result in constitutive ERK pathway activation. We thus experimentally assessed the ability of the mutations in this 3D cluster to induce ERK1/2 phosphorylation in a cellular model.

We found that expression of five of the mutated proteins, including G128D, Y130C, and also the previously characterized F53L, Q56P, and K57N mutations, induced downstream MAPK signaling as assessed by increased expression of phosphorylated ERK (Figure 5C). To test whether the Y130C mutant, which is not in a single-residue hotspot, but was nominated by 3D cluster analysis, was sensitive to MEK inhibition, we treated HEK-293T cells expressing the Y130C mutant, or as a positive control the Q56P mutant, with trametinib, an FDA-approved MEK inhibitor. Trametinib treatment resulted in significant downregulation of MAPK pathway activity (Figure 5D). As durable responses to MEK inhibitors have been reported in patients whose tumors harbor an activating mutation in *MAP2K1*[76], this example highlights the potential translational impact of 3D cluster analysis to guide patient care decisions.

As variants of unknown significance in MEK1 continue to be identified as potential drivers, MEK-targeted drugs will become increasingly important in cancer care. We thus sought to test the potency of various MEK1 inhibitors currently being tested in patients in cells expressing several additional common variants, including F53L, Q56P, Q56_60del, K57N, E102_I103del, P124L, and Y130C. These MEK1 mutations demonstrated varying levels of sensitivity to our panel of MEK inhibitors as measured by

changes in phospho-ERK levels at various time points, with the E102_I102del mutant being resistant to all inhibitors tested (Figure 6A, Figure 7A, Figure 8A). Most MEK1 variants also showed moderate resistance to the MEK inhibitor CH5126766 (Chugai) inhibitor, with the exception of P124L, which was very sensitive (Figure 6A). Interestingly, P124L was insensitive to selumetinib (Figure 7A), suggesting that mutant sensitivity to MEK inhibitors likely varies as a function of the mechanism whereby the drug inhibits MEK kinase activity.

Discussion

The mechanisms whereby the Ras/MAPK signaling pathway promotes tumor development has been well characterized over the past several decades, however, the differences in the biology of individual mutations in many of the genes within this pathway remains relatively unstudied. Our laboratory and clinical data suggest that cell type impacts the selection for different HER2 mutation types and may also impact sensitivity to HER2 kinase inhibitors. While kinase domain mutations are frequent in breast cancer, extracellular domain mutations are more common in bladder. In the 3T3 cell models, the V777L kinase domain mutation is a strong driver of colony formation. Fewer colonies were formed by the S310F extracellular domain mutation, although it is also an activating mutation. Differential responses to the HER2 targeted therapy neratinib were also seen in breast versus bladder patients. While the basis for this differential sensitivity is likely complex, it may be in part due to differences in the biology of kinase versus extracellular domain mutations. Further studies will be required to characterize these mutations in a tissue-specific context.

We also identified several activating MEK1 alterations that may be predictive biomarkers of sensitivity to MEK inhibition in patients. These studies highlight the importance of characterizing variants of unknown significance, even in genes that are less frequently mutated. The scientific community has largely identified the most commonly mutated genes and in several cancer types established the value of targeted therapies. We are now at a point where so much sequencing data is being generated prospectively that we are not able to use it all effectively. However, potential actionable mutations may not be appreciated in clinical sequencing data because their prevalence in the population is low. Models that are able to distinguish between actionable alterations and variants of unknown significance will be critical to achieving the full impact of precision oncology.

In addition to characterizing several novel mutations in MEK1, we demonstrated that MEK1 mutations have varying sensitivity to different classes of MEK inhibitors. Work recently published by Neal Rosen (MSKCC) demonstrated that some activating MEK1 variants drive MAPK signaling through dependence on RAF[74]. These mutations, including P124L, were shown to increase MAPK signaling as a result of increased RAF phosphorylation of the MEK1 variant. In the absence of RAF, this mutation was not highly activating. Activity of other mutations, including F53L and K57N, were only partially dependent on RAF phosphorylation.

These studies provide mechanistic insight into the varying sensitivity of MEK mutations to different MEK inhibitors observed in our analysis. The P124L mutation was very sensitive to the Chugai inhibitor, which functions through RAF inhibition, but was less sensitive to selumetinib. As P124L is dependent on RAF phosphorylation to activate

downstream signaling, it is more sensitive to the dominant negative effect of Chugai-bound MEK inhibiting RAF as well.

In the future, a major consideration of mutational characterization will be tissue specific context. We highlighted the importance of characterizing the effects of lineage in our studies of HER2 variants in breast and bladder cancers, but lineage is also likely relevant in dictating MEK-dependence in MEK1 mutant tumors, as co-mutations with RAF may impact function of MEK1 variants and their sensitivity to drug. Although studies in well characterized cell lines with low genetic variability will be helpful in understanding difference in drug sensitivity based on difference in the biology of individual mutant alleles, future studies will need to examine the impact of co-occurrence of other mutations both in the same pathways, like RAF and MEK, and other signaling pathways.

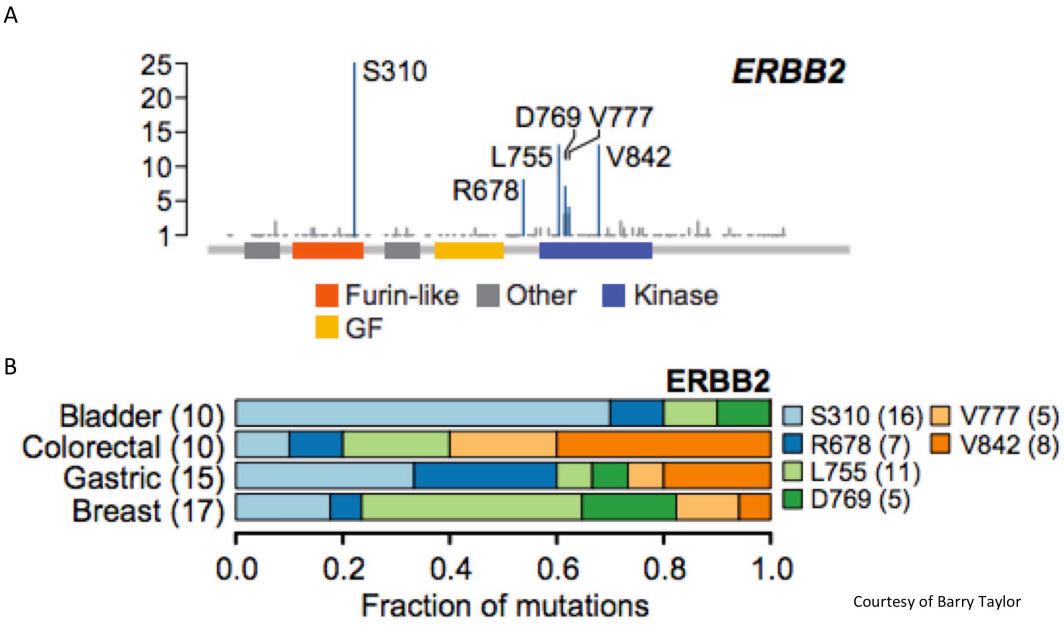

Figure 2: *ERBB2* variation frequencies across cancer types.

A: A number of "hotspot" mutations are found across the *ERBB2* gene. Known oncogenic mutations can be divided into extracelluar domain and the kinase domain. B: Occurrence of *ERBB2* mutations. Bladder cases consist of approximately 70% S310 mutations. In contrast, breast cases consist of approximately 80% kinase domain mutations. Figures generated by Barry Taylor.

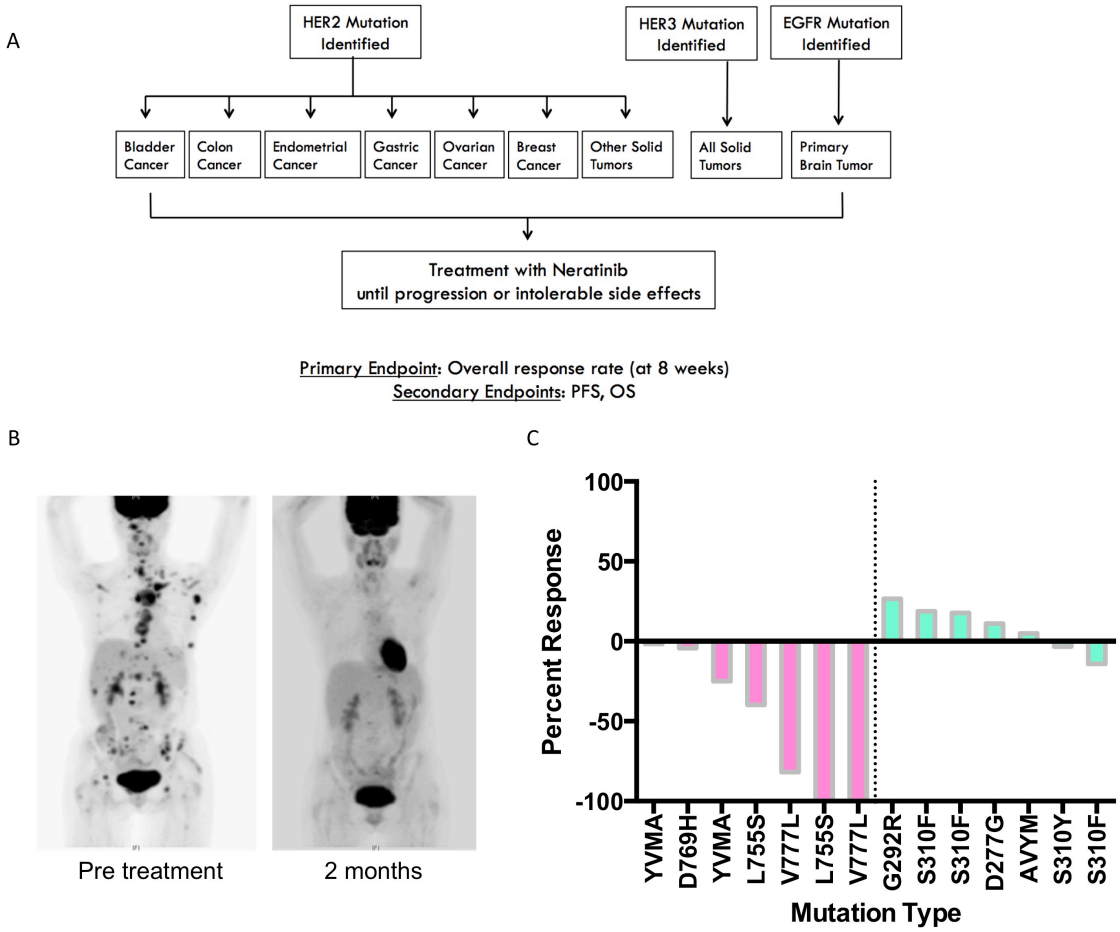

Figure 3: Patient response to neratinib, a tyrosine kinase inhibitor.

A: Schema of basket trial accrual. Patients with HER2 mutant bladder, colon, endometrial, gastric, ovarian, breast and other solid tumors were included in the trial. HER3 and EGFR mutant tumors formed separate baskets. B: PET images of patient with ERBB2 V777L mutant ductal breast carcinoma responding to neratinib therapy in trial MSK study 13-140. Images courtesy of David Solit. C: Waterfall plot showing overall patient response.

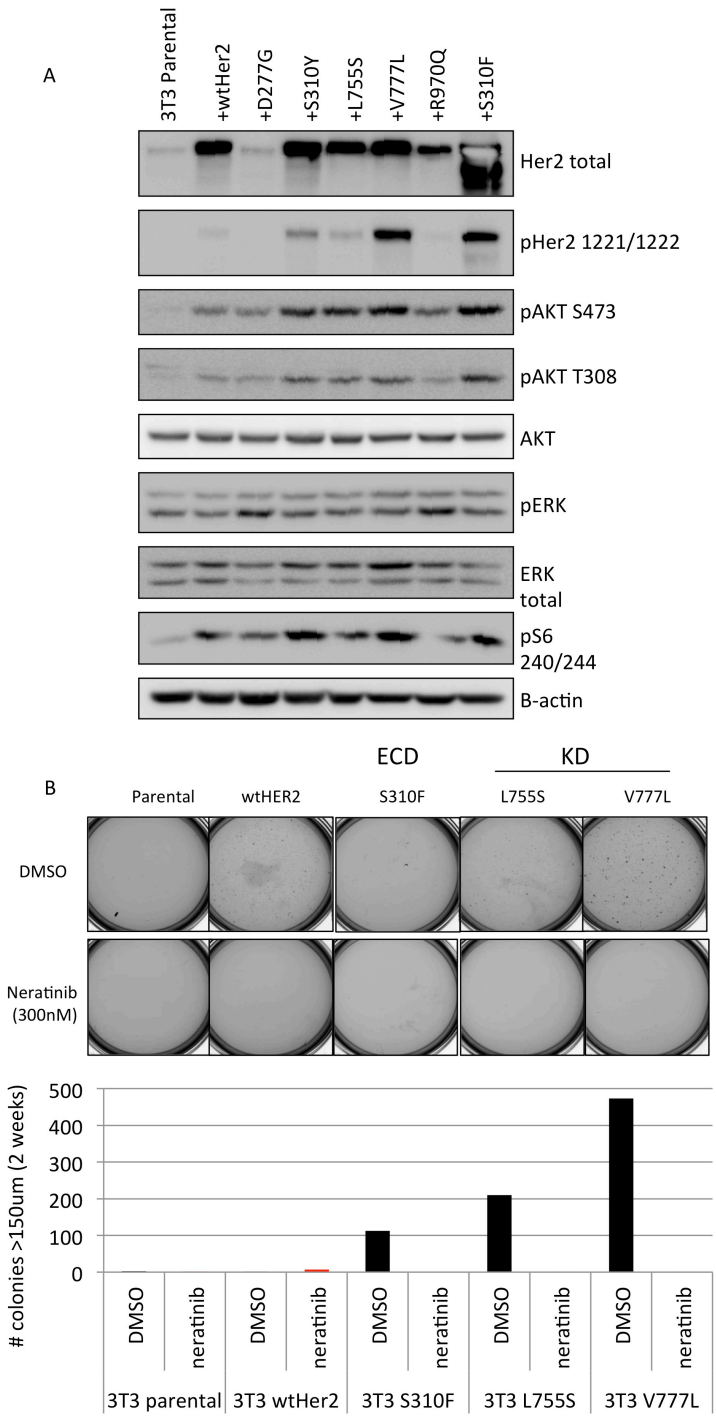

Figure 4: Select ERBB2 mutations are transforming and sensitive to neratinib.

A: Western blot analysis of NIH3T3 cell lines expressing various ERBB2 mutations. B: Soft agar assay was used to determine transforming ability of each mutant in the absence and presence of neratinib. Graph shows the number of colonies that grew for each mutation.

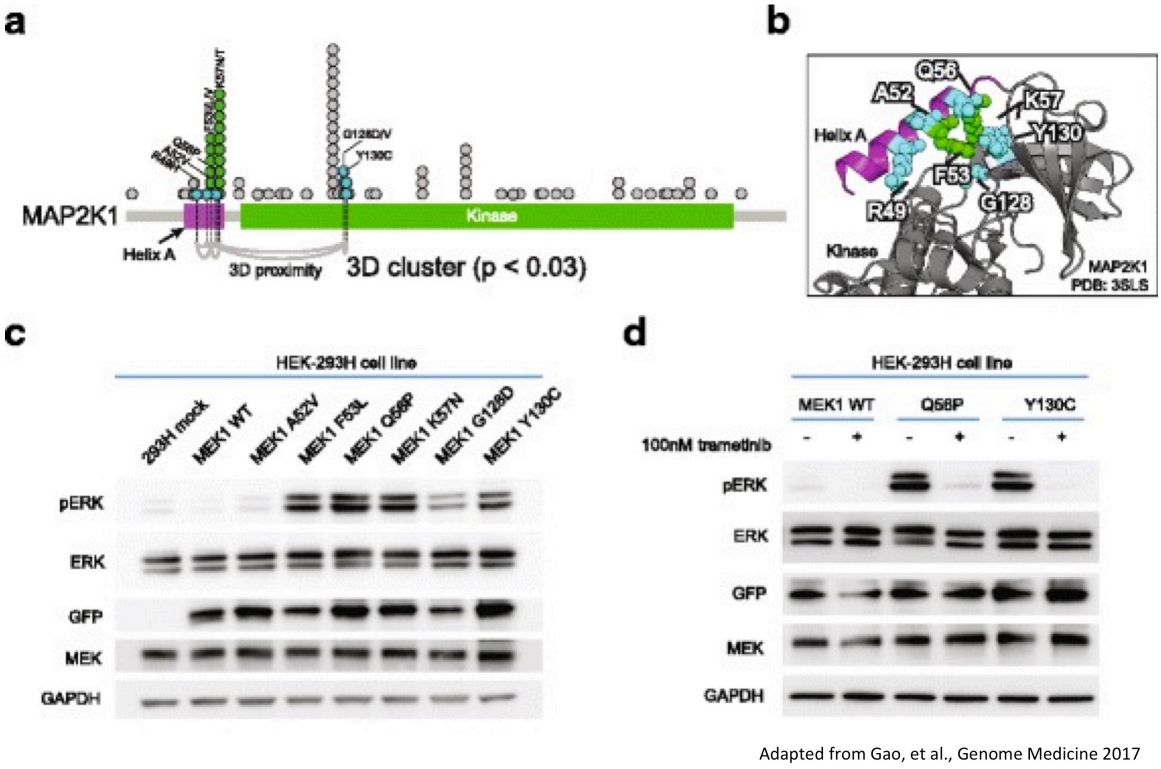

Adapted from Gao, et al., Genome Medicine 2017

Figure 5: Experimental validation of functional impact of mutations in 3D clusters in *MAP2K1*.

A: Seven residues in a 3D cluster in MAP2K1, in the context of the domain structure of the protein. Each circle is an occurrence in a sample; connecting lines (bottom) indicate cluster membership, i.e., statistically significant proximity in 3D in the protein structure. Figure generated by Matt Chang. B: The same cluster of mutated residues in the 3D structure of MAP2K1. The purple helix is known to negatively regulate the kinase activity of MAP2K1/MEK1. Figure generated by Matt Chang. C: Functional characterization of MAP2K1/MEK1 mutants in HEK-293H cells. Expression of G128D and Y130C (as well as the previously characterized F53L, Q56P, and K57N) mutants each resulted in increased expression of phosphorylated ERK compared to wild-type MAP2K1 but not the cluster member A52V. D: ERK phosphorylation was inhibited by trametinib in cells expressing the Q56P or Y130C MAP2K1 mutations in HEK-293H cells.

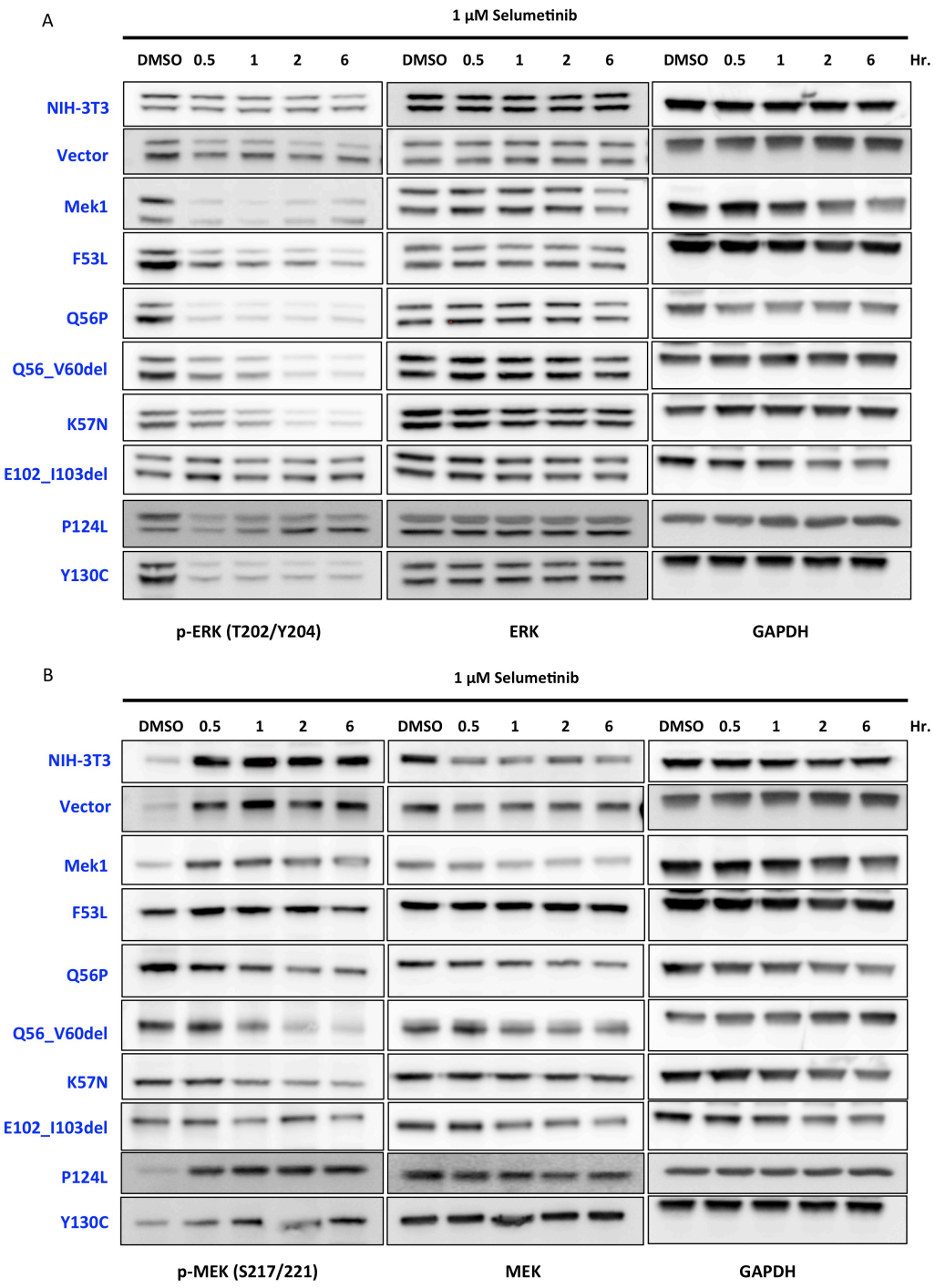

Figure 6: Sensitivity to selumentinib across *MAP2K1* mutants.

NIH-3T3 cells were transfected with vector, wild-type MEK1, or mutant MEK1. Cells were then treated with DMSO or 1μM of selumetinib and collected at 0.5, 1, 2 or 6 hours. Phospho-ERK (A), total ERK (A), phospho-MEK (B), and total MEK (B) levels were assessed by Western.

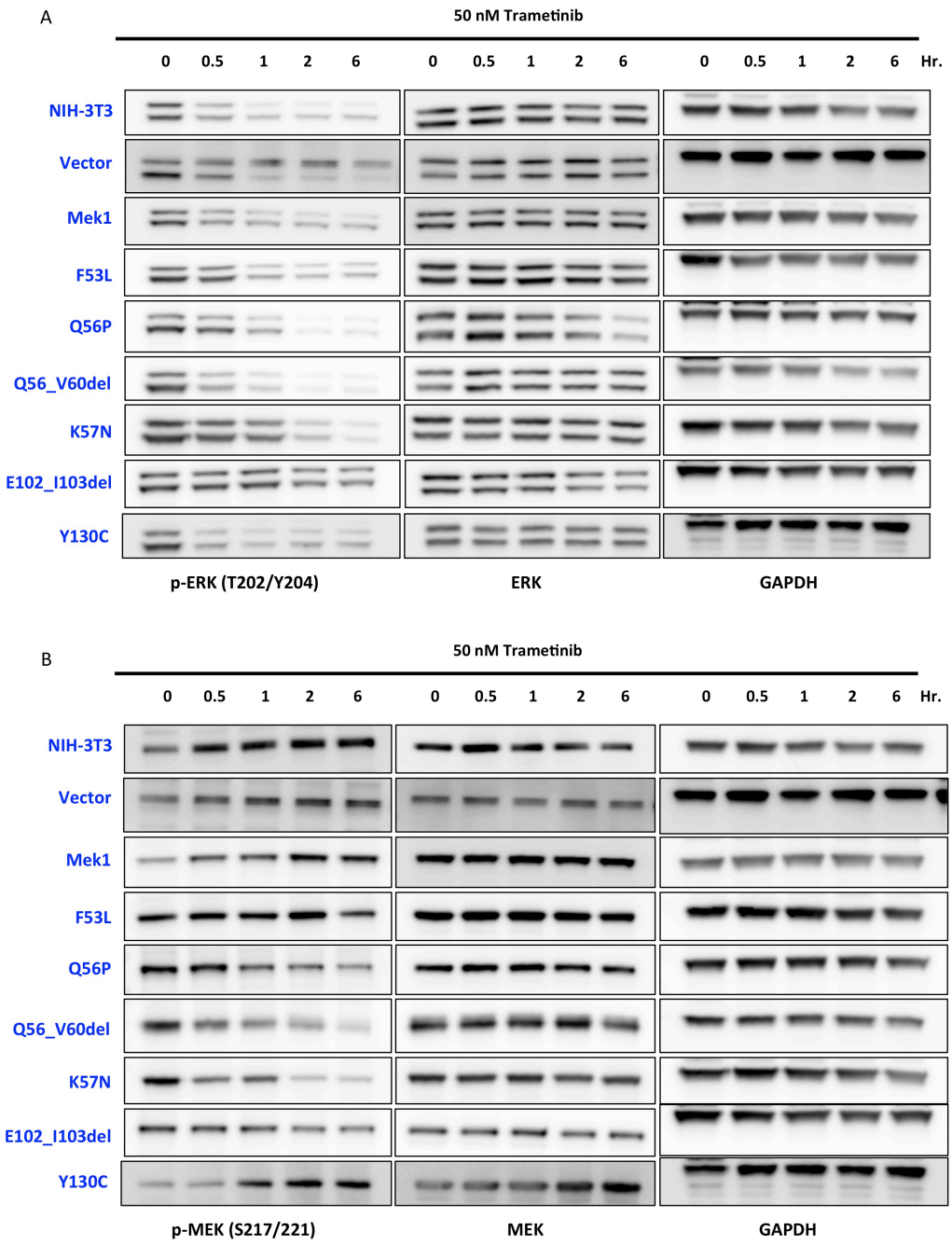

Figure 7: Sensitivity to trametinib across *MAP2K1* mutants.

NIH-3T3 cells were transfected with vector, wild-type MEK1, or mutant MEK1. Cells were then treated with DMSO or 50nM of trametinib and collected at 0.5, 1, 2 or 6 hours. Phospho-ERK (A), total ERK (A), phospho-MEK (B), and total MEK (B) levels were assessed by Western.

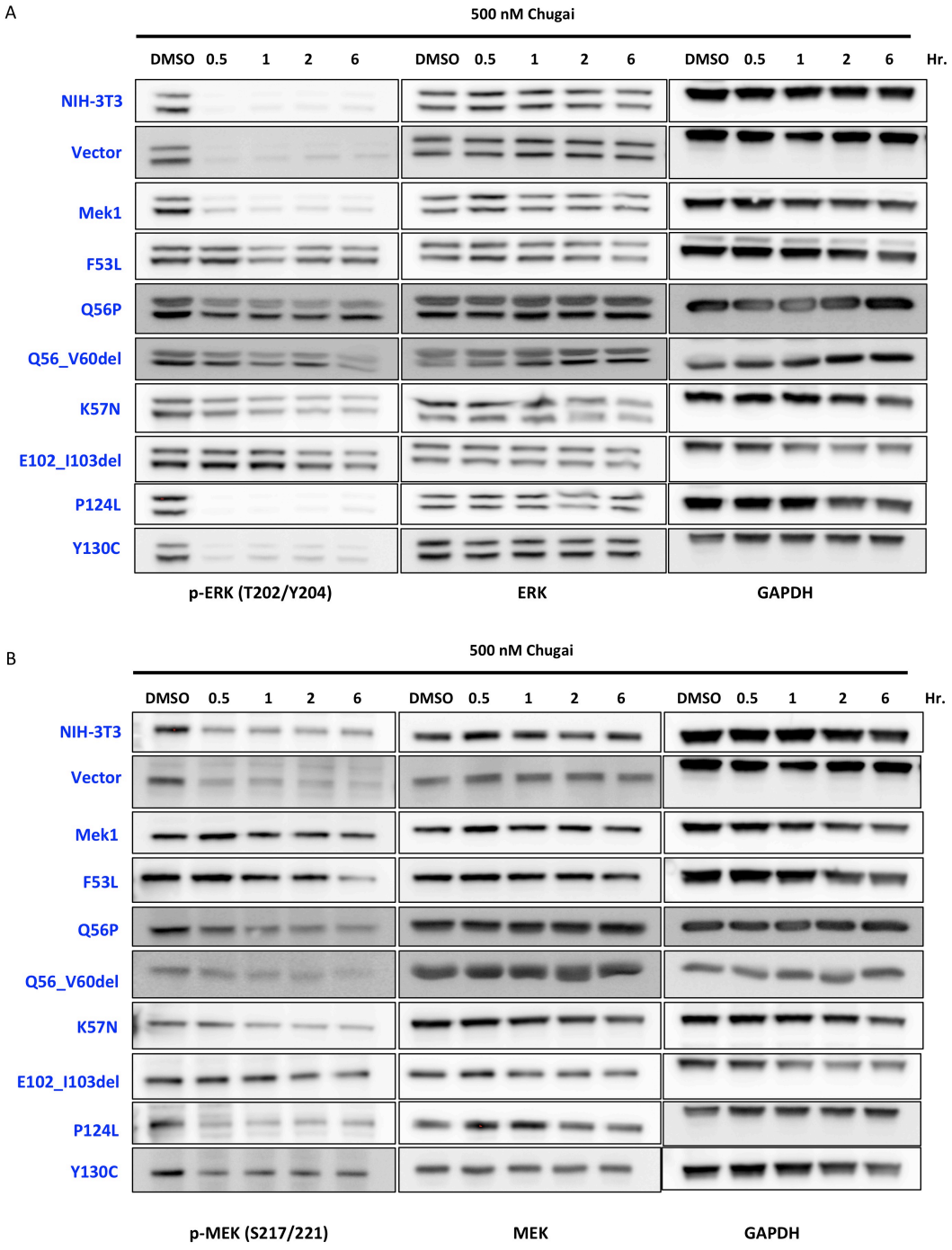

Figure 8: Sensitivity to Chugai across *MAP2K1* mutants.

NIH-3T3 cells were transfected with vector, wild-type MEK1, or mutant MEK1. Cells were then treated with DMSO or 500nM of Chugai and collected at 0.5, 1, 2 or 6 hours. Phospho-ERK (A), total ERK (A), phospho-MEK (B), and total MEK (B) levels were assessed by Western.

Chapter 2: Defining the biologic consequences of KDM6A loss-of-function *in vitro*

In 2014, the Cancer Genome Atlas Research Network published a comprehensive analysis of genomic landscape of muscle-invasive urothelial bladder carcinomas[34]. Commonly altered genes included cell cycle regulators such as *RB1*, *CDKN1A* and *CDKN2A*, and genes that regulate mitogenic signaling including *FGFR3*, *PIK3CA* and *TSC1*. Consistent with several prior reports, epigenetic modifiers, including *ARID1A*, *KMT2D*, *KDM6A* and *EP300*, were found to be altered in approximately 74% of cases, with *KDM6A* alterations present in 25%.

Several lines of evidence support a role for KDM6A in the pathogenesis of bladder tumors. First, introduction of wild-type KDM6A into *KDM6A*-null cancer cell lines results in a significant decrease in H3K27me3 and an increase in cell doubling time, suggesting a tumor suppressive role for KDM6A. Second, KDM6A has been shown to play a role in lineage specificity and cell cycle regulation. Removal of repressive H3K27me3 marks results in increased expression of the HOX gene cluster. Also, ChIP-qPCR has identified RB1 and Rb binding proteins as gene targets for KDM6A binding. Depletion of KDM6A resulted in reduced levels of RB1 and Rb binding proteins and increased S phase entry in primary human fibroblasts, providing additional evidence that KDM6A may promote tumorigenesis by modulating Rb pathway activity. Notably, alterations within KDM6A and Rb were mutually exclusive within a prospectively sequenced cohort of 157 bladder tumors analyzed at our institution, suggesting that these two genes may have overlapping functional roles.

While the role of KDM6A deletion has been investigated in development and other cell lineages, efforts to functionally characterize the role of KDM6A loss-of-function in a bladder specific context have been limited. Given the strong association of KDM6A truncating mutations specifically in bladder cancer, we sought to understand the role of KDM6A loss-of-function in bladder cancer initiation and development. To explore this question, we sought to develop an isogenic *in vitro* model in which KDM6A expression was lost in urothelial cell lines using CRISPR/Cas9.

Results

Genomic characterization of bladder cell lines

Previously, we had assembled a panel of 33 urothelial cell lines from various sources, including the American Type Culture Collection (ATCC), the Leibniz Institute of DSMZ, and Margaret Knowles (Leeds Institute of Cancer and Pathology, St James's University Hospital). To confirm the genetic background of these cell lines, we performed targeted next generation sequencing using MSK-IMPACT. The genetic mutations identified were consistent with the types of alterations previously identified in human bladder cancer and in most cases matched the mutation profiles for these cell lines if they had previously been reported in the literature. In addition, several cell lines were noted by MSK-IMPACT to harbor *FGFR3* fusions, including in the RT4 cell line.

Because most KDM6A mutations identified in bladder cancer patients are truncating mutations predicted to result in functional loss of protein expression, we sought to generate isogenic knockout models to study KDM6A loss-of-function *in vitro*. As KDM6A mutations are common in bladder cancers, we expected KDM6A loss-of-function alterations to be similarly prevalent in patient-derived cell lines. While

underrepresented as compared to the expected frequency of *KDM6A* mutations in bladder tumors, 4 out of 33 cell lines were found to harbor truncating mutations in *KDM6A* by MSK-IMPACT. However, the patterns of co-mutation among cell lines was highly variable and complex suggesting to us that direct phenotypic comparisons between KDM6A mutant and wild-type cell lines was likely to be uninformative. We thus utilized CRISPR/Cas9 technology to generate KDM6A knockout cell lines that could be directly compared to the parental cell line in order to probe the effects of KDM6A loss.

In order to select appropriate cell lines in which to knockout KDM6A, we reviewed the mutational profiles of the cell lines generated by MSK-IMPACT analysis and, with the help of Dr. Ricardo Ramirez, performed RNA sequencing (RNA-seq) to assess the levels of KDM6A expression in each (Figure 9A). We then compared relative KDM6A transcript levels to identify cell lines with high KDM6A levels. Cell lines with high KDM6A expression and lacking mutations in other chromatin modifying genes that could have similar biologic functions were considered best suited for this study. Because bladder cancer patients often harbor several potentially oncogenic mutations that may be contributing to tumorigenicity, it was challenging to identify cell lines in our panel with high KDM6A expression that lacked mutations that we felt could have similar biologic effects as KDM6A. While we did have access to an immortalized normal human urothelial cell line (TERT-NHUC), working with this cell line to generate CRISPR knockouts presented a number of technical challenges. In the end, this selection process led us to choose the RT4 and VMCUB2 cell lines as most appropriate models to study KDM6A loss *in vitro*.

To develop KDM6A isogenic models, we utilized a lentiCRISPRv2 plasmid provided to Addgene from the Zhang lab. Guide RNA's were targeted to exon 2 of the KDM6A protein to induce indels that would produce frameshift mutations that would result in protein truncation. First, cells were transduced with viral lentiCRISPRv2, and single-cell sorted after brief selection. Isogenic clones were then tested for loss of KDM6A expression by Western blot. Sanger sequencing was initially performed to characterize the mutational basis for the loss of KDM6A mutation in select clones. MSK-IMPACT sequencing was then performed on select single cell clones that had loss of KDM6A expression by western blot to confirm that the process of CRISPR gene editing and single cell selection had not resulted in selection of a sub-clone with other potentially confounding oncogenic mutations.

For the majority of our functional experiments, we chose to focus our analysis on studies of the RT4 parental cell line and CRISPR-mediated KDM6A knockout cell sub-lines derived from the RT4 cell line for a number of reasons. First, activating FGFR3 alterations are commonly co-occurrent with KDM6A alterations and RT4 harbors an FGFR3-TACC3 fusion, making it a representative model of KDM6A loss-of-function in the human disease. Second, the RT4 cell line is derived from a papilloma, which is a relatively benign neoplasm of the bladder. Therefore, analysis of the model would help us determine whether KDM6A loss could contribute to a higher grade, invasive, or metastatic phenotype.

Initially, with the help of Dr. Byron Lee, we generated two separate isogenic KDM6A-null RT4 cell lines, designated RT4 K2 and RT4 K3. After a number of passages, RT4 K3 appeared to regain KDM6A expression, possibly as a result of

contamination of a small subset of the original RT4 K3 population being KDM6A wild type and out competing the KDM6A knockout population. We thus chose to resort the RT4 K3 population into single cell clones to ensure a more homogenous population moving forward. This led to a subclone of K3, named K316, which was confirmed to have loss of KDM6A expression throughout all subsequent experiments. Furthermore, to minimize population drift, cell lines were not used for experiments beyond passage 20.

MSK-IMPACT sequencing of K2 and K316 confirmed that each had a likely pathogenic mutation in *KDM6A* predicted to result in loss of protein expression, which was confirmed by Western blot (Figure 9B). More specifically, Y116fs and Q117fs mutations were identified in the KDM6A null cell lines that were not present in the parental cell line. MSK-IMPACT sequencing also confirmed the presence of an FGFR3-TACC3 fusion in the RT4 parental cell line, in addition to a *TSC1* frameshift mutation and a hotspot *RHOA* A161V mutation. All other mutations identified by MSK-IMPACT sequencing were variants of unknown significance (VUS) that were shared between all cell lines, with the exception of an ELF3 frameshift deletion identified in RT4 K316 that may be oncogenic (Figure 10). We also examined copy number alterations in each cell line, and found 9p21 deletion across all the cell lines (Figure 11), a region which includes the *CDKN2B* and *CDKN2A* tumor suppressors.

To generate KDM6A knockouts in the VMCUB2 cell line, we used the lentiCRISPRV2 plasmid with the same KDM6A exon 2 targeted sgRNA's that was used in the RT4 cell line. Isogenic clones were similarly identified after single-cell sorting. As with the RT4 cells, clones with KDM6A loss by Western blot were selected for subsequent genetic and biologic characterization.

Functional Characterization of KDM6A loss

After confirming the genetic background of the RT4 parental and KDM6A knockout cell lines, we performed a series of phenotypic assessments to determine the effect of KDM6A loss-of-function. We first assessed whether loss of KDM6A expression was associated with enhanced cell proliferation, comparing two-dimensional growth of the RT4 parental line to that of the KDM6A knockout lines. We found that cells engineered to be KDM6A deficient grew faster than the KDM6A wild-type parental cells (Figure 12A).

We additionally assayed anchorage-independent growth in the isogenic cell lines. Anchorage-independent growth is a hallmark of tumorigenicity in cell lines that assesses the ability of the cells to form colonies in three-dimensional culture. Cells were grown in media with agar, and colonies were stained and counted after a specified number of days. Consistent with its derivation from a non-invasive bladder cancer, RT4 cells were unable to form colonies in soft agar. However, both the RT4 K2 and K316 cell lines demonstrated a significant increase in the number of colonies greater than 50um present after four weeks as compared to the parental line (Figure 12B,C).

After demonstrating that the KDM6A knockout cells had a growth and colony formation advantage, we wanted to determine if these cell lines were able to grow *in vivo* as another measure of tumorigenicity. We first examined tumor formation by subcutaneous injection of RT4 parental and RT4 K2 cell lines in the flank of athymic nude mice performed by the MSKCC Antitumor core facility. After 27 days, no statistical difference in tumor size was observed between the parental RT4 and K2 KDM6A

knockout cells, although the K2 cells did trend toward smaller tumor volume (Figure 13A).

Because truncating mutations in KDM6A are less commonly found in non-urothelial human tumors, we hypothesized that the specific tumor microenvironment found in the bladder may be important for the phenotype observed with KDM6A loss *in vitro*. The Antitumor core therefore performed orthotopic injections under direct surgical visualization of the bladder of the RT4 isogenic cells directly into the bladder wall of athymic nude mice. Prior to injection, the cell lines were infected with Luciferase to facilitate assessments of tumor growth. Following injection of the tumor cells, mice were imaged weekly, and tumor volume was calculated by luminescence levels. While the parental RT4 cell line again showed little growth over the observation period, in contrast to the results observed subcutaneously, mice injected with the RT4 K2 cell line developed large tumors that required the mice to be sacrificed after 45 days (Figure 13B,C). Hematoxylin and eosin (H&E) staining of the bladders showed that the parental RT4 cells were contained within the bladder wall, leaving the lumen visible and bladder structure relatively unaltered. In contrast, RT4 K2 cells were better at forming tumors than wild-type cells, and the resulting tumors were much more aggressive with the tumors growing into the lumen of the bladder, and completely taking over the bladder structure (Figure 13D).

KDM6A loss was also characterized in the VMCUB2 cell lines. KDM6A knockout was confirmed by Western blot (Figure 14A). To assess the effect of KDM6A loss on wound healing, VMCUB2 cells were plated in a well with a silicon insert and allowed to become confluent. The insert was removed, leaving empty space on the plate

representative of an artificial wound. Plates were imaged after 24 hours to determine the extent of cell migration to fill the wound. We observed increased migration in the K77 KDM6A knockout line compared to parental VMCUB2 cells. In addition, a Boyden chamber assay was also used to assess migration. Cells were plated in an upper well free of serum or growth factors, while lower well contained FBS and EGF. Cells were stained and counted after 24 hours to determine the number of cells able to migrate through the upper well. We observed increase migration again in the K77 KDM6A knockout line (Figure 14B).

RNA-sequencing of KDM6A knockout lines

As we found that KDM6A loss-of-function in RT4 cells resulted in increased cell proliferation, tumorigenicity, migration and invasion, we sought to explore the mechanistic basis of these phenotypes by examining differences in transcriptional activity among the isogenic cell lines. We thus performed RNA sequencing (RNA-seq) on the RT4 parental, RT4 K2 and RT4 K3 cell lines. Cells were collected 24 hours after plating, followed by RNA extraction. RNA sequencing was then performed by the Integrated Genomics core, with analysis performed by Drs. Wenhuo Hu and Byron Lee. The KDM6A knockout lines demonstrated a transcriptional program distinct from the parental RT4 cell line (Figure 15A). The two KDM6A knockout sub-lines also grouped separately from parental RT4 by principal component analysis (PCA) (Figure 15B).

Upon gene set enrichment analysis (GSEA), a number of pathways were identified that were differentially upregulated or downregulated in parental versus KDM6A knockout cells. Of particular interest, several negative regulators of the

mitogen-activated protein kinases (MAPK) pathway were found to be downregulated in the KDM6A knockout cells, including NF1, DUSP2, DUSP4, DUSP6, DUSP7, SPRY2, and SPRY4 (Figure 15C,D).

Because DUSPs and SPRYs are phosphatases responsible for downreglating Ras/MAPK signaling, we hypothesized that loss of expression of these feedback regulators may be responsible for the increased growth observed following KDM6A knockout. However, when the expression levels of these proteins were examined by Western blot, no consistent and reproducible difference was observed between RT4 parental and KDM6A knockout cells (Figure 15E). In addition, no difference was seen in the activation of several effectors of Ras/MAPK signaling. More specifically, levels of phospho-MEK and phospho-ERK expression were similar in the RT4 parental and KDM6A knockout cells (Figure 16). Other signaling pathways that have been implicated in growth and tumorigenicity of cancer cells were also investigated by Western blot, including the PI3K and JAK/STAT pathways. However, no differences in the activation of these pathways were observed in the KDM6A knockout cells as compared to parental RT4 cells (Figure 16).

ChIP-sequencing of KDM6A knockout lines

In an effort to further elucidate the mechanism of the phenotypic changes observed in KDM6A knockout cells, we performed chromatin-immunoprecipitation (ChIP) sequencing (ChIP-seq) on our isogenic cell lines. Cells were plated at 5 million cells per 10cm plate, collected after 24 hours and prepared as described in the materials section. Chromatin was probed with antibodies against trimethyl H3K27 (H3K27me3),

and IgG as a control. Sequencing was performed by the MSKCC Integrated Genomics Operation, and analysis was performed with the assistance of Dr. Wenhuo Hu.

In the RT4 parental cell line, we observed high H3K27me3 levels within 1000 base pairs of the transcriptional start site (TSS) across the genome. Approximately 25% of all H3K27me3 marks were found in a promoter region. In both KDM6A knockout cell lines, H3K27me3 marks were spread further from the TSS, with a large proportion of the marks located up to 3000 base pairs from the TSS (Figure 17A). In the KDM6A knockout cells, only approximately 10% of H3K27me3 marks were found in a promoter region. In contrast, more H3K27me3 marks were found in exons beyond the first exon and distal intergenic regions.

Previously, we had examined H3K27me3 global levels in the KDM6A knockout lines compared to wild type. By Western blot, we did not observe significant changes in global H3K27me3 levels. This was confirmed by the ChIP-seq experiments, which showed global levels of H3K27me3 to be relatively unchanged in the KDM6A knockout cell lines. However, significant differences in H3K27me3 levels were observed in individual genes. More specifically, we identified a set of 1517 genes that showed differential H3K27me3 levels in both KDM6A knockout lines as compared to the parental KDM6A wild-type RT4 cells. This suggested that KDM6A may play a role in regulating H3K27me3 of these genes and may therefore impact transcriptional regulation.

We further identified a subset of genes among these KDM6A target genes that were also differentially expressed in our RNA-seq data. For this analysis, we focused on genes that had a fold change in expression greater than 1.5 and an adjusted p value of less than 0.05. Additionally, because we wanted to identify direct targets of KDM6A activity,

we chose to include only genes that were downregulated compared to wild-type KDM6A expression. In this case, we expected KDM6A loss to lead to increased methylation at target genes, and therefore decreased expression. By focusing on genes that showed decreased expression rather than increased expression in the KDM6A knockout lines, we hoped to be able exclude genes whose expression may be impacted by upstream genes regulated by KDM6A activity, but are not directly affected by KDM6A themselves. While we have identified several candidate genes (Figure 17B) we believe that additional studies are need before any conclusions should be made.

EZH2 inhibition in KDM6A knockout cell lines

KDM6A is responsible for removing the inactivating trimethyl mark on H3K27. This mark has been shown in prior studies to be placed by the methyltransferase EZH2. The expression level of genes regulated by the Trithorax and PRC2 complex depend on the balance between the two complexes. Because loss of KDM6A function is hypothesized to result in unopposed EZH2 activity, we tested whether KDM6A knockout cell lines were more sensitive to EZH2 inhibition.

For these studies, we used several EZH2 inhibitors that had been shown in pre-clinical models of other cancer types to have efficacy in EZH2 mutant cell lines, including GSK126, GSK343, and GSK504. Because these drugs are predicted to alter histone placement, which occurs over several replication cycles, cell lines were treated with drug at varying concentrations ranging from 156nM to 20μM for at least one week with drug replenished every 3-4 days. Surprisingly, in 2D growth conditions, none of

these drugs showed greater efficacy in RT4 K2 cell line as compared to the parental RT4 cells, at concentrations up to 20μM (Figure 18A, B, C).

Two additional EZH2 inhibitors were subsequently tested in soft agar assay. For these studies, JQEZ5 (JQE) and EPZ011989 (EPZ) were plated with RT4 parental and K2 cells in soft agar. As with the 2D growth assays, co-culture with JQE and EPZ had not effect on the number of colonies formed by K2 as compared to DMSO control (Figure 18D, E). Notably, this lack of selective sensitivity in KDM6A null cells with EZH2 inhibitors was similar to the lack of correlation between EZH2 sensitivity and KDM6A mutational status in organoid models reported by our collaborator Dr. Michael Shen (Columbia University)[139].

As a prelude to testing possible combination strategies, we next examined whether EZH2 inhibition had an effect on signaling pathways predicted to drive bladder cancer growth. We thus treated the RT4 parental, K2, and K3 cell lines with 1μM of GSK126 for one week with drug replenished every 3-4 days. No changes were observed in the expression of phospho-CRAF, phospho-ERK, phospho-ERBB2, phospho-S6, and phospho-AKT (Figure 19). In KDM6A knockout GSK126 treated cells, there was an increase in phospho-STAT3. Based upon this result, we hypothesized that activation of JAK/STAT signaling by GSK126 could sensitize these cells to JAK inhibition. However, after treating cells with JAK inhibitor AZD1480 alone or in combination with GSK126 for one week, we observed no difference in the sensitivity in RT4 parental cells compared to the KDM6A knockout cells to the JAK inhibitor (Figure 20).

In the GSK126 experiment, we also observed there was no change in H3K27 trimethyl levels in GSK126 treated cells. Because of a concern that the drug had lost

efficacy, thus leading to the lack of EZH2 sensitivity observed in the KDM6A knockout cells, we tested EPZ011989, as well as an EED inhibitor, EED-226, also shown to effectively inhibit PRC2 activity, in a BAP1 mutant cell line that has been shown to be sensitive to EZH2 inhibition[140]. Cells were split every 3-4 days to allow for complete reprogramming of the epigenetic structure. However, no difference in growth was observed between DMSO and inhibitors (Figure 21A). To confirm that the inhibitors were effectively targeting PRC2 activity, we performed histone extraction on cells after treatment with drug for 18 days. We indeed observed a reduction in H3K27 trimethyl levels in the EZH2 and EED inhibitors, demonstrating that while these drugs are actively targeting PRC2 activity, growth in 2D culture was not affected (Figure 21B).

Discussion

While the critical role played by epigenetic regulators in embryonic development, tissue maturation and human disease has become increasingly clear, the accumulating literature strongly indicate that cellular context, both tissue cell lineage and the complement of co-altered genes, greatly affect how these regulators function. As chromatin modifying gene mutations are present in the majority of bladder cancer, we sought to explore the mechanisms whereby alterations in these genes promote tumor development and progression. To this end, we developed a bladder specific model to study KDM6A loss-of-function. We observed increased proliferation, migration and invasion in KDM6A null cells. Loss of KDM6A led to global changes in transcriptional activity and H3K27me3 markers.

Studying KDM6A loss *in vitro* in bladder cell lines posed several technical challenges. First, consistent with large-scale genetic studies in bladder cancers including the TCGA and MSK-IMPACT cohorts, most bladder cell lines have a complex mutational profile with multiple known and likely pathogenic mutations present in each. Therefore, choosing appropriate cell lines with an applicable genetic background to study the biologic consequences of KDM6A was crucial. KDM6A is frequently co-mutated with FGFR3, so the RT4 FGFR3-TACC3 fusion cell line was deemed an ideal candidate. However, we also wanted to be able to validate key biologic insights in additional cell lines to ensure that the phenotypes observed in the RT4 knockouts were of broad applicability and not cell line specific.

Finding additional appropriate cell lines for studying KDM6A knockout proved to be a greater hurdle than initially predicted. While we were able to collect a large panel of over 30 bladder cancer cells lines, many cell lines had likely oncogenic alterations in other epigenetic regulators that could potentially confounding the phenotype of KDM6A knockout. Furthermore, the vast majority of cell lines were derived from high grade aggressive tumors, a phenotype in which KDM6A alterations are underrepresented. In such backgrounds the nuances of KDM6A loss in the setting of a very strong oncogenic driver may have been lost. As mechanisms of epigenetic regulators continue to be investigated, consideration of the background in which to investigate these alterations will be critical. Discoveries in cell lines that are not representative of the human disease may not prove to be applicable to patients. This will be a major issue as epigenetic targeted therapies continue to be a focus of drug development in bladder and other cancer types.

In addition to genetic considerations, we also faced challenges studying the phenotypic consequences of KDM6A loss. While we identified a global change in transcriptional activity in KDM6A knockout cells compared to wild type, a large number of genes were altered and most of these did not replicate in subsequent experiments. For example, our RNA sequencing initial studies identified regulators of the Ras/MAPK signaling pathway as altered in both KDM6A knockout sub-lines of RT4. Subsequent studies noted that changes in ERK pathway output in RT4 cells were highly dependent on culture conditions (cell passage number, time since addition of new media, confluence) and thus we were unable to confirm the signaling changes predicted by the RNA sequencing analysis at the protein level. Although each of these variables could potentially be controlled for in technical replicates, the effects of KDM6A loss on signaling pathway may be too subtle to detect in vitro.

Surprisingly, we observed that KDM6A loss did not sensitize the RT4 cells to EZH2 inhibition despite the fact that knockout of *KDM6A* was associated with clear oncogenic gain-of-function. Although other investigators have suggested KDM6A null cells are more sensitive to EZH2 inhibition, we were unable to reproduce these findings. This was despite treatment of cells over multiple doubling times to allow for complete histone reprogramming. While it is possible the discordance between our results and those of others are due to differences in the models employed, a separate concurrent collaboration between the Solit laboratory and that of Dr. Michael Shen (Columbia) also did not observed greater sensitivity for EZH2 inhibitors in *KDM6A* mutant versus wildtype organoid models[139].

These latter results suggest that the oncogenic effects of KDM6A loss observed in our hands may have been due to KDM6A targets that do not overlap with PRC2 activity. If so, EZH2 inhibition would not be predicted to have a major effect on KDM6A loss. Another possibility is that the EZH2 inhibitors that we have tested to date were not sufficiently potent to inhibit bladder cancer cell growth. The Solit laboratory is thus seeking to obtain several more recently developed selective inhibitors of EZH2 to test in our isogenic model. In sum, while we were able to establish that KDM6A loss was sufficient to induce cell proliferation, colony formation in soft agar and tumorigenicity in an orthotopic mouse model, we did not find that current EZH2 inhibitors are likely to have meaningful anti-tumor effects in bladder cancer patients, at least as monotherapy. Further studies should thus seek to explore whether EZH2 inhibitors can enhance that activity of other potential therapeutic options.

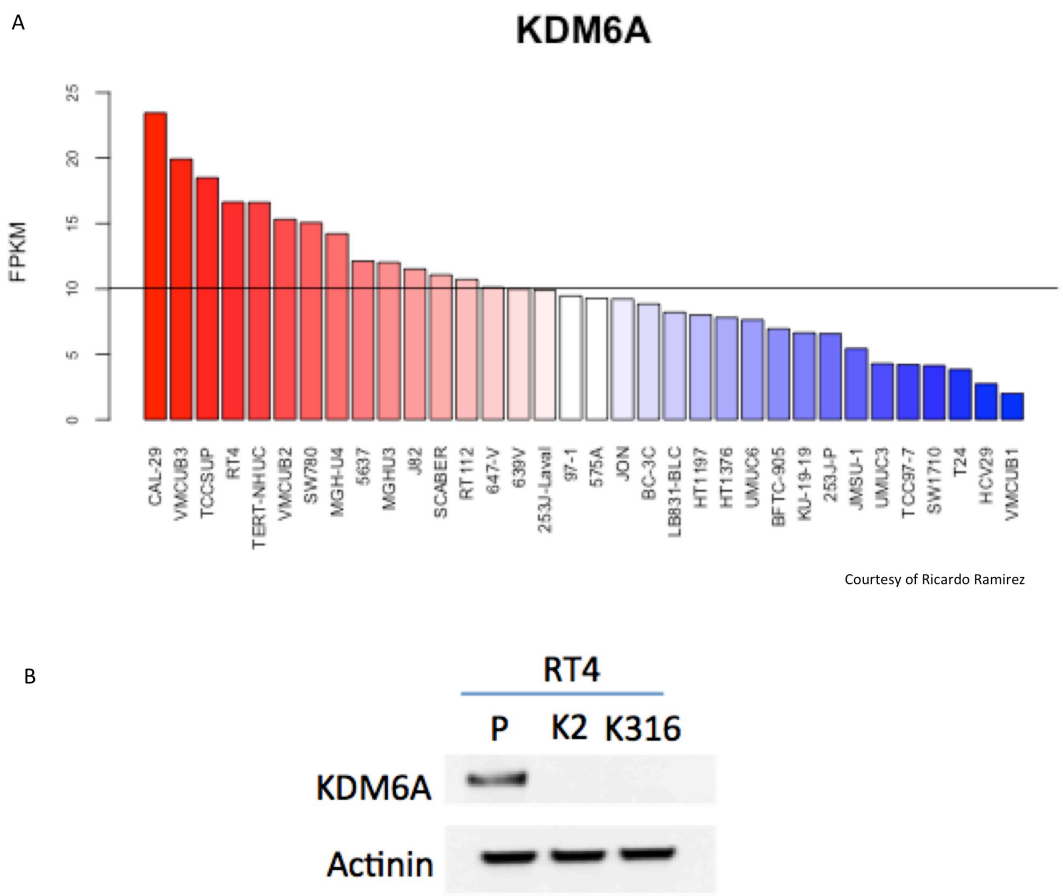

Figure 9: Cell line selection for KDM6A knockout.

A: RNA-seq was performed on a panel of urothelial cell lines. KDM6A levels were graphed across all cell lines. Cell lines with KDM6A expression above 10FPKM were considered ideal candidates for KDM6A knockout. Figure generated by Ricardo Ramirez. B: Western blot confirming KDM6A knockout. RT4 cells were infected with viral CRISPR/Cas9 particles targeting exon 2 of KDM6A. Cells were single-cell sorted and allowed to grow up to form isogenic clones. KDM6A knockout was confirmed by Western blot.

Tumors	Gene	Protein Change	Annotation ▼	Mutation Type	Allele Freq
❶ ❷ ❸	FGFR3	*FGFR3-TACC3 fusion*		Fusion	
❹	FGFR3	*FGFR3-TACC3*		Fusion	
❶ ❷ ❸ ❹	TSC1	*L557Cfs*72*		FS del	▮▮▮▮
❷ ❸	KDM6A	*Y116Tfs*64*		FS del	▮
❷ ❸	KDM6A	*Q117Sfs*64*		FS ins	▪
❸ ❹	KDM6A	*Y116Lfs*6*		FS del	▪▪
❶ ❷ ❸ ❹	RHOA	*A161V*		Missense	▪▪▪▪
❹	ELF3	*V217Wfs*35*		FS del	▮
❶ ❷ ❸ ❹	TERT	*Promoter*		Other	▪▪▪▪
❶ ❷ ❸ ❹	TGFBR1	*X27_splice*		Splice	▪▪▪▪
❶ ❷ ❸ ❹	DNMT3A	*S129L*		Missense	▪▪▪▪
❶ ❷ ❸ ❹	EPHB1	*C284R*		Missense	▪▪▪▪
❶ ❷ ❸ ❹	EPHB1	*C284F*		Missense	▪▪▪▪
❶ ❷ ❸ ❹	INPP4A	*G227S*		Missense	▪▪▪▪
❶ ❷ ❸ ❹	NOTCH4	*C733S*		Missense	▪▪▪▪
❹	PPARG	*T475M*		Missense	▮
❶ ❷	PTPRS	*T966M*		Missense	▪
❷ ❸	KDM6A	*S114C*		Missense	▮
❷ ❸	KDM6A	*S114A*		Missense	▮
❷ ❸	KDM6A	*A115T*		Missense	▮
❸ ❹	KDM6A	*Y119_Q123del*		IF del	▮▮
❶ ❷ ❸ ❹	KMT2D	*S5385L*		Missense	▪▪▪▪
❶ ❷ ❸ ❹	SPEN	*D1419G*		Missense	▪▪▪▪
❶	BRD4	*P956Tfs*137*		FS ins	▪
❶ ❷ ❸ ❹	ARID1B	*P450dup*		IF ins	▪▪▪▪
❶ ❷ ❸	TACC3	*TACC3-FGFR3 fusion*		Fusion	
❹	TACC3	*TACC3-FGFR3*		Fusion	

Figure 10: Mutational background of RT4 cell line by MSK-IMPACT.

RT4 parental and KDM6A knockout lines K2, K3 and K316, a subclone of K3, were run on MSK-IMPACT to determine genetic background. Black circles under "Tumors" with corresponding number denote the cell line that contains a certain mutation. RT4 parental: 1, K2: 2, K3: 3, K316: 4. All gene and protein changes called by MSK-IMPACT are listed. "Annotation" denotes level of evidence for a particular mutation that has been curated by precision oncology knowledge base OncoKB. Blue circles indicate alterations that have evidence for oncogenicity. A number of associated with a blue circle indicates an alteration has therapeutic indications at varying levels. Level 1: FDA-approved biomarker predictive of response. Level 2: standard care biomarker predictive of response. Level 3: Compelling clinical evidence supports biomarker as predictive of response. Level 4: Compelling biological evidence supports biomarker as predictive of response. Grey circles indicate variants of unknown significance that have not been reviewed by OncoKB. Mutation type indicates the mutation type observed for a particular variant. Allele frequency shows the frequency of a particular alteration in each sample with 1 at the left and 4 at the right.

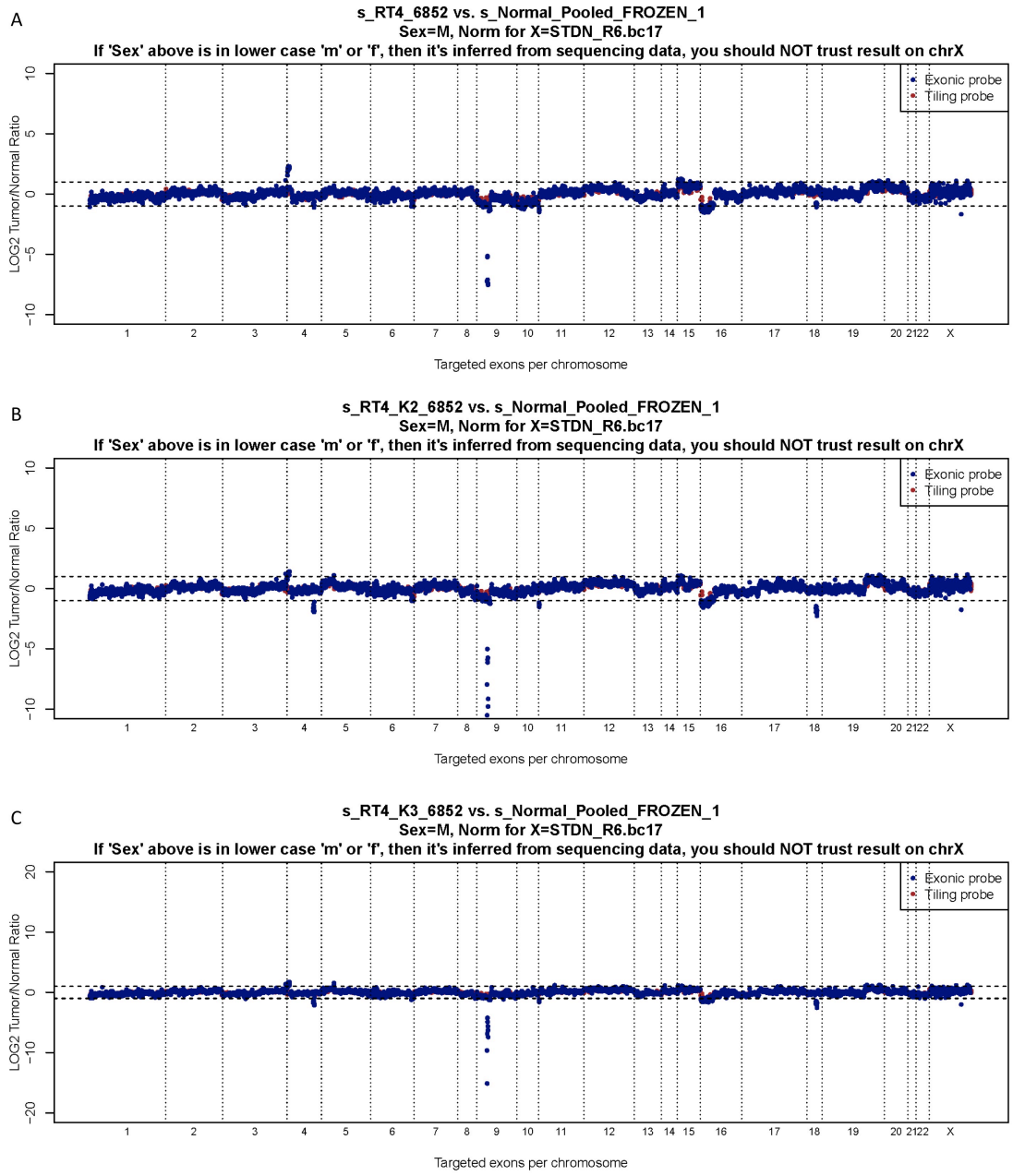

Figure 11: Copy number alterations in KDM6A knockout cell lines.

FACETS analysis was run using MSK-IMPACT data to identify copy number alterations in the RT4 parental and KDM6A knockout cell lines. FACETS pipeline includes sequencing BAM file post-processing, joint segmentation of total- and allele-specific read counts, and integer copy number calls corrected for tumor purity, ploidy and clonal heterogeneity, with comprehensive output and integrated visualization. Y-axis shows copy number log-ratio of total sequence read count in the cell line compared to a pooled "normal," as cell lines do not have a normal tissue control, across chromosomes on the X-axis. Figures generated by the MSKCC Integrated Genomics Operation core. A: RT4 parental, B: K2, C: K3.

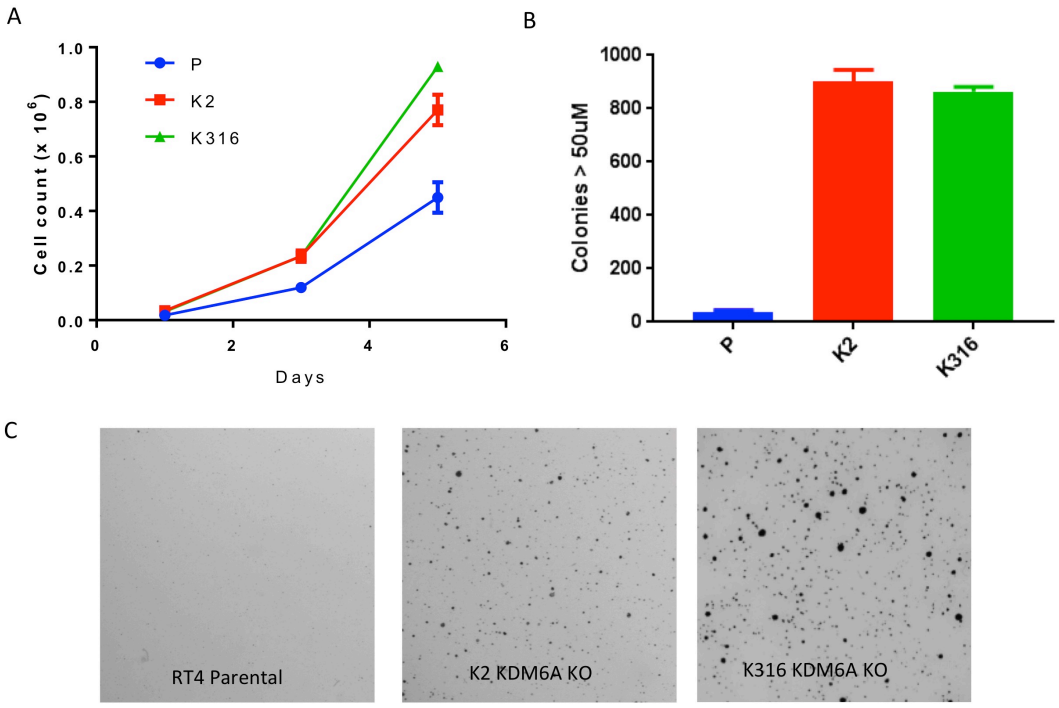

Figure 12: Characterization of KDM6A loss in RT4 cells.

A: Growth curves comparing RT4 parental and KDM6A knockout lines, K2 and K316. Cells were plated in a 6-well plate at 25,000 cells per well and counted at day 1, 3, and 5. B: Soft agar assay comparing colony formation potential of RT4 parental, K2, and K316. Cells were plated in 6-well plates in 0.33% agar at 10,000 cells per well. After 4 weeks, colonies were visualized by MTT reagent and counted. C: Representative images of soft agar assay after 4 weeks as quantified in B.

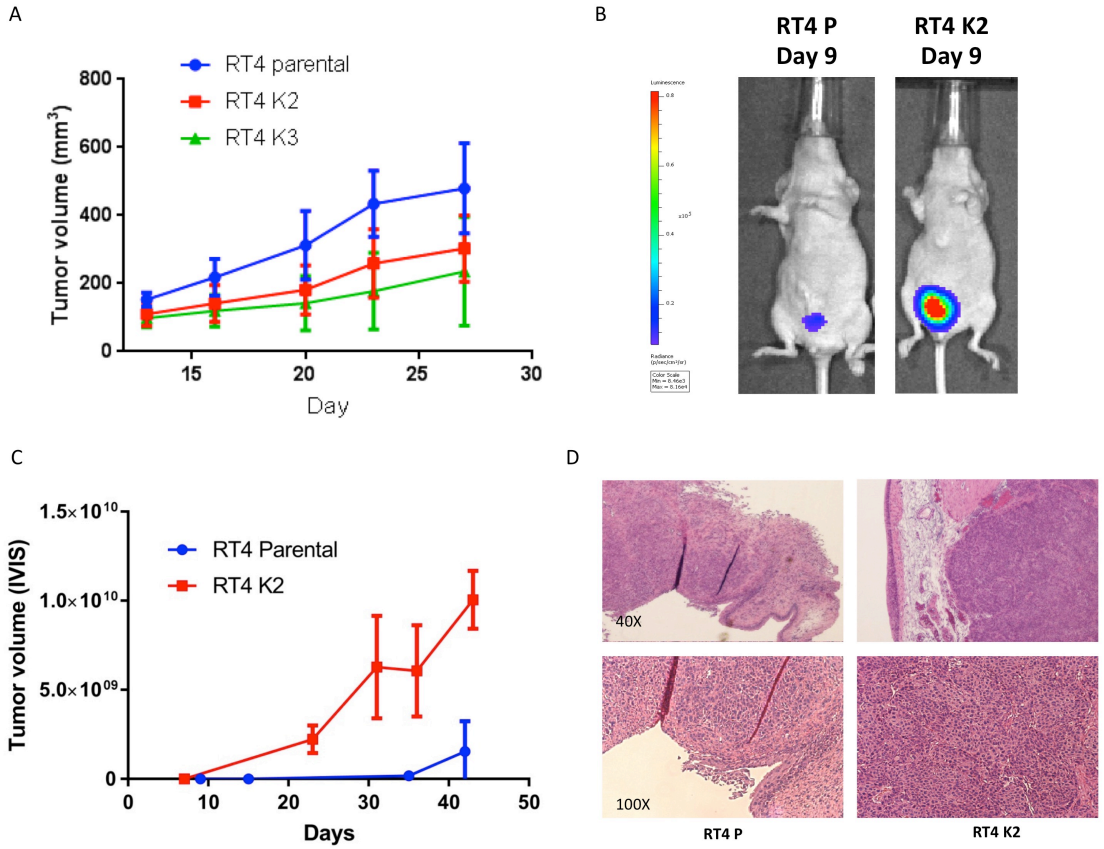

Figure 13: KDM6A loss promotes growth in orthotopic bladder models

In vivo growth potential of RT4 parental and KDM6A knockout cells was assessed by subcutaneous (A) and orthotopic (B-D) xenografts. A: Cells were injected with Matrigel subcutaneously on the flank in 7 mice. Tumor measurements (mm^3) are plotted over 27 days. B-D: Cells were infected with luciferase to allow quantification by IVIS, and orthotopically injected into bladders of athymic nude mice. B shows a representative image of IVIS monitoring at day 9, quantified weekly over 45 days in C. After 45 days, mice were euthanized and bladders were fixed, with representative H&E staining shown in D. Images courtesy of the MSKCC Antitumor core.

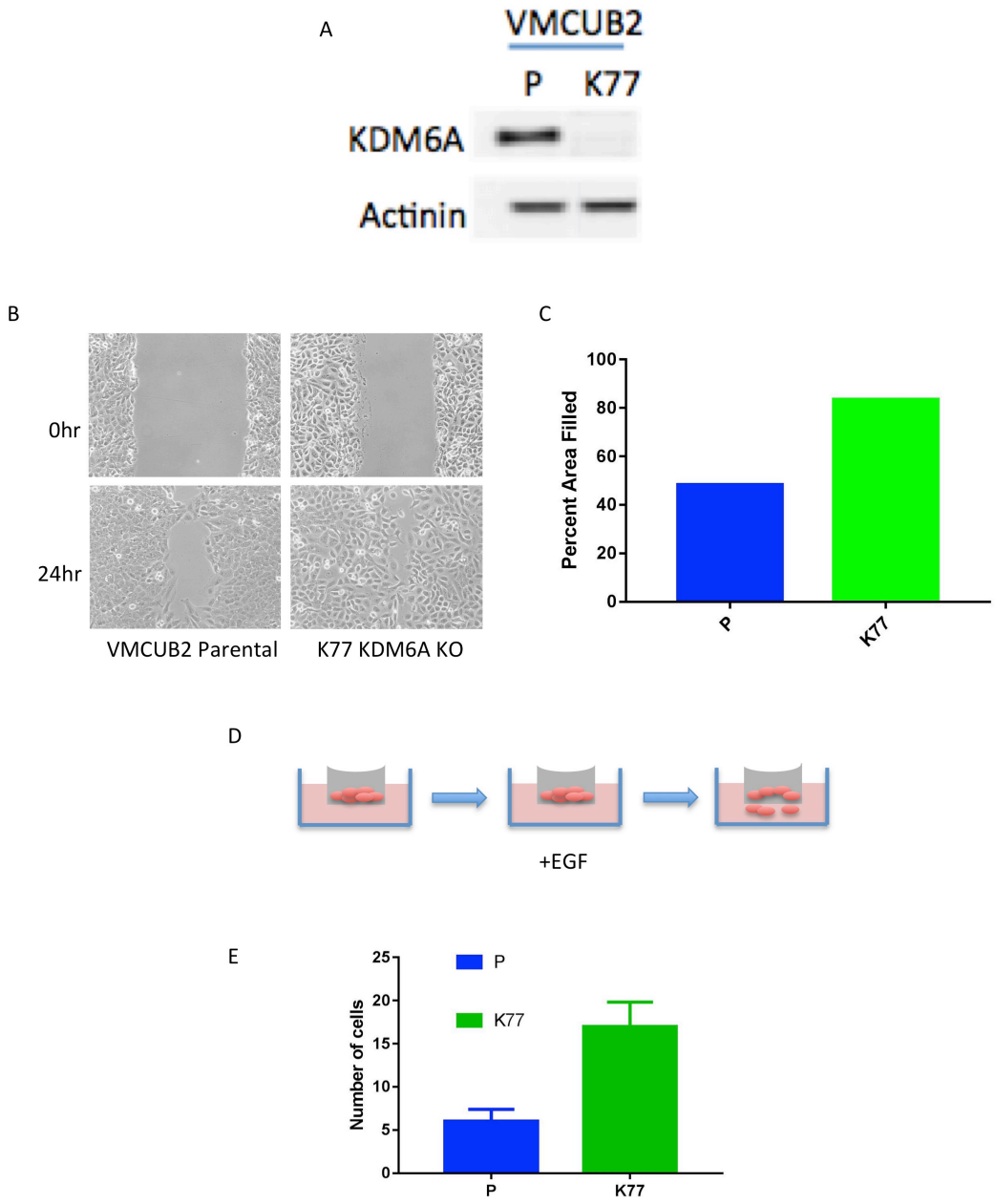

Figure 14: Characterization of KDM6A loss in VMCUB2 cells.

A: Western blot demonstrating KDM6A knockout in the K77 subclone compared to parental VMCUB2. B: Representative images of wound healing assay. Cells were imaged at 0 hrs and 24 hrs, and the percent of area filled by cells was calculated, quantified in C. D: Schematic of Boyden chamber assay. Cells were plated in a transwell in serum-free media, then placed in serum-full media + EGF. Cells that migrated through the transwell were stained and counted by microscope, quantified in E.

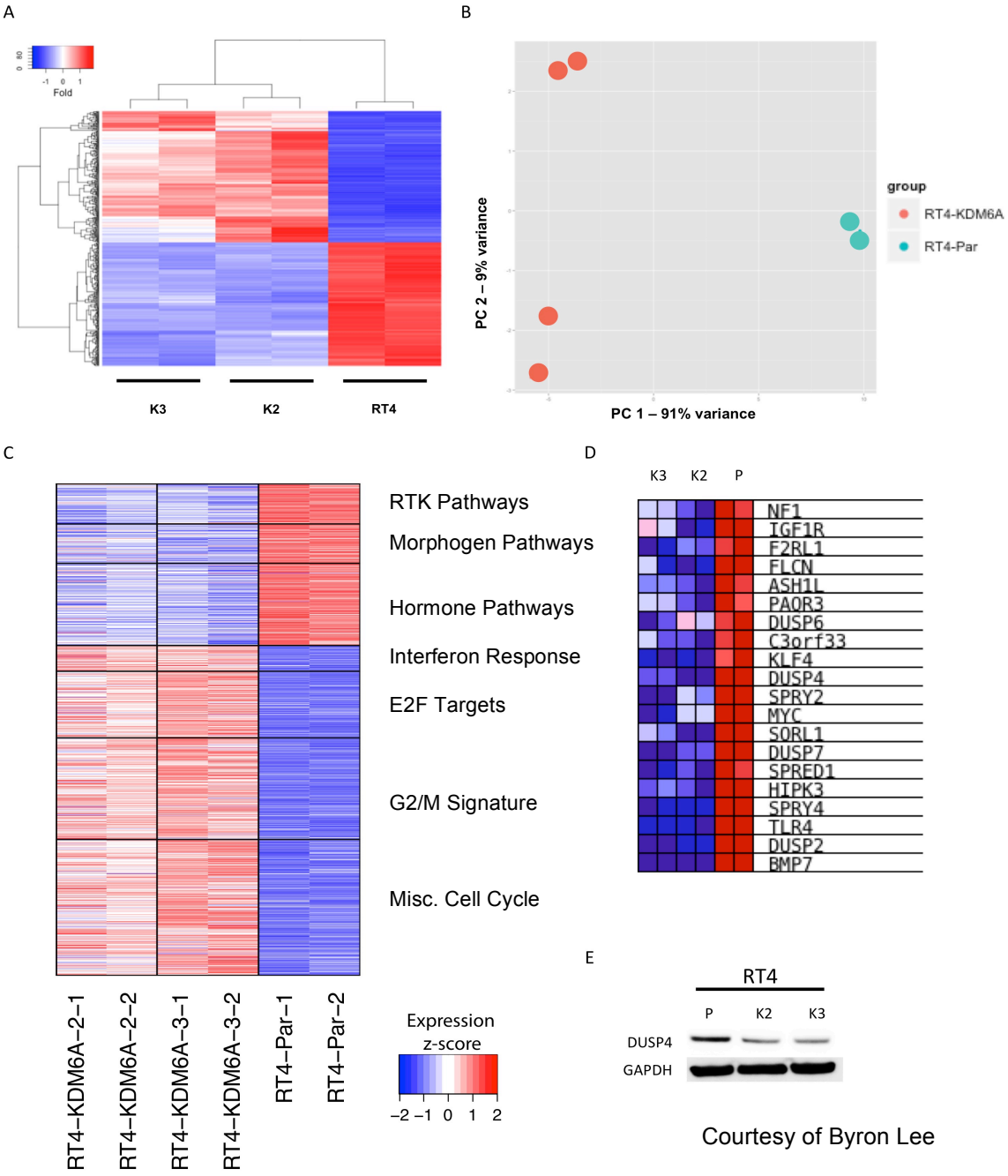

Figure 15: RNA-sequencing analysis of KDM6A knockout cells.

A: Unsupervised hierarchical clustering of significantly differentially expressed genes in RT4 and KDM6A knockouts. Each row represents an individual gene with a p-value <0.05. Columns represent individual samples. Figure courtesy of Byron Lee. B: Principle component analysis of RT4 parental and KDM6A knockout lines. Figure courtesy of Byron Lee. C: RNA expression data clustered by gene sets, with representative genes listed from the RTK pathway set in D. Figures courtesy of Byron Lee. E: Western blot showing DUSP4 protein levels in RT4 parental, K2 and K3 cells.

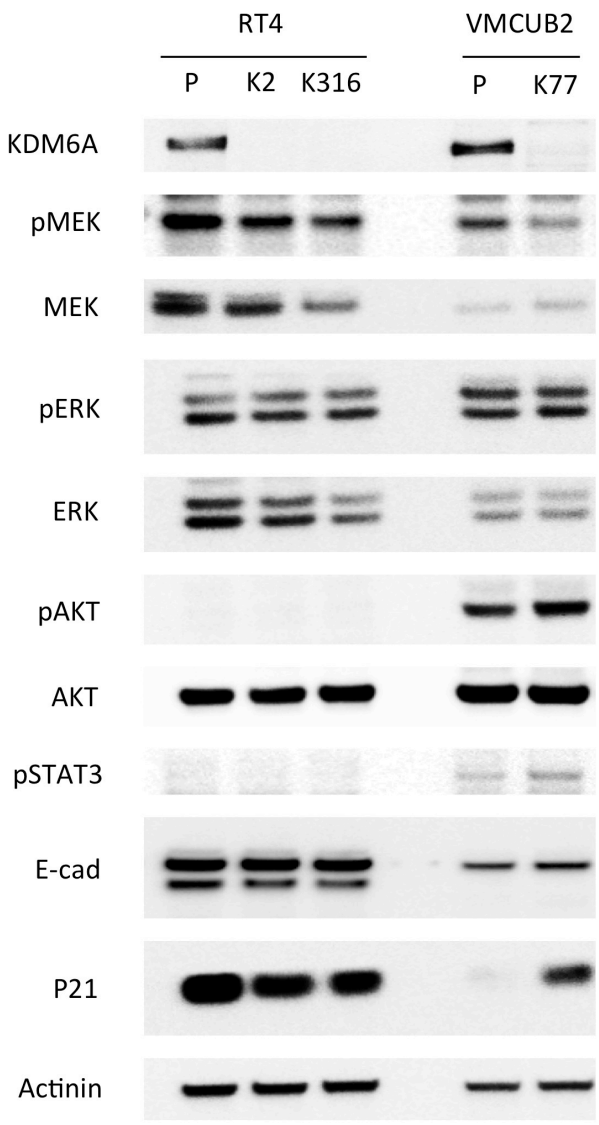

Figure 16: Western blot analysis of signaling pathways in KDM6A knockout lines.

All cell lines were collected after 48 hours at approximately 80% confluency. Signaling activity of Ras/MAPK pathway were assessed by phospho-MEK and phospho-ERK levels. Signaling activity of PI3K pathway was assessed by phospho-AKT levels. Signaling activity of JAK/STAT pathway was assessed by phospho-STAT3 levels.

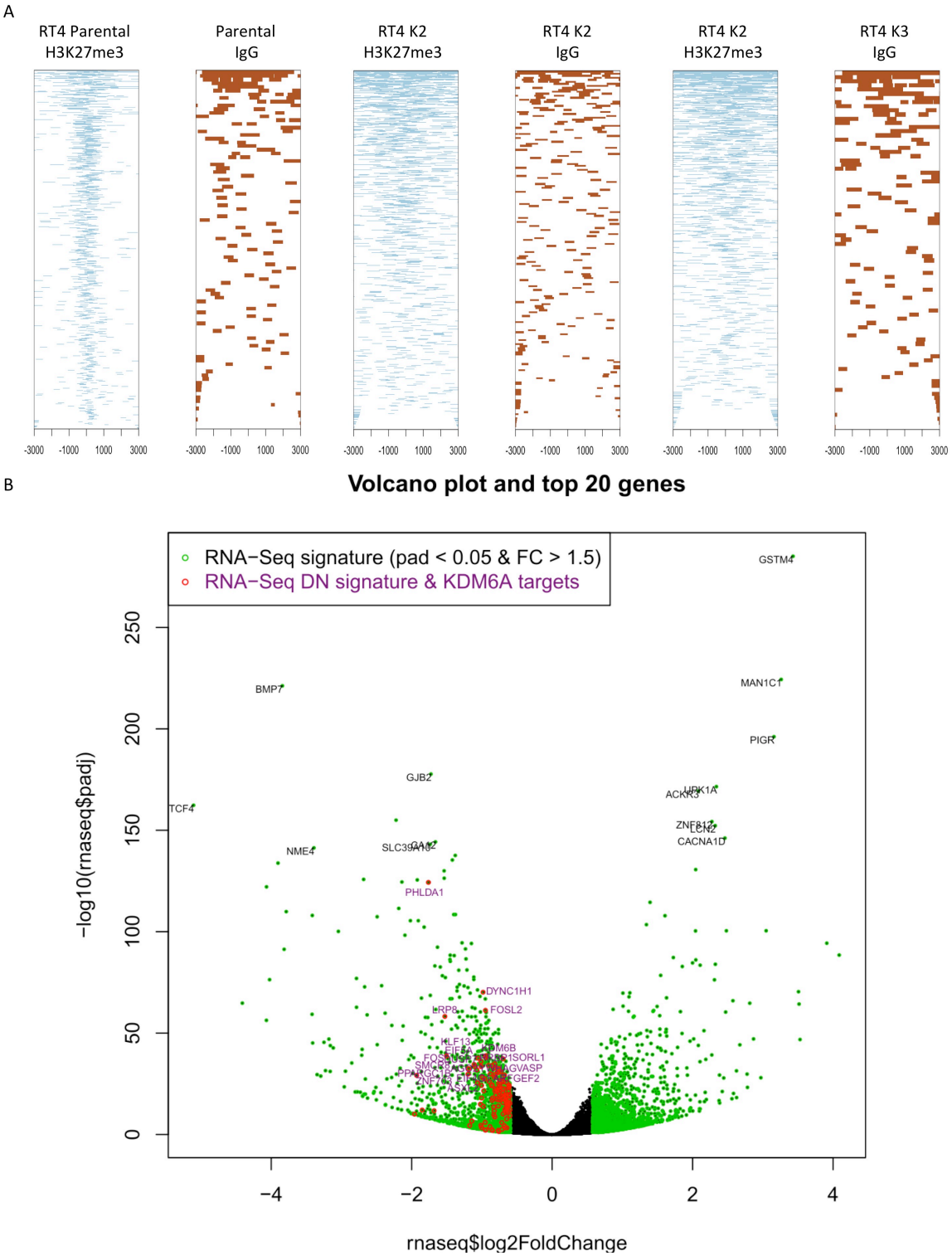

Figure 17: ChIP-sequencing analysis of KDM6A knockout lines.

Cells were plated at 1 million cells per well in a 10cm plate and collected after 48 hours, with cells at approximately 80% confluency. ChIP was performed with antibodies against H3K27me3 and IgG as a control, and reads were aligned to UCSC genome assembly hg19. A: Individual reads were oriented around the transcriptional start site (TSS) across

the genome, and plotted as distance in base pairs from the TSS. Reads were plotted for H3K27me3 and control IgG in the RT4 parental line and K2 KDM6A knockout line. Figure generated by Wenhuo Hu. B: Genes with variable H3K27me3 levels between parental and KDM6A knockout line were identified as KDM6A targets. Genes from the RNA-seq data showing a fold change greater than 1.5 and P value greater than 0.05 were graphed as a volcano plot, showing fold change as a function of P value. KDM6A targets are highlighted in purple. Figure generated by Wenhuo Hu.

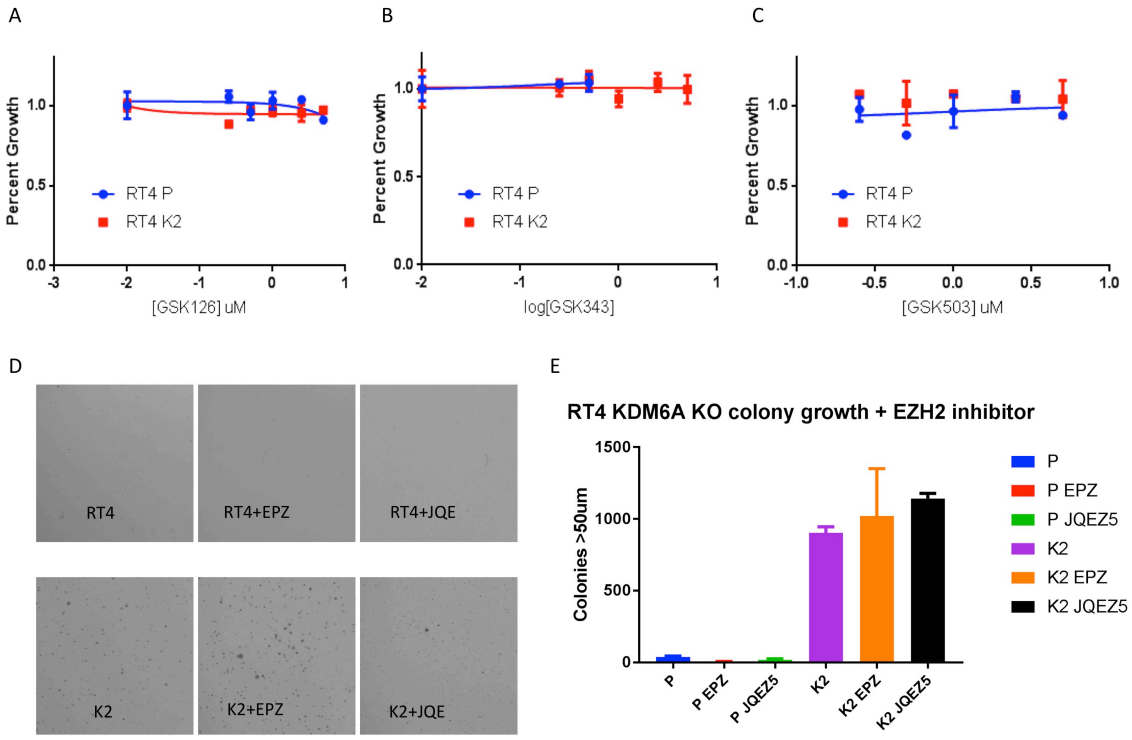

Figure 18: EZH2 inhibition in KDM6A knockout cell lines.

A-C: Dose response curves for EZH2 inhibitors in RT4 parental and K2 cell lines. Cells were plated in triplicate in varying concentrations of GSK126 (A), GSK343 (B), or GSK503 (C) starting at a concentration of 10μM. Growth was measured by MTT signal on Day 7 relative to a DMSO control. D: Soft agar assay with EZH2 inhibitors. Cells were plated for soft agar in the presence of 5μM DMSO, EPZ011989, or JQEZ5. After 4 weeks, colonies were stained with MTT reagent and counted, quantified in E.

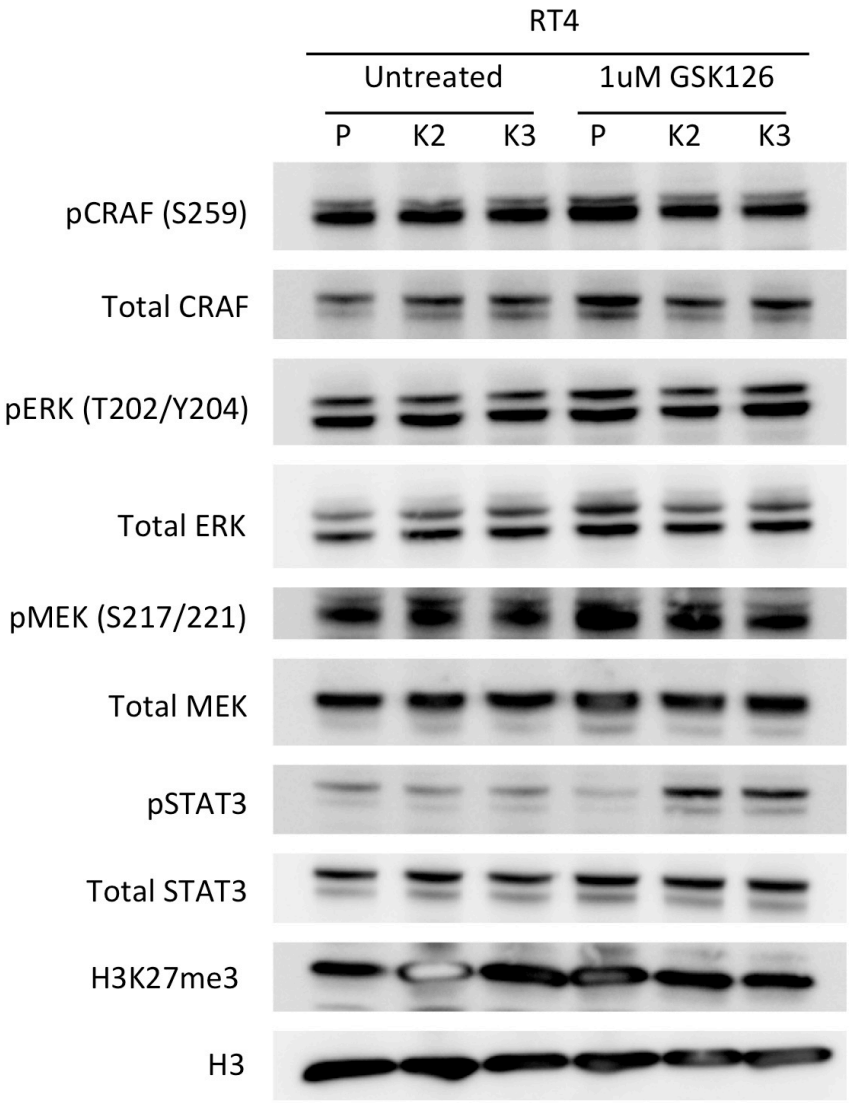

Figure 19: Effect of EZH2 inhibition on signaling pathways.

Activity of the Ras/MAPK and JAK/STAT signaling pathways in response to EZH2 inhibition were assessed by Western blot. Cells were pre-treated with 1μM GSK126 for one week, then replated again with drug and collected after 24 hours. Ras/MAPK pathway activation was examined by phospho-CRAF, phospho-ERK and phospho-MEK. JAK/STAT pathway activation was examined by phospho-STAT3.

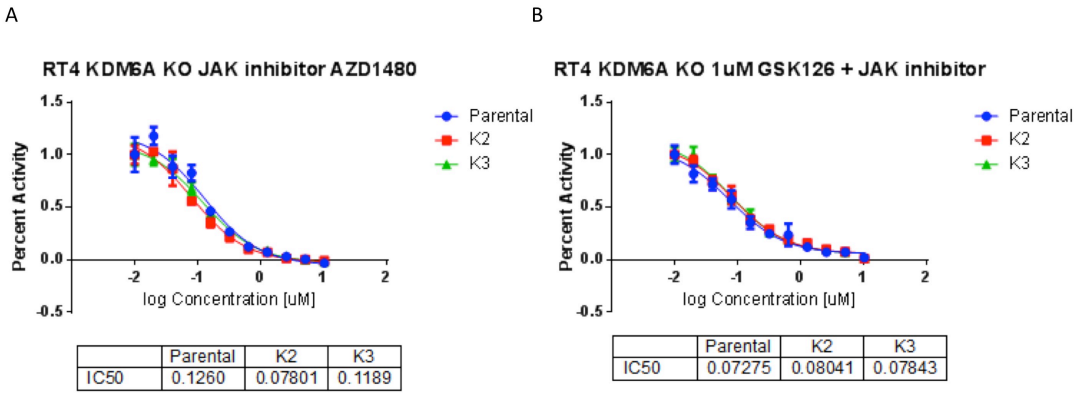

	Parental	K2	K3
IC50	0.1260	0.07801	0.1189

	Parental	K2	K3
IC50	0.07275	0.08041	0.07843

Figure 20: EZH2 inhibition in combination with FGFR3-targeted therapy.

A: Dose response curve to JAK inhibitor AZD1480. Cells were plated in triplicate in varying concentrations of AZD1480, starting at a concentration of 5μM. Cell growth was measured by MTT signal at day 7. B: Cells were grown in 1μM of GSK126 for one week before being plated for AZD1480 dose response as in A.

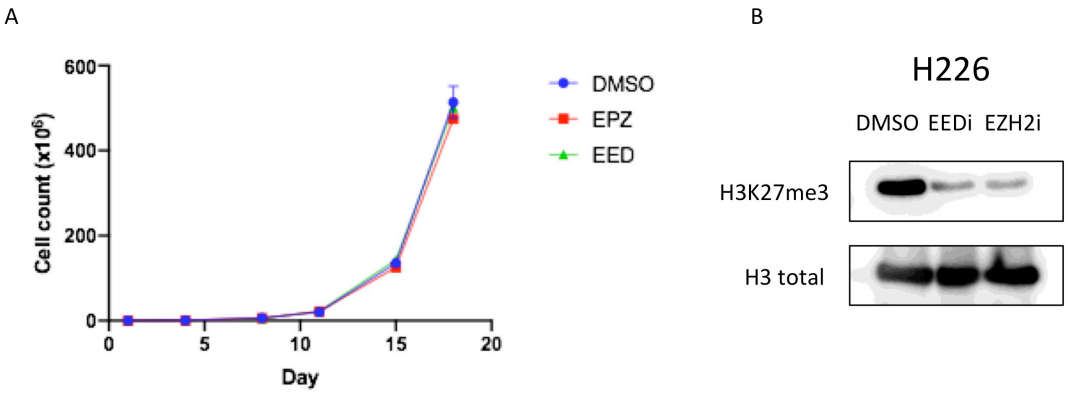

Figure 21: EZH2 and EED inhibition in BAP1 mutant cell line H226.

A: Proliferation of H226 cell line in the presence of 5μM DMSO, EPZ011989, or EED-226. Cells were replated every 3-4 days to allow for continual growth over 18 days and multiplied by the split factor to get total cell count. B: Western blot analysis of H226 histone extract in the presence of 5μM DMSO, EPZ011989, or EED-226 after 18 days.

Chapter 3: Modeling urothelial carcinoma *in vivo*

Our *in vitro* data suggest that KDM6A plays a tumor suppressor role in bladder cancer oncogenesis, and that loss of KDM6A results in a reprogramming of the epigenetic landscape, leading to over-activation of proliferative pathways, and accelerated tumor growth. However, our *in vitro* studies only allowed us to examine the effects of KDM6A loss in cell lines that were already transformed.

Because our human tumor studies suggest that KDM6A loss is an early alteration in bladder cancer pathogenesis (see **Chapter 4**), KDM6A may play an additional role in the process of tumor development beyond induction beyond acceleration of cell growth. Based upon our initial RNA sequencing analysis and the observation that TP53 mutations are underrepresented in *KDM6A* mutant tumors, we hypothesized that KDM6A loss may play a role in overcoming oncogene-induced senescence (OIS). Although this reprogramming manifests as increased mitogenic signaling and cellular proliferation in a transformed setting, a major function of KDM6A loss-of-functional alterations in bladder cancer tumorigenesis may be the abrogation of OIS induced by other oncogenic alterations, such as *FGFR3* and *ERBB2* mutations or PTEN inactivation.

To test this hypothesis, we utilized a $Pten^{flox/flox}p53^{flox/flox}$ mouse model of bladder cancer developed by the Abate-Shen laboratory[141]. When Adenovirus containing Cre recombinase is administered directly into the bladder through intravesical injection, these mice develop large invasive bladder tumors with 100% penetrance by six months. In this model, we hypothesize that PTEN loss promotes cell proliferation, whereas TP53 provides a permissive environment for such proliferation at least in part by preventing

OIS. In an analogous fashion, TP53 has also been shown to overcome growth arrest caused by acute PTEN inactivation in the PTEN/TP53 prostate cancer mouse model[142] We hypothesized that KDM6A may play a similar role in creating a permissive environment for aberrant cell proliferation through global changes in the epigenetic landscape.

In addition to testing the role of KDM6A in tumor initiation, we aimed to add to and improve on currently available mouse models of bladder cancer, which poorly reflect the genomic complexity of the human disease. As a consequence, while investigators interested in other cancer types have several well-characterized and readily available *in vivo* models, investigators interested in bladder cancer remain at a disadvantage given of the lack of biologically and genomically relevant models to study tumor initiation, progression and drug response *in vivo*.

Results

Genetically engineered mouse models in bladder cancer

Because of the lack of genetically engineered mouse models (GEMM) available in bladder cancer, we worked closely with collaborators in the Abate-Shen laboratory at Columbia University to utilize a GEMM model previously shown by their laboratory to develop invasive urothelial carcinomas. First, we aimed to confirm that their model was reproducible in our hands. We thus obtained $Pten^{flox/flox}$ knockout mice and $Trp53^{flox/flox}$ mice from the Jackson Laboratory (JAX), and crossed these mice to generate $Pten^{flox/flox}Trp53^{flox/flox}$ mice. In these mice, loxP sites flank the PTEN and P53 alleles. These sites are recognized by Cre recombinase, which then induces deletion of the area between the two loxP sites.

The original GEMM model developed by the Abate-Shen laboratory utilized adenoviral Cre recombinase (Adeno-Cre) to deliver Cre to cells to induce recombination within the *Pten* and *Trp53* genes. Because all of the cells in these mice are PTEN and P53 floxed, Adeno-Cre must be injected directly into the bladder urothelium to minimize the likelihood of developing tumors in other organs of the body (Figure 22A). Surgery was thus performed on each mouse to visualize the bladder and inject Adeno-Cre into the badder urothelium. This procedure has limitations. The mice must be subjected to a major surgical procedure, with incisions made in the abdominal muscle wall. Mice are also at risk of complications from anesthesia, which is influenced by the length of surgery. Surgeries can be up to 45 minutes per mouse. Post-surgery, mice are monitored and administered daily pain medication. Because this is a time intensive procedure, cohorts are limited to smaller numbers.

In addition to the above considerations, our initial experience with this model revealed additional technical limitations. While mice developed tumors in the abdomen, we found these tumors to be very aggressive, leading to death at 2.5 months. Upon histological examination, these tumors were poorly differentiated and thus it was unclear if they were derived from urothelial cells, or some other cell of origin.

With each cohort of *Pten/Trp53* knockout mice, we included a Rosa-LacZ reporter mouse to confirm recombination in the urothelium. These mice contain the gene for β-galactosidase (β-gal), lacZ, under the control of the Rosa26 promoter, preceded by a floxed stop cassette (citation). Cre expression results in removal of the stop cassette and subsequent β-gal expression[143]. Tissue can then be stained with X-gal, an analog of lactose, which is hydrolyzed by β-gal and yields an intensely blue insoluble compound.

Because the histology of the tumors was difficult to confirm, we examined the reporter mice to determine in which cells recombination was most likely occurring. After staining performed by the MSKCC Center of Comparative Medicine and Pathology, the Rosa-LacZ reporter mice showed some recombination in the urothelium of mice, but also revealed high levels of staining throughout the surrounding muscle layer (Figure 22B).

Because many of the resulting tumors had a dedifferentiated sarcomatoid appearance on histologic review, our collaborator, Hikmat Al-Ahmadie (GU Pathology), ultimately classified these tumors as sarcomas and not as urothelial carcinomas (Figure 22C). This experience was also consistent with a personal communication from David Kwiatkowski (Dana Farber), who also found that use of the Adeno-Cre model could result in the development of mesotheliomas likely due to leakage of the virus into the peritoneal cavity. Furthermore, our results were consistent with PTEN and TP53 loss being strong drivers of sarcoma development[144,145]. While it is possible that recombination was happening in both the urothelium and muscle layers, the loss of *Pten* and *Trp53* expression in the surrounding muscle layer may have been a stronger driver of sarcoma development than urothelial carcinoma initiation.

Bladder-specific expression of Cre recombinase

In an effort to develop a more robust bladder tissue specific GEMM, we turned to a newer Cre-estrogen receptor (Cre-ER) system that allows for tissue-specific expression of Cre in the bladder urothelium. In this model, Cre recombinase is expressed as a fusion protein with ER under the control of a tissue specific promoter. In the absence of tamoxifen, ER is sequestered from the nucleus in the cytosol, preventing the fused Cre

recombinase from encountering loxP sites in the DNA. In the presence of tamoxifen, ER is bound by tamoxifen and released into the nucleus, bringing along Cre to induce recombination at the loxP sites[146].

For our model, we utilized the cytokeratin 5 promoter, which is a cellular marker expressed in epithelial cells[147]. Of note, urothelial carcinomas have been shown to arise from the CK5 expressing basal cells in the urothelium[148,149]. We therefore can limit Cre expression to CK5 expressing cells. However, this model precludes the systemic administration of tamoxifen, as other cell types in the body express CK5 as well. To overcome this limitation, we administered tamoxifen intravesically via ultrasound-guided injections directly into the bladder (Figure 23A).

In this CK5-targeted model, we were able to successfully generate recombination specific to the urothelium (Figure 23B), although some recombination was also seen in other epithelial tissue throughout the body, including the skin, lungs, and gallbladder. We also generated CK5 Cre-ER *Pten/Trp53* knockout mice to determine if these mice would develop tumors similar to the Adeno-Cre model used by the Abate-Shen lab, with a plan to further cross these mice with the *Kdm6a*$^{flox/flox}$ mice if successful. In our hands, these mice did not, however, develop bladder tumors. A number of mice did develop tumors of the neck and face, which we presumed was due expression of the CK5 promoter in epithelial cells located in these regions.

Carcinogenic mouse models of bladder cancer

Due to the technical challenges of developing a genetically engineered bladder cancer model of KDM6A knockout, we have also utilized a carcinogenic model of

bladder cancer in mice. In this model, mice are fed N-butyl-N-(4-hydroxybutyl)nitrosamine (BBN) in their drinking water daily[150,151]. After four months, these mice begin to develop CIS in the urothelial lining, and after six months develop bladder tumors that are histologically similar to the human disease (Figure 24A).

To further define the timeline of tumor development in mice treated with BBN, we treated cohorts of mice with 1% BBN for varying lengths of time from 8 to 26 weeks. We also treated one group with 0.5% BBN for 26 weeks (Figure 24B). Indeed, mice began to develop large tumors in the bladder at 4-6 months. We used bladder mass as a proxy for tumor size. Mass increased with length of BBN treatment. After 8 weeks, mice had an average weight of 31mg, similar to the control group at 30mg. In contrast, mice at 20 and 26 weeks had a bladder mass of 56mg and 55mg, respectively (Figure 24C).

In addition to the timing of tumor development, we were also interested in the genetic profile of the resulting BBN-induced bladder tumors. We thus performed whole exome sequencing (WES) on several of these tumors. As expected with a carcinogen-induced model, the BBN-induced tumors had a very high mutation burden. On average, each tumor had more than 6,000 genes mutated. We also observed very low allele frequencies for the majority of these mutations below 0.1, although a large portion of mutations had allele frequencies between 0.2 and 0.4. This is in contrast to allele frequencies observed in human samples examined in the TCGA cohort. Allele frequencies in this cohort were evenly spread between 0.1 and 0.5 (Figure 24E).

Although there were thousands of mutations identified in the mouse BBN tumors, we sought to compare the genes mutated in these bladder tumors to the genes mutated in the TCGA cohort. Many of the genes identified by the TCGA cohort were also mutated

in the BBN mice. Of the six mice sequenced, all had likely oncogenic mutations in *Kmt2c*, *Nf1*, and *Trp53*. Five of six had mutations in *Atm*, *Notch2*, *Notch4*, *Pik3c2g*, and *Ros1*. Four of six had mutations in *Ep300*, *Kmt2a*, and *Kmt2d*. Fifty percent of mice had mutations in *Crebbp* and *Kdm6a*, and 2 of 6 had mutations in *Arid1a*, *Rb1*, *Erbb3* and *Pik3ca* (Figure 24D).

Combining GEMM and carcinogenic models

While we were able to confirm the BBN model robustly induced bladder tumor formation, the latency was quite long. Furthermore, we felt that studying the biology of any one specific gene or set of genes and their involvement in bladder cancer initiation was likely not realistic using the BBN model because of the confounding factor that so many other genetic alterations were present. However, we hypothesized that combining the BBN model with our GEMM mice could provide insight into whether loss of *Kdm6a* or *Trp53* could cooperate with a chemical carcinogen such as BBN to induce bladder cancer initiation.

We hypothesized that *Kdm6a* loss prior to BBN treatment may create an environment more conducive to oncogenic mutations promoting tumor growth, therefore accelerating tumor development upon BBN exposure. We therefore utilized our CK5 Cre-ER GEMM mice to look at the effects of *Kdm6a* alone, *Trp53* alone, and *Kdm6a*/*Trp53 double* knockout prior to BBN treatment in a small, preliminary study. Tamoxifen was delivered daily over four days directly to the bladder by ultrasound-guided injections, and knockout was confirmed in paired reporter mice in each cohort, and later by Western blot of tumor tissue. One month after tamoxifen injections, mice

were started on 1% BBN in the drinking water and monitored until the size of the bladder tumors required that mice be euthanized (Figure 25A).

The control group consisted of mice that were *Kdm6a* floxed or *Trp53* floxed, but were wild type for CreER expression therefore precluding any knockout. These control mice followed a similar disease timeline as the BBN alone mice. However, mice were allowed to progress on BBN until time of death or euthanasia was required because of disease. Control mice began to succumb to their disease beginning at 4 months, with all mice dead by 8 months. The average survival of the control mice was 5.78 months. *Kdm6a* knockout mice followed a very similar trend, with average survival of 5.35 months. *Trp53* knockout mice had an average survival of 5.55 months, whereas *Kdm6a*/*Trp53* double knockout mice had an average survival of 4.74 months (Figure 25B).

Although *Trp53* alone and *Kdm6a* alone mice had similar average survival compared to wild-type mice, all *Trp53* mice died from their tumors before 6 months. In contrast, the tail of the survival curve for the *Kdm6a* mice and control mice extended to 8 months. *Kdm6a*/*Trp53* double knockout mice had the shortest survival with all double knockout mice dead within 5.2 months. *Trp53* loss appeared to expedite tumor growth and death from disease, whereas *Kdm6a* loss alone did not have a significant impact compared to the control group (Figure 25C).

When mice required euthanasia, the bladder tumors were collected before euthanasia and divided into two parts. Half was fixed in paraffin for H&E staining, while the other half was frozen for Western blotting. All tumors analyzed by H&E staining were confirmed to be of urothelial origin and consistent with urothelial carcinoma (Figure

25C). While we hypothesized that *Kdm6a/Trp53* double knockout expedited tumor growth, we wanted to confirm that the tumors did indeed have loss of KDM6A and/or P53 expression. As shown in Figure 25D, we were able to confirm both KDM6A and P53 loss of expression in the BBN tumors.

Using GEMM mice to generate KDM6A knockout mouse cell lines

Although we were unable to develop an *in vivo* tumor model from the KDM6A, P53 and KDM6A/P53 knockout mice, we were able to utilize these mice to generate cell lines with targeted deletion of these genes to further study the biology of KDM6A loss. These cell lines have a potential advantage over patient-derived cell lines because of the lack of other confounding oncogenic mutations typically found in the patient-derived cancer cell lines. In addition, these cells are taken from the bladder of mice before tumors develop, allowing us to examine the potential impact of KDM6A loss in the early stage of tumor development.

To facilitate the cell lines studies, the CK5 CreER mice were crossed with a reporter mouse known as mT/mG. In these mice, the fluorescent membrane-targeted tandem dimer Tomato (mT) is expressed in all cells prior to Cre-mediated recombination. LoxP sites flank the mT gene, and after recombination-induced excision of mT, the promoter drives expression of membrane-targeted enhanced green fluorescent protein (mG)[152]. Cells that have Cre expressed in them will become green, while cells without Cre expression remain red.

Breeding was then performed to generate mT/mG CK5 CreER *Kdm6a* floxed, *Trp53* floxed, and *Kdm6a/Trp53* floxed mice. Because these mice were not going to be

aged long enough for head and neck tumor development, we induced recombination by systemic tamoxifen intraperitoneal (IP) injections once daily for four days. Two weeks after the last tamoxifen injection, mice were euthanized and cells were collected (Figure 26A).

Because recombination was induced in other cell types throughout the body with this method, urothelial cells were specifically collected by removing the bladder followed by cell dissociation with collagenase. Cells were then sorted by flow cytometry for epithelial cell adhesion and activating molecule (EpCAM) as a marker for epithelial cells to avoid contamination of other cell types[153,154]. After EpCAM sorting, cells were sorted for GFP positivity.

Overall, IP injections led to higher levels of recombination in EpCAM positive cells. In wild-type mice with IP injections, 24% percent of EpCAM positive cells were GFP positive, while only 16% of EpCAM positive cells were GFP positive in mice with ultrasound-guided injections. This was consistent with immunohistochemistry (IHC) staining in IP injected mice compared to ultrasound-guided injected mice. A higher frequency of GFP positive cells was observed in the urothelial layer (Figure 26B).

Compared to wild-type mice, KDM6A knockout led to an increase in the number of GFP positive EpCAM positive cells. In the IP injected KDM6A mice, 50% of EpCAM positive cells were GFP positive, compared to 24% in wild-type mice. Ultrasound-guided injection of KDM6A mice resulted in 26% of EpCAM positive cells being GFP positive, compared to 16% in wild-type mice. Again, more recombination was seen in the IP injected mice compared to those that had ultrasound-guided injections. The increase in GFP positive cells observed in KDM6A knockout mice compared to wild-type mice

suggested that KDM6A loss was inducing the proliferation of urothelial cells (Figure 26B).

After sorting for GFP positivity, these cells were plated in 6cm plates. In addition to *Kdm6a* knockout, cells were also collected from *Trp53* knockout mice and *Kdm6a*/*Trp53* double knockout mice. Of these three subsets, cells from *Kdm6a*/*Trp53* knockout mice grew best on plastic. *Trp53* knockout cells also grew relatively well, though not as rapidly as the double knockout cells. *Kdm6a* knockout urothelial cells grew poorly in cell culture, but after many weeks a cell could be passaged. However, these cells were not robust and died soon after re-plating. We were able to collect sufficient cells from all three genotypes for Western blotting to confirm KDM6A loss in the *Kdm6a* single and *Kdm6a*/*Trp53* double knockout lines, whereas high levels of KDM6A were still seen in the *Trp53* single knockout line (Figure 26C).

While the *Kdm6a* knockout derived urothelial cells grew poorly on plastic, we were able to collect sufficient cells for RNA-seq with the goal of assessing the changes in gene expression resulting for loss of KDM6A and TP53. Cells from four wild-type mice and six KDM6A knockout mice were submitted for RNA-seq, with unique transcriptional signatures noted with each group, as revealed by PCA (Figure 27A, B). Though this was a preliminary analysis, several of the genes differentially expressed in the Kdm6a mutant wild-type cells have been previously shown to play a role in tumor initiation (Figure 26C).

Discussion

Developing bladder specific mouse models remains a challenge in the field. While targeted knockout of *Pten* and *Trp53* in the bladder urothelium has been shown to induce bladder cancers by the Abate-Shen laboratory, we encountered several technical challenges with the use of this model, which will likely impede its large-scale adoption. More recent attempts to develop tissue specific models support this as the field moves away from nonspecific Cre introduction.

Our work with tissue specific models also highlighted several challenges in generating GEMM mice that develop urothelial bladder cancers. In our hands, *Pten/Trp53* double knockout mice did not develop bladder tumors. This result may be due to the fact that this genetic combination may not be a strong driver of bladder cancer development. In fact, co-occurring *TP53* and *PTEN* alterations are only present in only about 1% of bladder cancer patients. This genomic profile is therefore not representative of the human disease.

As an alternative, we attempted to use a CK5 driven tumor model, but found that Cre expression in these mice was not adequately specific to the bladder. Because CK5 is widely expressed in other epithelial tissues in the body, we were required to perform ultrasound-guided injections of tamoxifen directly into the bladder. Still, the CK5 allele had some leakiness and recombination was observed in various other tissues throughout the body. Again, because *PTEN* and *TP53* may not be the most potent inducers of bladder cancer development, mice were developed off-target head and neck tumors requiring euthanasia before any bladder tumors could likely developed.

Two possible solutions to overcome this limitations of the models employed may warrant further investigation in the future. First, GEMM should be developed that better represent the genomic landscape of the human bladder disease. To this end, the development of KDM6A/FGFR3 co-altered mice would be valuable, although knock in mice pose additional technical challenges to develop. In addition, the combination of RB1/P53 could be studies as alterations in these genes are both common in patients with high grade invasive disease. In patients with bladder cancer, mutations in the *RB1* and *TP53* genes are associated with more aggressive tumors, and combination with a CK5-Cre, bladder tumors may arise before off-target tumors require euthanasia. Furthermore, as CRISPR becomes a viable tool for the development of mouse models, even more complex genetic combinations may be feasible that are more representative of the genomic complexity of the human disease.

The alternative solution may lie in methods that can better restrict Cre recombination to the bladder urothelium. There are several promoters that are specific to the urothelium. Uroplakin3 (UPK3) has been identified as one. Our data showed that systemic administration of tamoxifen led to higher recombination rates. By using a urothelial-specific driver, tamoxifen could be administered systemically without concern for the development of tumors at other sites. However, a major consideration of this driver is the cell of origin in urothelial carcinoma. CK5 expression is largely in the basal layer of the urothelium, which is thought to be the cell of origin for most human bladder cancers. In contrast, UPK3 expression is limited to superficial umbrella cells. Whether the tumors that would form in UPK3 mice are representative of the biology of the human disease is an area of active debate.

Our work also highlighted the potential value of combining GEMM and the carcinogenic BBN model. While *Trp53* deletion appeared to accelerate death, a larger cohort of mice will be needed to confirm our preliminary findings. Other studies have also examined the effect of KDM6A loss in males vs. females and found that KDM6A loss accelerates tumor growth in the BBN model[155]. Because sex may influence phenotype, it will be critical to compare the phenotype of male and female mice.

Another caveat of our study was the use of death as an endpoint. While *Trp53* loss appeared to accelerate death, *Kdm6a* knockout did not appear to have an major effect on time to death. However, our *in vitro* data suggest that KDM6A may play a role in tumor initiation. Therefore, close monitoring of the bladder by ultrasound throughout BBN treatment will be an important data point in future studies. Mice may develop slow-growing tumors faster following BBN exposure in *Kdm6a* knockout as compared to wild-type mice, but we were not able to assess this in our model.

Lastly, molecular profiling of the tumor arising in our GEMM mice may provide additional insight into the role of KDM6A in tumor development. In preliminary studies, we found that BBN-induced tumors were highly mutated, with over 6,000 mutations in each tumor. Because KDM6A may create a permissive environment for tumor formation, BBN tumors in KDM6A knockout mice may have fewer mutations than tumors arising in wild-type mice. Molecular analysis could confirm that biallelic loss of Kdm6A was present in the BBN-induce tumors arising in these mice.

Overall, the field still lacks mouse models of bladder cancer that reflect the genomics of the human disease. *In vivo* models will likely be crucial for studying the mechanisms whereby loss of chromatin modifying genes such as KDM6A cooperate with

other recurrent genetic alterations to induce tumor formation. Such models would also be valuable to testing novel therapeutic approaches that show promise in *in vitro* studies. Finally, as immunotherapy is now a component of the standard treatment for bladder cancer patients with metastatic disease, mouse models will be needed to prioritize which combinations of agents warrant testing in patients.

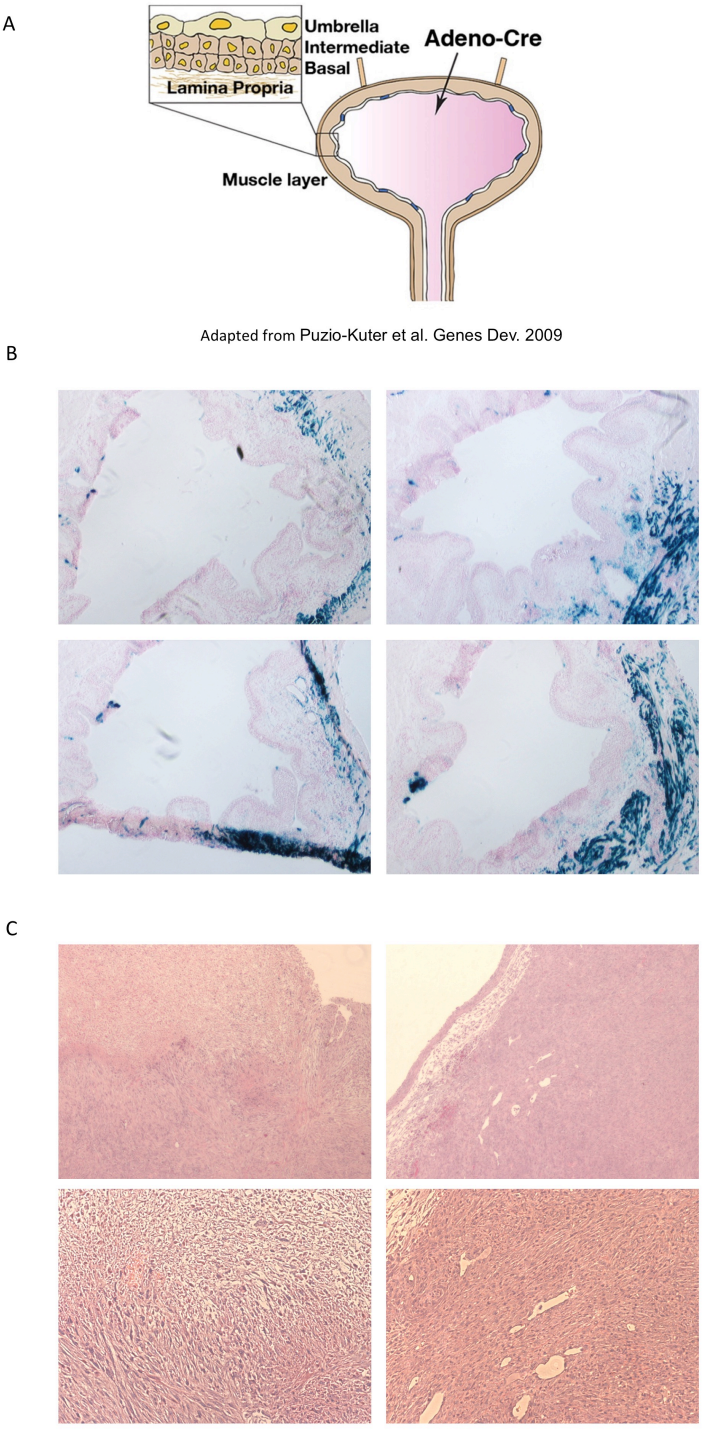

Figure 22: Adeno-Cre delivery results in non-specific recombination.

A: Schematic describing Adeno-Cre delivery to the bladder developed by the Abate-Shen laboratory (Columbia University Irving Medical Center). B: X-gal staining of fixed

bladders from Rosa-LacZ reporter mice. Images show bladder lumen in the center. The urothelial layer can be observed as the darker pink layer lining the lumen. Dark blue cells are indicative of recombination. Images courtesty of Sebastien Monette. C: H&E staining of fixed bladders from PTEN/P53 knockout mice 6-8 weeks post Adeno-Cre delivery. Bladder lumen is not defined as tumors grew aggressively and took over lumen. Images courtesy of Sebastien Monette.

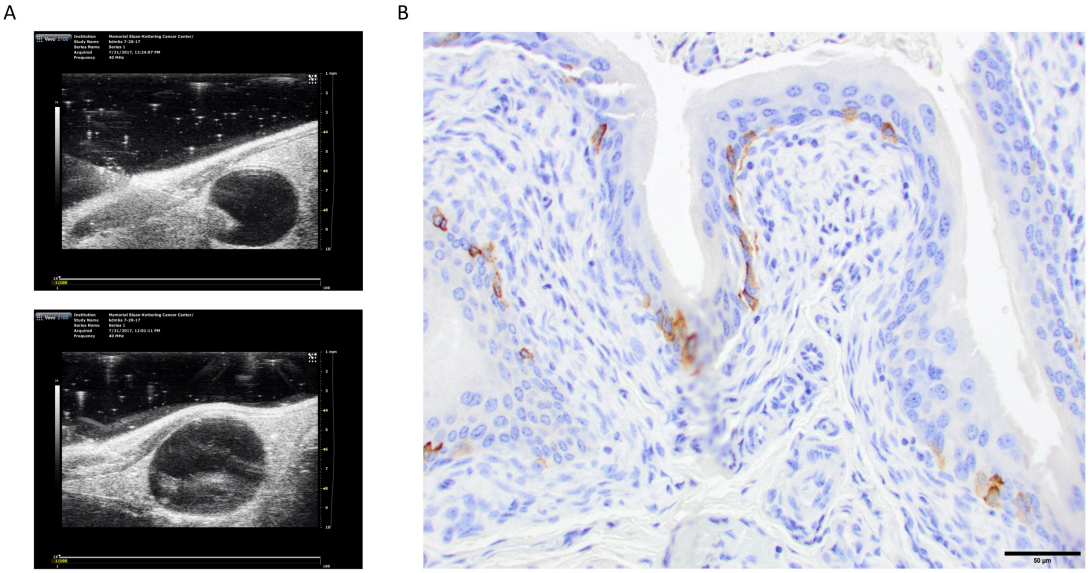

Figure 23: Utrasound-guided tamoxifen injections in Cre-ER driven model provides urothelial-specific recombination.

A: Representative images of ultrasound-guided injections. Bladder lumen is visualized by ultrasound as black space just below the abdomen. Tip of needle can be observed at the far left side of the bladder. B: Representative IHC GFP staining of fixed bladder from mT/mG mouse. Dark brown color is indicative of GFP positive cells. Image courtesy of Sebastien Monette.

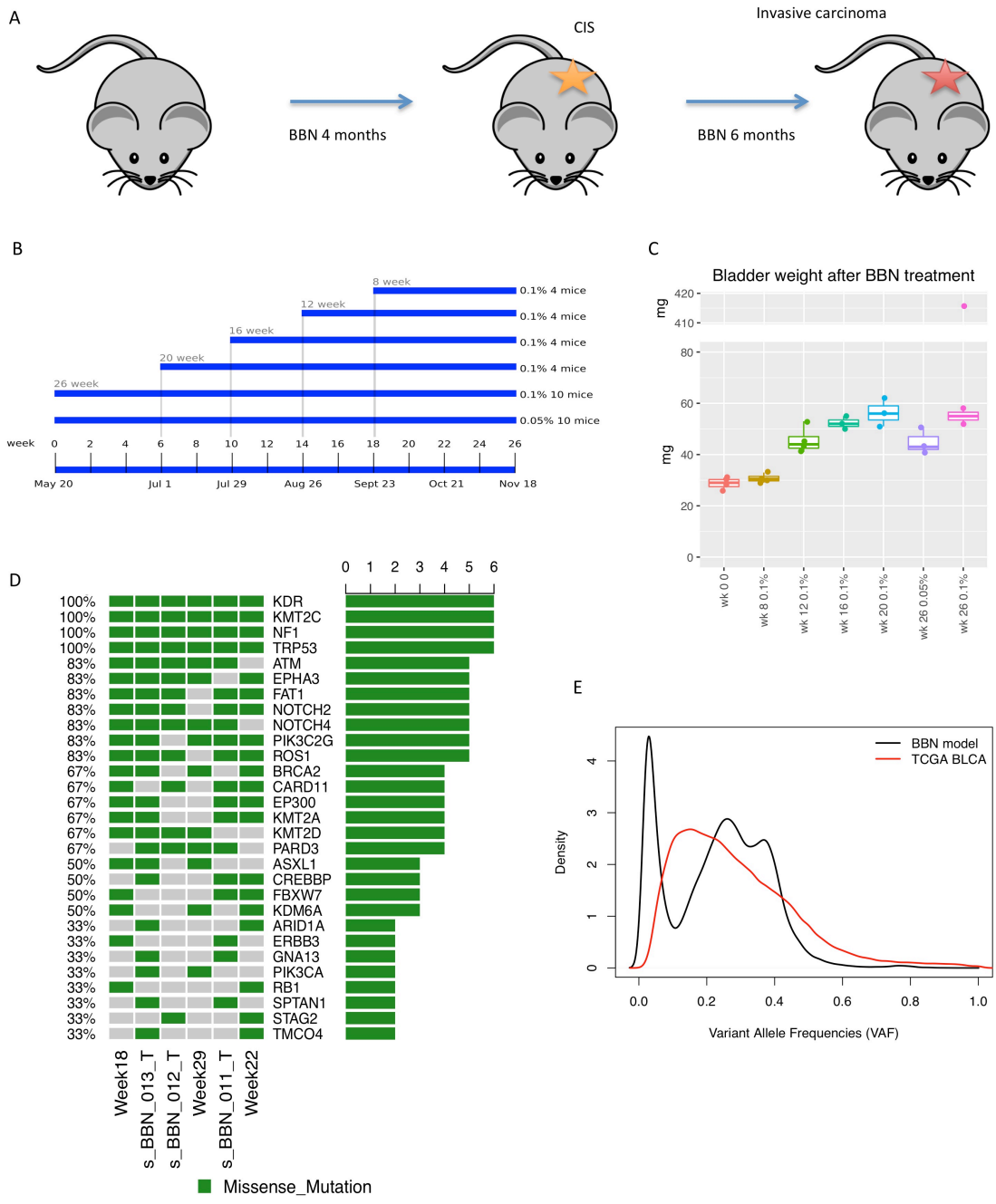

Figure 24: BBN-derived tumors in mice show similar genetic profile to human bladder disease.

A: Schematic of BBN tumor development. B: Schematic of BBN treatment groups and collection time points. Groups consisted of 0.1% BBN treatment with collection at 8, 12, 16 and 20 weeks, with 4 mice in each group. Two additional groups of 10 mice were treated with 0.1% and 0.5% BBN with collection at 26 weeks. C: Bladder weight of each treatment group at collection time point is graphed after BBN treatment. Figure generated

by Wenhuo Hu. D: Oncoprint of mutated genes. WES was performed on bladder tumors from 6 mice. On the left, each column represents a gene and each row a different mouse. Green denotes presence of a mutation. On the right, the frequency of mutation in the cohort for each gene is graphed. Figure generated by Wenhuo Hu. E: Variant allele frequency of all mutations identified in the BBN mice cohort compared to frequencies observed in the muscle invasive bladder cancer TCGA cohort. Figure generated by Wenhuo Hu.

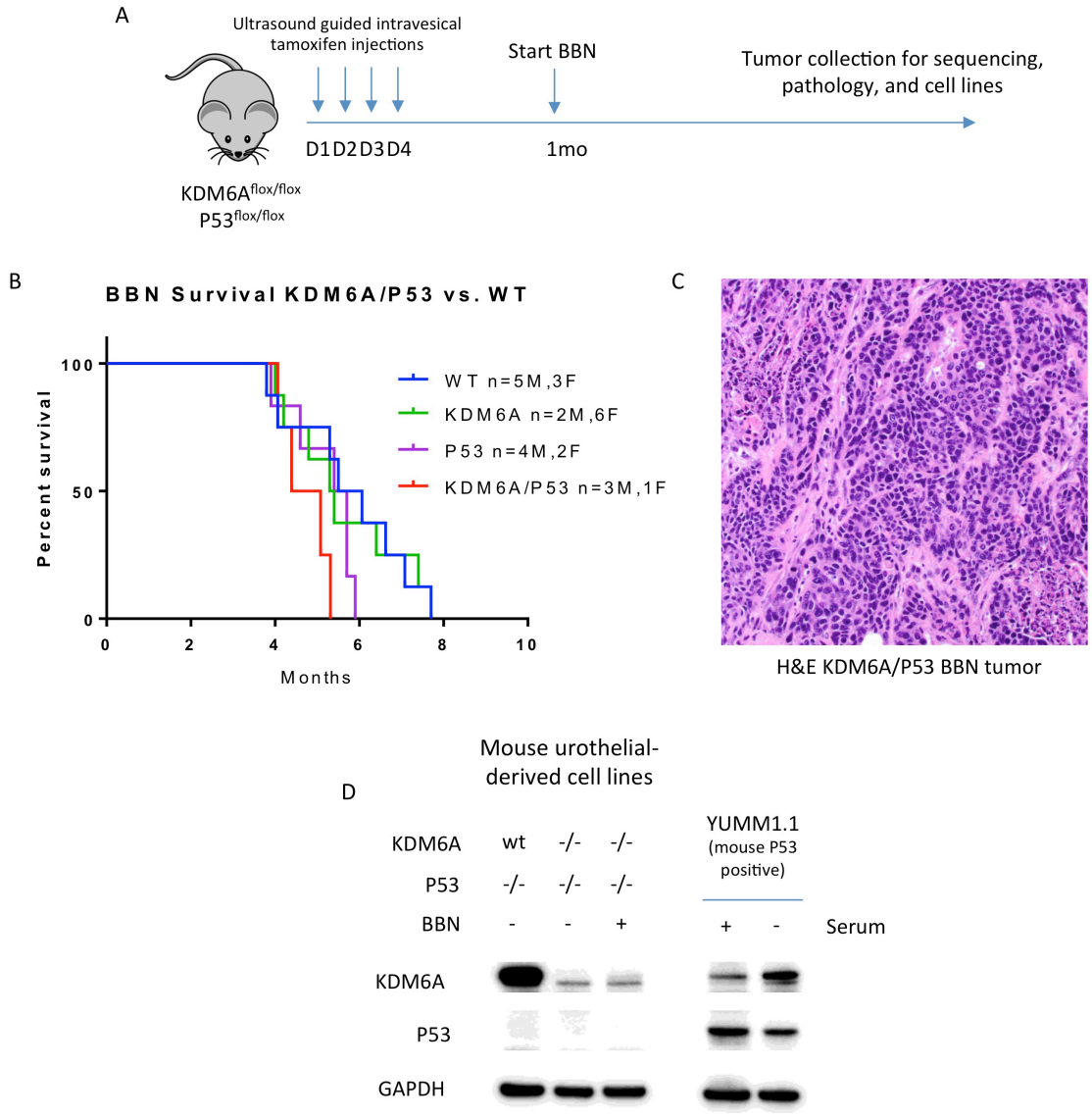

Figure 25: Combining BBN carcinogenic model with GEMM.

A: Schematic showing timing of tamoxifen injections and BBN treatment. B: Kaplan-Meier survival of BBN treated mice in a wild type, KDM6A, P53, and KDM6A/P53 knockout background. C: Representative H&E staining of fixed bladder from a KDM6A/P53 knockout mouse with BBN tumor. Image courtesy of Sebastien Monette. D: Western blot analysis of mouse urothelial-derived KDM6A and KDM6A/P53 knockout cell lines, and tissue from a KDM6A/P53 knockout mouse with BBN tumor.

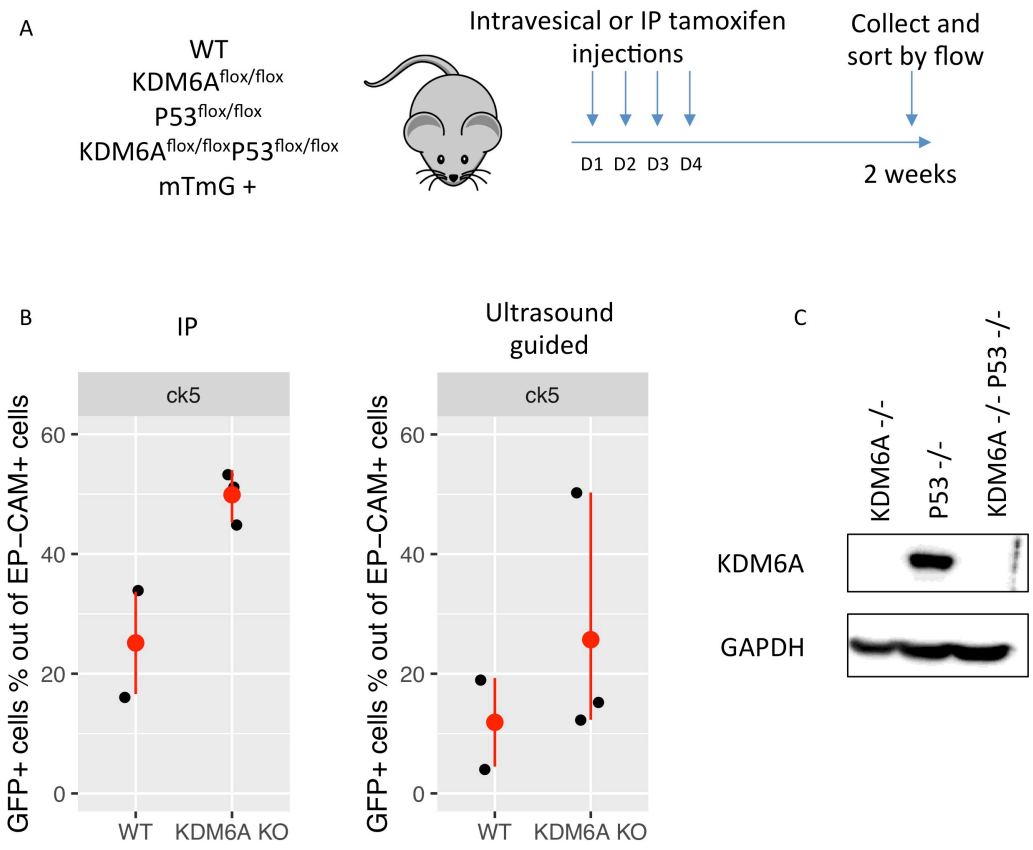

Figure 26: Generating mouse urothelial-derived cell lines.

A: Schematic showing experiment design. Mice were injected with tamoxifen intravesically or intraperitoneally once daily four days in a row. Two weeks after injections, bladders were collected and cells were dissociated and sorted by flow cytometry. B. GFP positive cell counts in wild-type and KDM6A knockout mice after sorting on EpCAM. Counts for IP injections are the left, and counts for intravesical injections are on the right. Figure generated by Wenhuo Hu. C. Western blot confirming KDM6A knockout in mouse urothelial-derived cell lines. After sorting, cells were plated and allowed to grow up.

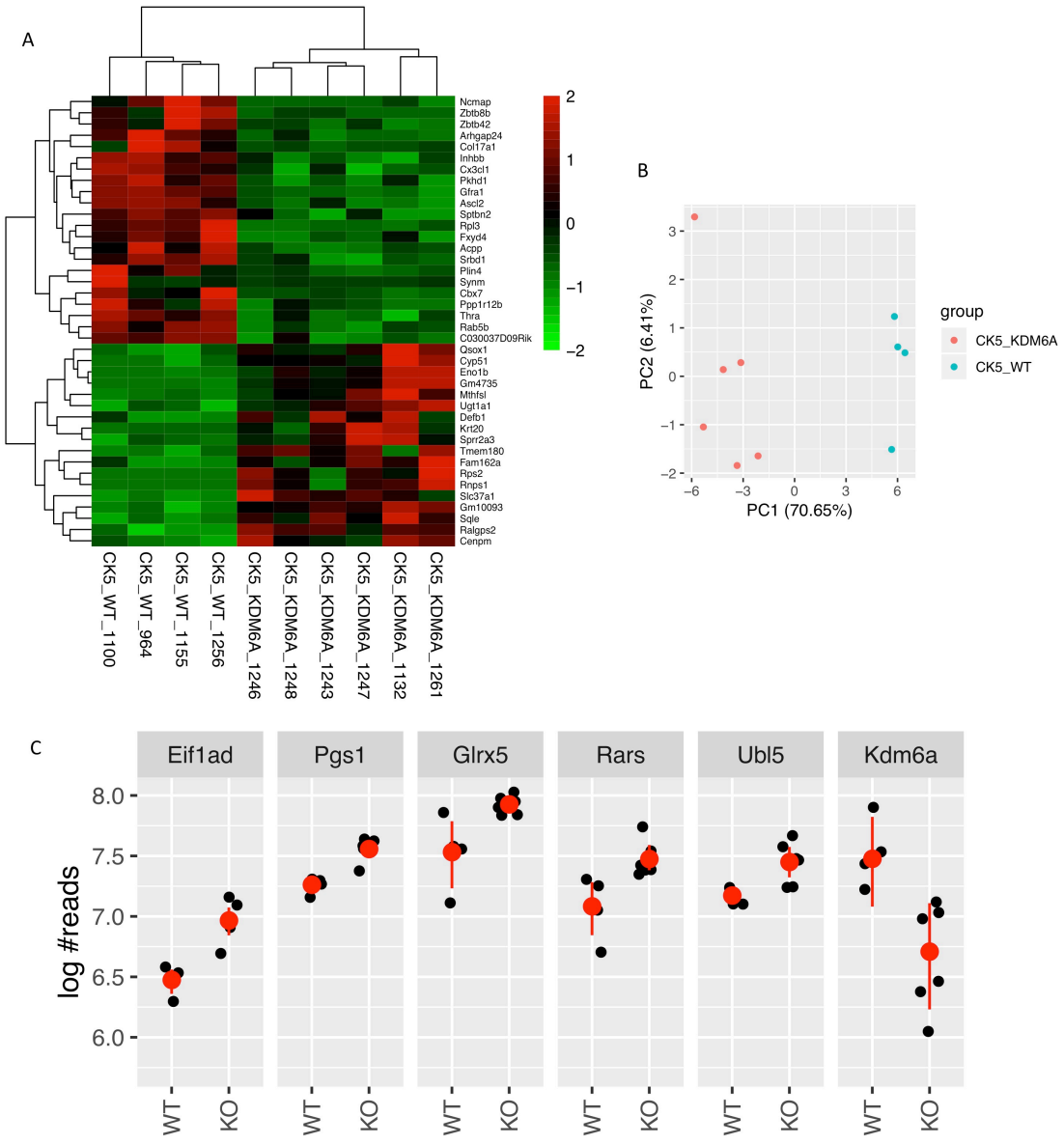

Figure 27: RNA-seq analysis of mouse urothelial-derived KDM6A knockout cells.

A: Unsupervised hierarchical clustering of significantly differentially expressed genes in wild-type and KDM6A knockout mice derived cells. Each row represents an individual gene with a p-value <0.05. Columns represent individual samples. Figure generated by Wenhuo Hu. B: Principle component analysis of wild-type and KDM6A knockout cells. Figure generated by Wenhuo Hu. C: Representative genes with variable RNA expression in wild-type compared to KDM6A knockout cells. Number of expression reads is plotted on the y-axis. Figure generated by Wenhuo Hu.

Chapter 4: Defining the evolution of epigenetic alterations in urothelial carcinoma

Several large-scale efforts have sought to define the genomic landscape of invasive bladder cancers with the goal of identifying novel therapeutic targets. The most notable finding was the identification of mutations in genes that regulate chromatin state in the vast majority of bladder cancers. Mutations in *KDM6A*, *ARID1A*, *KMT2D*, and *EP300* are most commonly observed and present in approximately 75% of cases.

To determine the timing at which mutations in chromatin modifying gene arise during disease pathogenesis and the role played by alterations in these genes in promoting disease initiation and progression remains poorly understood. In contrast to other cancer types, molecular alterations identified by clinical tumor sequencing are not yet commonly used to guide disease management in patients with urothelial cancer. Rather primary disease management is based primarily on classification of bladder cancers as low grade or high grade and non-muscle invasive (NMIBC) or muscle invasive (MIBC) largely based on nuanced pathology. While NMIBC has a high overall survival rate, patients with non-invasive tumors have a 50% recurrence rate and a subset progress to more lethal MIBC[156]. Recent studies have examined the genomic landscape of NMIBC and MIBC individually, revealing an enrichment of *FGFR3* and TERT mutations to NMIBC, whereas *RB1* and *TP53* are more commonly altered in MIBC[34,105].

While several groups have sought to define the prevalence of mutations in NMIBC and MIBC, few studies have examined the genomic landscape by grade. Typically, many NMIBC are low grade whereas all MIBC are high grade tumors.

However, a subset of NMIBC are high grade and such high grade non-muscle invasive lesions are more likely to progress to MIBC and metastatic disease. Small cohort studies have shown that alterations in individual genes, including *ARID1A* and *TP53*, are associated with high grade invasive disease[157]. However, most prior studies profiled only primary tumors and few metastatic cancers have been profiled to date. Hence, the genomic evolution of individual bladder cancers over the course of disease progression remains largely unexplored.

We therefore leveraged the prospective MSK-IMPACT sequencing cohort to identify differences in the prevalence of mutations in low and high grade, invasive and muscle invasive tumors. We also used this unique institutional cohort to identify patients for whom paired primary and metastatic tumors from the same patient could be analyzed. We began with a cohort of 969 patients with bladder cancer. We divided these patients into low grade, high grade, and metastatic cohorts and characterized the landscape of alterations present in each category.

In addition, we were able to collect matched primary and metastatic tissue samples in a subset of 56 patients. With these matched pairs, we performed whole exome and/or targeted next generation sequencing to determine the clonality and timing at which genomic alterations arose during disease progression. While the genomic profiles of the primary and metastatic samples were largely concordant, we found that targetable mutations including those in *FGFR3*, *PIK3CA*, *ERBB2* and *TSC1* were commonly discordant. Furthermore, our data suggests that *KDM6A* mutations, when present arise early in tumor development (concordant in both the primary and metastatic samples),

whereas *ARID1A* alterations were present only in the metastatic sample in a minority of cases.

Results

Clinical and Histological Data

The unmatched cohort consisted of 1057 bladder tumor samples collected from 969 patients for whom extensive clinical data was available. Based on the biology and clinical management of bladder cancer, the unmatched tumor samples were divided into three cohorts: primary low grade (6.1%, n=65), primary high grade (70.2%, n=742), and metastatic (23.7%, n=250). Metastatic sites included lung (35.2%, n=88), retroperitoneal or distant lymph node (28.8%, n=72), bone (16%, n=40), liver (9.2%, n=23), and pelvic metastatic mass (6%, n=15), recurrences that were deemed on expert curation of the clinical histories to be locoregional metastases.

Mutational profiling of the MSKCC unmatched cohort

We first compared the genomic profile of the MSK-IMPACT bladder cancer patients to the previously published TCGA bladder cancer cohort. Overall, the pattern genetic alterations identified in the MSKCC unmatched cohort varied only slightly from the 2017 TCGA muscle invasive bladder cancer (MIBC) studies (Figure 28A). Of note, *FGFR3* was altered at higher rates in the MSKCC unmatched cohort compared to the TCGA cohort. *FGFR3* was altered in 14% of tumors in the 2017 TCGA study, while a mutation frequency of 27% has been seen to date in the MSKCC cohort. The higher frequency of *FGFR3* alterations in the MSK cohort was likely the result of inclusion of

patients low grade and non-muscle invasive disease, which were excluded from the TCGA analysis.

As previously identified by large scale sequencing efforts, epigenetic regulators were altered in a large proportion of samples in the MSKCC unmatched cohort. More specifically, epigenetic alterations were identified in 76.1% of tumor samples, with the most frequently mutated genes being *KDM6A* (26%), *KMT2D* (28%) and *ARID1A* (27%) (Figure 28A). Alterations in *KDM6A* were typically truncating mutations (frameshift, nonsense mutations) distributed throughout the protein. These mutations are predicted to result in loss of protein expression or disruption of the enzymatically active Jumanji C domain of the protein.

Comparing mutation frequencies more broadly across the cancer types analyzed by the TCGA revealed that *KDM6A* alterations were strongly associated with a diagnosis of bladder cancer and rare in most common solid tumor types. The tumor type with the second highest prevalence of *KDM6A* mutation was esophageal cancer, with mutations identified in 13.7% of cases (Figure 29A). No other cancer type had a *KDM6A* mutational frequency of greater than 10%. Mutations in *ARID1A* were more broadly present across cancer types, most frequently in uterine (43.7%), stomach (27.1%) and bladder cancers (26%) (Figure 29B). In addition to bladder cancer, *KMT2D* was also recurrently mutated in a number of cancer types, including uterine (27.6%), diffuse large B-cell lymphoma (27.1%), lung (23%) and melanoma (22.8%) (Figure 29C).

Given the high prevalence of *KDM6A* and *ARID1A* alterations in bladder cancer and the poorly defined roles played by mutations in these gene in urothelial cancer pathogenesis and progression, we sought to define the timing at which these alterations

arose during the natural history of the disease. With assistance from Drs. Nima Almassi and Tim Clinton, we divided the MSKCC unmatched cohort into low grade, high grade, and metastatic cohorts. We then integrated the genetic profiles derived from MSK-IMPACT with patient demographic and cancer outcome data. This analysis revealed several genes that were more frequently mutated in low grade samples as compared to high grade and/or metastatic samples, including *KDM6A*, *FGFR3*, *PIK3CA*, *CREBBP*, and *KMT2C* (Figure 28B). Conversely, several genes were found to have higher alteration frequencies in high grade and metastatic samples, including *TP53*, *ARID1A*, *RB1*, and *ERBB2* (Figure 28B).

We next inferred the cancer cell fraction of the mutations in the most recurrently mutated genes using FACETS and then compared the clonality of the mutations in these genes across the primary and metastatic cohorts. Our ongoing analyses suggest that the genes more likely to be mutated in low grade tumors had a higher cancer cell fraction in both cohorts (Figure 30). Conversely, mutations in genes more likely to be altered in the high grade primary and metastatic samples were more likely to be sub-clonal in the primary samples as compared to the metastatic cohort (Figure 30). This suggested that alterations associated with low grade disease were more commonly clonal in the tumors in which they are present, whereas alterations more frequently present in the tumors of patients with high grade or metastatic disease were more likely to be subclonal (if present at all) in low grade samples, arising as later gain-of-function alterations that may be promoting tumor progression and or metastasis.

WES on Matched Pair Cohort

A limitation of MSK-IMPACT platform is that it can only identify alterations in genes included in the assay design. Furthermore, those mutations enriched in metastatic samples may not be discordant in the respective primary samples of the patients in which they were found. Rather, such mutations may have arisen in the primary samples where they confer an increased risk for the subsequent development of metastatic disease. Therefore, to take an unbiased approach to comparing the genomic landscape of primary and metastatic paired samples, we performed whole exome sequencing (WES) of the primary and metastatic samples from 23 bladder cancer patients for whom DNA of adequate quantity and quality was available for WES analysis, in collaboration with Drs. Shweta Chavan and Barry Taylor. Sequencing was performed by the MSKCC Integrated Genomics Operation, with analysis performed by Dr. Chavan. Metastasic sites included the lung, liver, lymph nodes, and pelvic recurrences deemed to be metastases.

Tumor specimens were sequenced to an average median coverage of 154-fold. Purity, ploidy, genome doubling, and cancer cell fractions for all mutations in all specimens were then inferred. Tumor purity ranged from 17 to 88% tumor cell content as estimated from sequencing data using the FACETS algorithm[158]. Evolutionary relationships among clones and metastatic sites were then inferred using the union of somatic mutations called in any of the tumors for a given patient. Somatic variants included in this analysis were those that were 1) covered at 20-fold or greater depth in both the tumor and matched normal specimens, 2) supported by greater than 3 reads in the tumor, 3) present in zero reads in the matched normal, and 4) with a mutant allele fraction in the affected tumor of greater than 2%.

While the mutational profiles of the primary and matched pairs were largely concordant, several notable discordances were observed in the whole exome sequencing analysis. For example, consistent with the higher frequency of *ARID1A* mutations in metastatic tumor samples, two patients had *ARID1A* mutations only in the metastatic samples.

One was Patient 7, who was originally diagnosed with a low grade bladder tumor for which a transurethral resection (TUR) was performed. Over the next 15 months, the patient developed 4 subsequent bladder tumors, each of which were resected by TURBT and all of which were high grade tumors despite treatment with Bacillus Calmette-Guerin (BCG). The last prompted a radical cystectomy. Six months later, the patient developed metastatic lung disease, which was treated with gemcitabine/carboplatin, though ineffective, leading to the patient's death 6 months later.

The primary sample analyzed by WES was derived from the cystectomy, whereas the metastatic sample was as lung biopsy collected 6 months later. In the primary sample, 70.4% of mutations identified by WES had a CCF above 0.75 and were thus deemed to be clonal. Only 18.5% of mutations were sub-clonal with a CCF below 0.25, most of which were unique to the primary. The majority of clonal mutations identified in the primary sample were also clonal in the metastatic sample. Three mutations that were clonal in the primary sample were not present in the metastasis. Likely oncogenic mutations present in both the primary and metastatic samples included mutation in *FGFR3* (S371C, a known activating hotspot mutation), *KDM6A* (S295*), *CDKN1A* (C117Lfs*12), *CREBBP* (K1051*), *PIK3CA* (H1047R), *TP53* (D281Y), and *TP53*

(V173M) mutations. Notably, two mutations in *ARID1A* (E1783* and E2078K) were detected only in the metastatic samples (Figure 32).

The other case was Patient 13, a former smoker with an initial diagnosis of muscle invasive bladder cancer and underwent radical cystectomy. One year post-operatively, the patient developed an obturator internus recurrence and bone metastases, which was treated with gemcitabine/cisplatin. However, the patient had progression in the bone metastases, prompting pembrolizumab treatment. Ultimately, the patient died of widely metastatic urothelial carcinoma.

The primary sample from this patient came from the radical cystectomy, while the metastatic sample was a biopsy of bone metastasis at progression, post gemcitabine/cisplatin treatment. Consistent with the trend observed in patient 7, a higher fraction of mutations in the metastasis were clonal. In this second example, both the primary and metastasis shared *CDKN1A* Q10* and *STAG2* Q167* mutations. Notable mutations unique to the primary included *ELF3* C235Lfs*66* and *FBXW7* R505S, whereas mutations unique to the metastatic sample included *ARID1A* X1665_splice, *ARID2* S1307*, *ARID2* R1745Kfs*10, and *FBXW7* R505G. In contrast to the WES data on Patient 7, however, we observed significantly greater genomic divergence between the two tumors with over half of the mutations identified in only the metastatic sample (Figure 33).

Expansion of the matched pair cohort using MSK-IMPACT analyis

Given the observation that two of primary and metastatic pairs analyzed by WES had mutations in *ARID1A* present only in the metastatic lesions, we sought to build upon

this finding by analyzing a broader cohort of tumors for known or likely oncogenic mutations using the MSK-IMPACT platform. We thus performed MSK-IMPACT on additional 33 primary and metastatic tumor normal pairs. We also performed MSK-IMPACT on the 23 pairs that had undergone WES to validate the oncogenic mutations identified by WES and to determine whether the lack of discordance in some cases was the result of low sequence coverage. Overall, the mutational frequencies of genes found to be commonly mutated in other bladder cancer cohorts were similar in this 56 patient cohort, with mutations in the *TERT* promoter in 73.9% (n=34), *KDM6A* in 33.9% (n=19), *ARID1A* in 26% (n=12), *TP53* in 47.8% (n=22), FGFR3 in 32.6% (n=15), and *CDKN1A* in 17.4% (n=8) (Figure 2).

Consistent with the WES data, we observed that the majority of mutations were concordant. However, a number of potentially actionable genes including *ERBB2*, *PIK3CA* and *TSC1* were observed to be strikingly discordant among the primary and metastatic pairs. More specifically, 3/8 *ERBB2*, 5/14 *PIK3CA*, and 2/8 *TSC1* known or likely pathogenic alterations in these genes were present in only the primary or metastatic samples but not in both. As an example, two patients had activating *ERBB2* alterations only in the primary tumor whereas one had an *ERBB2* mutation only in the metastasis.

Consistent with our hypothesis that *KDM6A* mutations arise early in disease pathogenesis (See Chapter 2), *KDM6A* mutations, when present, were found in both the primary and metastatic samples, with rare exceptions. Careful analysis of two tumors in which *KDM6A* was discordant suggested that the primary and metastatic pairs in these patients almost certainly represented two distinct primary cancers. Among the other chromatin modifying genes, *CREBBP* and *KMT2C* were occasionally altered in the

primary samples only, but not in the metastatic samples. Strikingly, building upon our observation from the WES data, *ARID1A* mutations were unique to the metastatic samples of four patients, providing additional support to the notion that *ARID1A* mutations arise later in disease evolution and may thus play a role in driving metastatic progression.

Discordant samples identified by MSK-IMPACT often represent second primary tumors

MSK-IMPACT has the ability to identify clinically relevant somatic mutations, novel noncoding alterations and mutational signatures shared by common and rare tumor types. By comparing the mutational signatures of the primary tumors to that of the patient matched metastatic lesions, we sought to determine whether any of the pairs represented second independent primary cancers as opposed to metastatic lesions. Furthermore, in our search for matched primary and metastatic samples, we identified a number of patients with two samples that had been classified as two primaries of different cancer types. Upon further investigation, the sequencing results revealed that in some of these patients the presumed second primary was in fact clonally related to the bladder primary cancer. These patients highlight the importance of sequencing the tumors of patients with a history of multiple primary tumors to ensure the correct disease diagnosis.

In one such case, the patient had a partial cystectomy for a urachal adenocarcinoma (stage IIIA Sheldon, enteric type, negative margins, 0/17 negative lymph nodes). Postoperatively, the patient was followed with surveillance scans during which time he was found to have a new 8mm left upper lobe lung nodule. Pathologic review of the biopsy of this lung lesion was consistent with non-small cell lung cancer with

prominent giant cell features. Despite the lack of morphologic similarity between the bladder and lung tumors, MSK-IMPACT analysis of the bladder primary tumor and the lung biopsy revealed that the two were genetically similar with 8 mutations shared. In sum, the genetic profiles indicated that the two tumors were clonally related with the lung tumor representing a metastasis from the primary bladder adenocarcinoma. As the treatment of bladder and lung adenocarcinomas are distinct, this finding ultimately impacted the systemic therapy delivered to the patient.

A second example was a 75-year-old female with a history of breast cancer. She subsequently developed a low-grade non-invasive papillary urothelial carcinoma in 2014 and then in 2016 cervical biopsies were interpreted as primary cervical squamous cell carcinoma (HPV-negative). MSK-IMPACT testing of the cervical biopsy demonstrated a mutation profile nearly identical to that of the bladder biopsy with known or likely oncogenic mutations found in *FGFR3*, *KDM6A*, *MLL2*, and TERT promoter mutations.

Discussion

With the goal of defining the timing at which mutations arise during bladder cancer initiation and development, we integrated tumor genomic sequencing data with detailed clinical annotation for a large cohort of bladder cancers. We first examined bladder cancer alterations in an unmatched cohort of 969 patients. Overall, the alteration frequencies observed in this cohort were largely similar to those reported in other large-scale sequencing studies, including the TCGA. However, these prior studies included few low grade samples or samples collected from metastatic sites. We found that certain alterations, including *KDM6A* and *FGFR3* were more frequently altered in low grade

tumors, whereas *TP53*, *RB1* and *ARID1A* were more common in high grade primary tumors and metastatic biopsies.

To determine whether differences in the distribution of mutations between primary tumors and metastases were a reflection of their variable prognostic impact, we then assembled and profiled a cohort of matched primary and metastatic samples. We found that *KDM6A* mutations, when present, were concordant in matched primary and metastatic samples from individual patients. In contrast, in 4 of 16 patients with *ARID1A* alterations, the ARID1A mutation was present only the metastatic sample .

As *KDM6A* alterations were also more frequently associated with early stage disease and were largely clonal, this suggests that *KDM6A* is an early alteration that is important in tumor initiation. Our data indicate that *ARID1A,* in contrast, likely arises later in tumor development, at least in some patients, and is associated with more aggressive disease course. While *ARID1A* mutations are still observed in some primary samples, mutations in this gene were often sub-clonal in the primary sample but clone in the metastasis, again suggesting that ARID1A alterations may promote metastatic progression.

Our analysis of matched pairs also showed that genetic relationship between primary and metastatic samples varies. Patient 7 showed very similar genetics in primary and metastatic sample, with a few additional alterations observed in the metastatic sample. Patient 13, in contrast, had a more diverse, subclonal primary with a number of mutations that were lost in the metastatic setting, and many that arose only in the metastasis.

In our identification of the primary and metastatic matched cohort, we also realized the possibility of several additional matched cohorts that can be investigated in the future. Many patients had samples pre- and post-BCG and chemotherapy. We also identified patients that had progressed from low grade to high grade disease, as well as patients with multiple recurrences. All of these matched pairs can provide information about disease progression and treatment response, and has the potential to greatly benefit patients in understanding the evolution of bladder cancer.

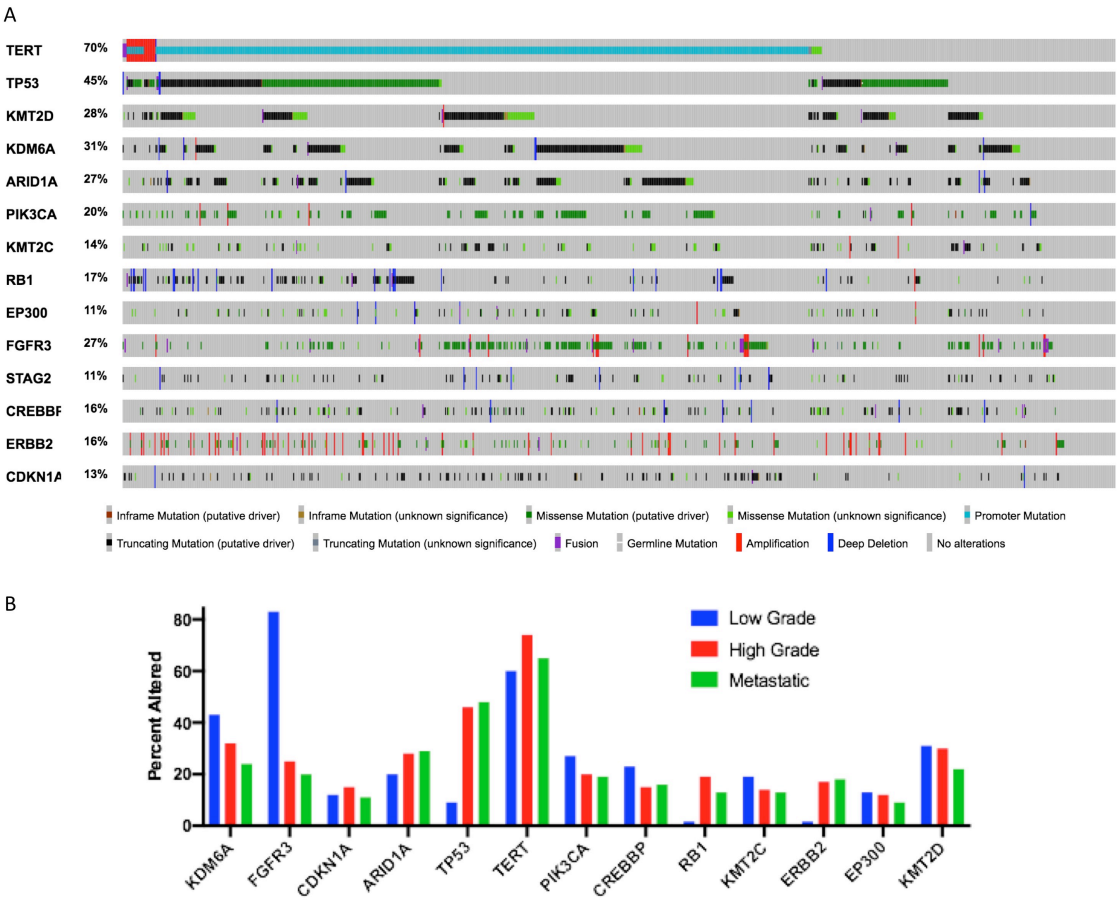

Figure 28: Mutation frequencies in the MSKCC unmatched bladder cohort.

A: Each column represents an individual tumor sample in the unmatched MSK sequencing cohort, and each row represents the mutational status of the gene listed on the left. Grey box denotes no alteration in a gene, red denotes amplification, blue denotes deep deletion, black line denotes truncating mutation, and green line denotes missense mutation. B: Mutational frequencies of commonly altered genes identified in the unmatched MSK sequencing cohort broken down by low grade, high grade, and metastatic disease. Frequency of gene alteration in each subgroup is plotted.

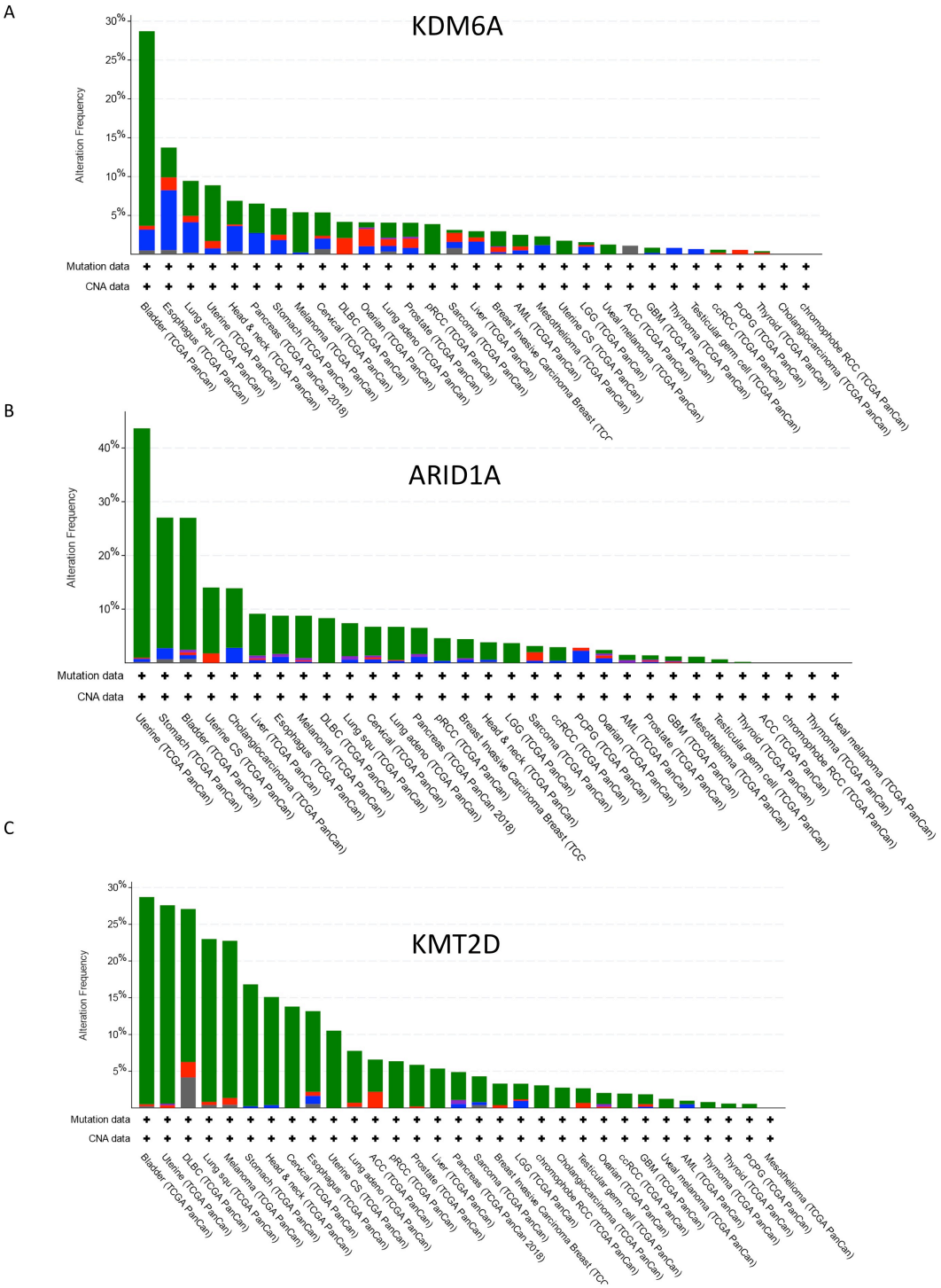

Figure 29: Mutational frequencies of epigenetic regulators across cancer types.

Mutation frequencies were taken from the TCGA pan-cancer studies. Frequency of gene alteration for KDM6A (A), ARID1A (B) and KMT2D (C) are plotted for the cancer types most commonly associated with alteration of the respective gene.

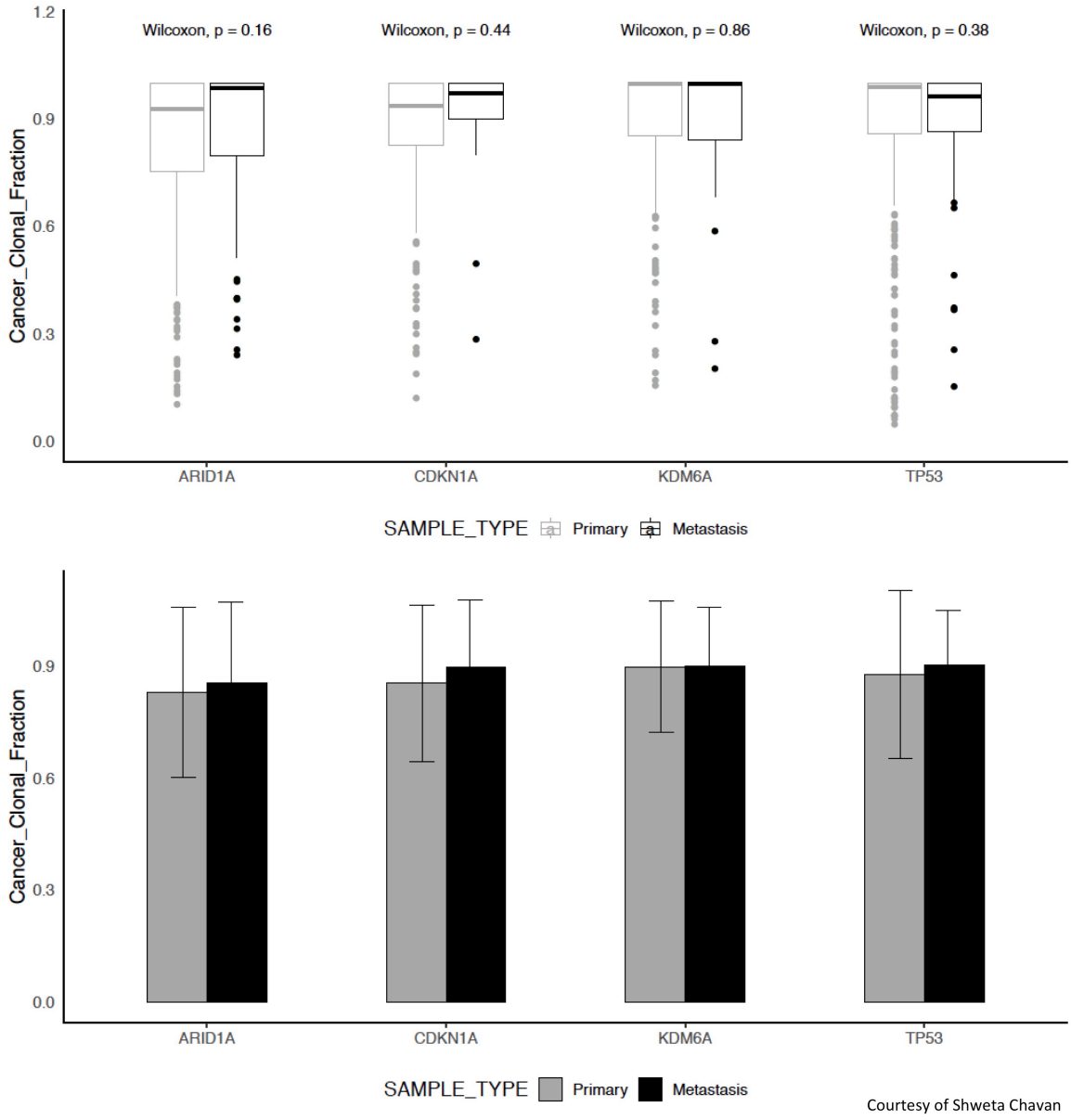

Figure 30: Cancer cell fraction of commonly altered genes in primary versus metastatic samples.

FACETS calculated from MSK-IMPACT data in the unmatched cohort was used to determine the CCF for ARID1A, CDKN1A, KDM6A and TP53 in primary versus metastatic samples. Figure generated by Shweta Chavan.

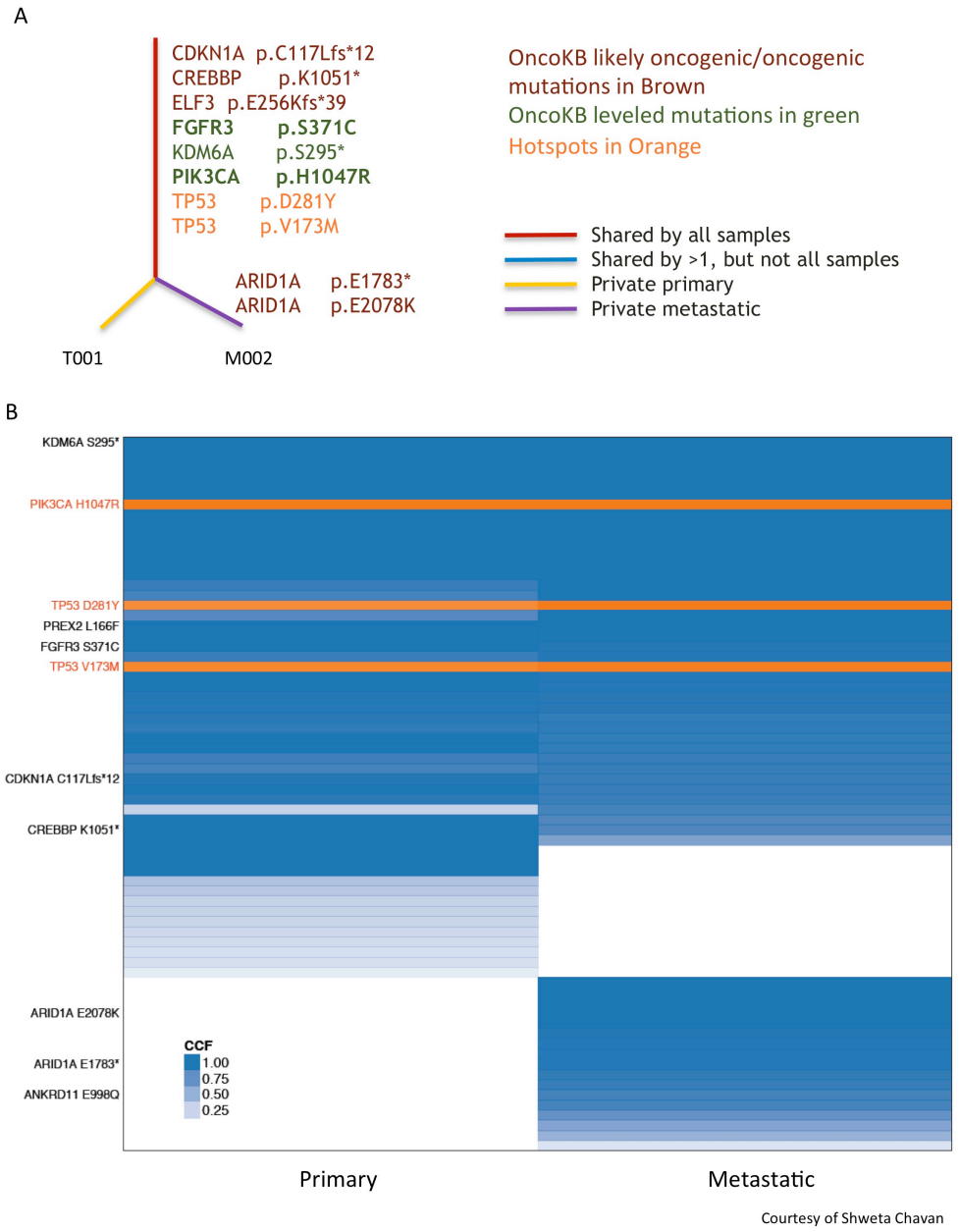

Figure 31: WES analysis of Patient 7.

A: Evolutionary trees were generated from WES data for OncoKB designated oncogenic mutations and hotspots. T001 denotes primary sample, M001 denotes metastatic sample. Figure generated by Shweta Chavan. B: CCF for each mutation identified by WES in primary versus metastatic sample, where each row is an identified mutation in the primary or metastatic sample, or both. Darker blue denotes higher CCF. Orange highlight denotes hotspot mutations. White space denotes that a mutation was not identified in that specific sample, but was identified in the other sample. Figure generated by Shweta Chavan.

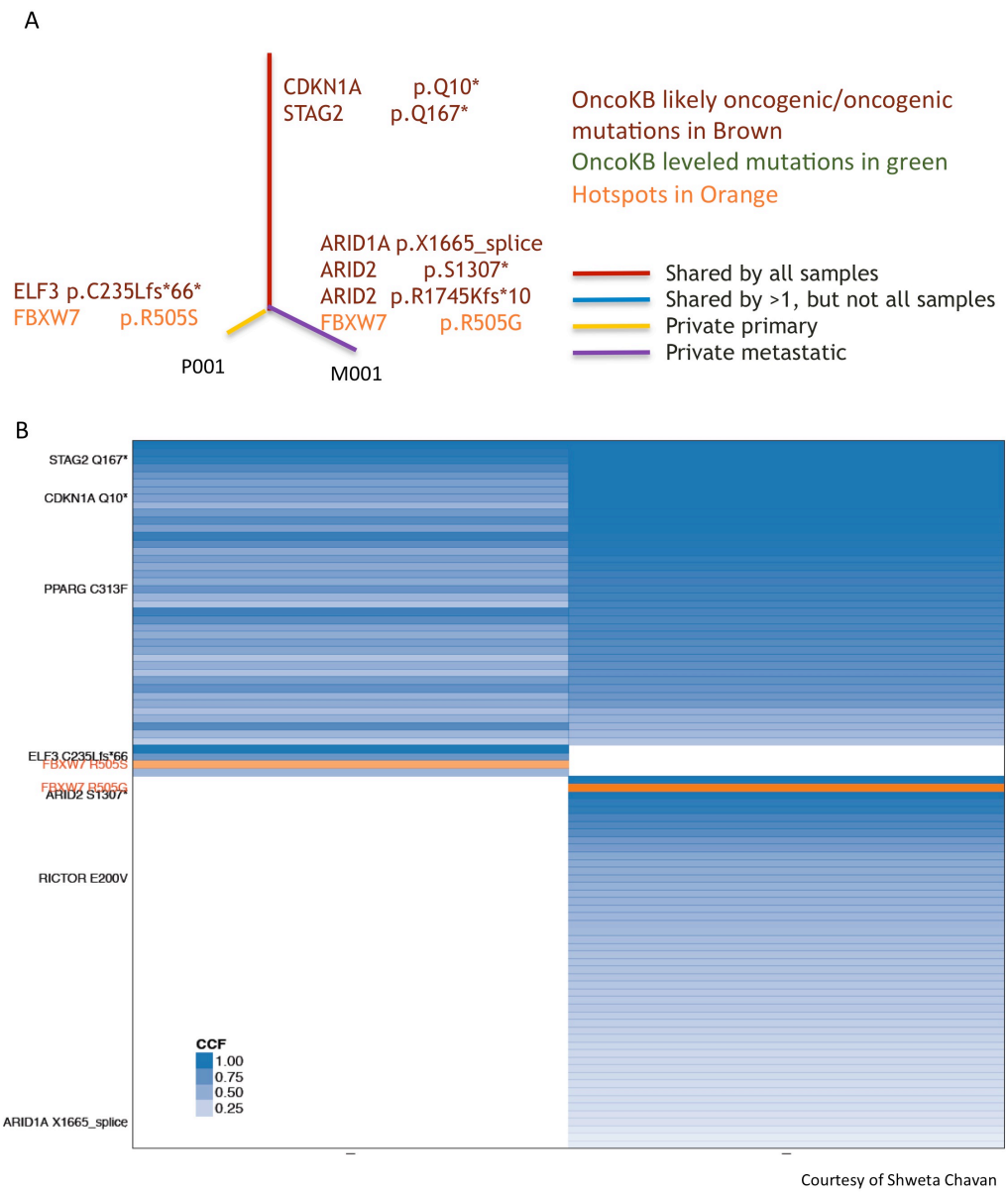

Figure 32: WES analysis of Patient 32.

A: Evolutionary trees were generated from WES data for OncoKB designated oncogenic mutations and hotspots. T001 denotes primary sample, M001 denotes metastatic sample. Figure generated by Shweta Chavan. B: CCF for each mutation identified by WES in primary versus metastatic sample, where each row is an identified mutation in the primary or metastatic sample, or both. Darker blue denotes higher CCF. Orange highlight denotes hotspot mutations. White space denotes that a mutation was not identified in that specific sample, but was identified in the other sample. Figure generated by Shweta Chavan.

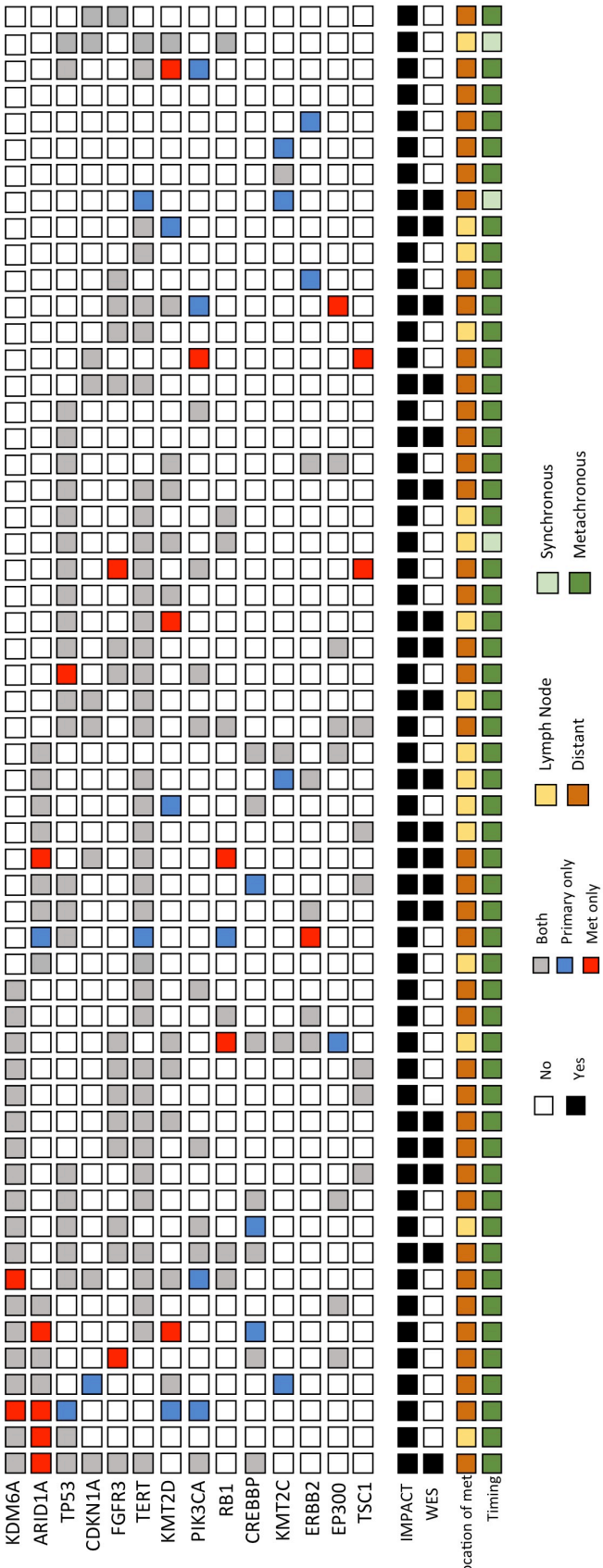
KDM6A
ARID1A
TP53
CDKN1A
FGFR3
TERT
KMT2D
PIK3CA
RB1
CREBBP
KMT2C
ERBB2
EP300
TSC1
IMPACT
WES
Location of met
Timing
No
Yes
Both
Primary only
Met only
Lymph Node
Distant
Synchronous
Metachronous

Figure 33: Concordance of mutations in matched primary and metastatic samples.

Summary of mutations identified by MSK-IMPACT in the matched 56 patient cohort. Each column is an individual patient, and each row is a mutation or clinical characteristic. Grey boxes denote a mutation identified in both primary and metastatic samples. Blue boxes denote a mutation identified in the primary sample only. Red boxes denote a mutation identified in the metastatic sample only. White boxes denote no mutation. For each patient, samples were sequenced by MSK-IMPACT, WES or both. Location of metastatic sample is provided for each patient, with yellow indicating lymph node metastasis and dark brown indicating distant metastasis. Timing of primary and metastatic samples was also included. Light green indicates synchronous diagnosis of primary and metastatic sample, while dark green indicates metachronous diagnosis.

Implications

Working in a translational lab that helped bridged the gap between cellular biology and clinical impact was a priority for my graduate studies. This work demonstrates the value of understanding the mechanisms behind patient disease and how targeted therapies can have varying efficacy based on those mechanisms. Going forward, we hope this work can help guide clinical decisions, leading to new biological questions to be answered in the lab.

In HER2 and MEK1 mutant cancers, we identified mutations with varying levels of activity. As more studies characterize these alterations, there will still be a tail of infrequent variants in all genes that are less likely to be studied. Predictive models using protein homology and 3D modeling can help guide the prioritization of characterizing these variants of unknown significance. By focusing on predicted activating mutations, patient cancers that may be driven by these otherwise uncharacterized mutations have the potential to benefit therapeutically.

As functional studies continue to define activating mutations in genes, we have demonstrated the importance of analyzing these mutations in a tissue specific manner with applicable co-alterations. This will be a major consideration moving forward with basket trials. Basket trials support testing targeted therapies across many cancer types with alterations in a designated target. While basket studies provide an advantage in rare alterations or tumor types that pose difficulties with patient accrual, the implications outlined in this work must be considered going forward.

First, the same alteration cannot be assumed to have the same effect in different cancer types. The function of epigenetic regulators is especially dependent on the genetic

background, but co-alterations can also affect the activity of mutations in canonical signaling pathways, like RAF-dependent MEK1 mutations. With HER2 alterations, mutation type correlated with cancer type, where kinase domain mutations were common in breast cancer and extracellular domain mutations were more common in bladder cancer. Future studies should consider if particular mutants are associated with higher frequency in different cancer types, and if co-mutations vary depending on cancer type.

Second, in vitro drug sensitivity assays must also be considered in a context-dependent manner. We demonstrated differential sensitivity of *MAP2K1* variants to MEK inhibitors based on co-mutations in RAF and the mechanism of action of the specific MEK inhibitor CH5126766. Therefore, functional studies of specific variants should consider the co-mutational patterns observed in patient sequencing studies with that variant. In one genetic context, a mutation may demonstrate limited tumorigenicity, but co-mutation of another gene may provide a functional advantage, as observed in the RAF-dependent MEK1 mutations. Understanding the combination of mutations seen in particular patient populations will also help guide combination therapy.

A context-dependent switch in function is also well defined in epigenetic regulators. EZH2, for example, has been shown to have gain-of-function mutations in lymphoid malignancies, but loss-of-function mutations in myeloid proliferative disorders[159,160]. ARID1A function has also been shown to be dependent on genetic context ovarian cancer, acting as a tumor suppressor in APC/PTEN mutant tumors, but acting as an oncogene in a PIK3CA mutant background[161]. Again, functional studies in the future must be guided by careful analysis of mutational context in specific tissue types.

One of the challenges of studying epigenetic regulators known to have variation in outcome is considering and controlling for the many different factors involved in that variation, including genetic background, cell type, timing of mutation, passage, and environment. In our KDM6A *in vitro* studies, we observed a change in transcriptional signature in the RT4 KDM6A knockout lines compared to parental RT4. However, specific targets were difficult to confirm due to lack of reproducibility. Although the RT4 cell line was chosen carefully for its genetic context and experiments were carefully repeated for technical replicates, the phenotype of KDM6A loss *in vitro* may be too subtle to accurately assess *in vitro*.

Another caveat of our *in vitro* KDM6A studies was studying KDM6A loss in already tumorigenic cell lines. Cancer cell lines already contain driver mutations, which may impact the ability to see phenotypic changes of more subtle drivers. Additionally, cell lines may not be appropriate models in which to study genetic functions associated with tumor initiation. Although the RT4 cell line was relatively benign, we were yet unable to study the role of KDM6A loss in normal urothelial cells undergoing tumor initiation. Based on our patient data, KDM6A is likely involved in mediating these early stage processes.

In order to overcome this, the development of more accurate mouse models of bladder cancer will be critical to understanding the function of genes with evidence of a role in early tumorigenesis. Limited by tissue-specific expression, GEMM will need to rely heavily on the correct context of genetic alterations to drive bladder specific tumor growth. Ideal mice would be FGFR3 fusion mice with KDM6A loss to study low grade disease, and a combination of P53 and RB1 loss for high grade disease. These models can

also be used in creative ways to further *in vitro* studies. We demonstrated that mouse cell lines with few genetic alterations could be generated from mouse models. These thoughtful approaches can be combined with *in vivo* models to thoroughly probe specific combinations of genetic alterations.

Mouse models will also play a role in understanding drug response. These models not only better replicate how the human body processes drugs compared to *in vitro* cultures, but also allow study of the immune system. With the high frequency of high mutational burden in bladder cancers, immunotherapy is a viable option for many patients. Mouse models that represent these patients, such as BBN models, will help understand the efficacy of immunotherapy in bladder cancer in a way that cannot be assessed *in vitro*.

We also demonstrated the value of utilizing large-scale clinical sequencing data to support functional studies *in vitro* and *in vivo*. A large clinical cohort allowed us to divide patients into low grade, high grade, and metastatic subgroups. In KDM6A and ARID1A, mutational frequency and CCF varied in these subgroups compared to the overall cohort. Subgroup analysis in the future will provide mechanistic and potential therapeutic insights into specific patient populations that are only accessible through large-scale studies.

Going forward, matched samples will be also important to understand the progression of disease in individual patients. While cohort-wide analysis can provide generalizable conclusions, matched pairs can provide a unique perspective and demonstrate potentially discordant targetable alterations. Sequencing at multiple times throughout the patient's course of treatment can also give insight on how a patient

responds to therapies in real time, while identifying potentially targetable alterations that were not previously identified. With the development of cell-free DNA sequencing (cfDNA), we can follow the genetic makeup of a tumor as it evolves in response to therapies.

Next generation sequencing is rapidly transforming the clinical management of cancer patients. While technologic improvements and reductions in sequencing costs will inevitably result in an expansion of the breadth of clinical tumor profiling assays, these diagnostic innovations will need to be closely integrated with biologic and clinical studies designed to elucidate allele- and lineage-specific factors that dictate drug sensitivity. The precision medicine field also needs to be more nuanced as to how it defines clinical actionability. However, we believe thoughtful design of functional *in vitro*, *in vivo*, and patient studies will provide a strong foundation for improvement in bladder cancer care in the near future.

References

1. Siegel RL, Miller KD, Jemal A. Cancer statistics, 2019. *CA Cancer J Clin*. 2019;69(1):7-34. doi:10.3322/caac.21551
2. Kirkali Z, Chan T, Manoharan M, et al. Bladder cancer: Epidemiology, staging and grading, and diagnosis. *Urology*. 2005;66(6):4-34. doi:10.1016/J.UROLOGY.2005.07.062
3. The American Cancer Society. Bladder Cancer Staging | Bladder Cancer Stages. https://www.cancer.org/cancer/bladder-cancer/detection-diagnosis-staging/staging.html. Published 2019. Accessed September 26, 2019.
4. Compérat EM, Burger M, Gontero P, et al. Grading of Urothelial Carcinoma and The New "World Health Organisation Classification of Tumours of the Urinary System and Male Genital Organs 2016." *Eur Urol Focus*. 2019;5(3):457-466. doi:10.1016/j.euf.2018.01.003
5. Holmäng S, Johansson SL. Stage Ta-T1 Bladder Cancer: The Relationship Between Findings At First Followup Cystoscopy And Subsequent Recurrence And Progression. *J Urol*. 2002;167(4):1634-1637. doi:10.1016/S0022-5347(05)65168-3
6. Pich A, Chiusa L, Formiconi A, Galliano D, Bortolin P, Navone R. Biologic Differences Between Noninvasive Papillary Urothelial Neoplasms of Low Malignant Potential and Low-Grade (Grade 1) Papillary Carcinomas of the Bladder. *Am J Surg Pathol*. 2001;25(12):1528-1533. doi:10.1097/00000478-200112000-00009
7. Compérat E, Larré S, Roupret M, et al. Clinicopathological characteristics of urothelial bladder cancer in patients less than 40 years old. *Virchows Arch*. 2015;466(5):589-594. doi:10.1007/s00428-015-1739-2
8. Samaratunga H, Makarov D V, Epstein JI. Comparison of WHO/ISUP and WHO classification of noninvasive papillary urothelial neoplasms for risk of progression. *Urology*. 2002;60(2):315-319. doi:10.1016/S0090-4295(02)01705-3
9. Pan C-C, Chang Y-H, Chen K-K, Yu H-J, Sun C-H, Ho DMT. Prognostic significance of the 2004 WHO/ISUP classification for prediction of recurrence, progression, and cancer-specific mortality of non-muscle-invasive urothelial tumors of the urinary bladder: a clinicopathologic study of 1,515 cases. *Am J Clin Pathol*. 2010;133(5):788-795. doi:10.1309/AJCP12MRVVHTCKEJ
10. Humphrey PA, Moch H, Cubilla AL, Ulbright TM, Reuter VE. The 2016 WHO Classification of Tumours of the Urinary System and Male Genital Organs—Part B: Prostate and Bladder Tumours. *Eur Urol*. 2016;70(1):106-119. doi:10.1016/J.EURURO.2016.02.028
11. Bosschieter J, Nieuwenhuijzen JA, van Ginkel T, et al. Value of an Immediate Intravesical Instillation of Mitomycin C in Patients with Non–muscle-invasive Bladder Cancer: A Prospective Multicentre Randomised Study in 2243 patients. *Eur Urol*. 2018;73(2):226-232. doi:10.1016/j.eururo.2017.06.038
12. Messing EM, Tangen CM, Lerner SP, et al. Effect of Intravesical Instillation of Gemcitabine vs Saline Immediately Following Resection of Suspected Low-Grade Non-Muscle-Invasive Bladder Cancer on Tumor Recurrence: SWOG S0337 Randomized Clinical Trial. *JAMA*. 2018;319(18):1880-1888. doi:10.1001/jama.2018.4657

13. Babjuk M, Oosterlinck W, Sylvester R, et al. EAU Guidelines on Non–Muscle-Invasive Urothelial Carcinoma of the Bladder, the 2011 Update. *Eur Urol*. 2011;59(6):997-1008. doi:10.1016/j.eururo.2011.03.017
14. Hall MC, Chang SS, Dalbagni G, et al. Guideline for the Management of Nonmuscle Invasive Bladder Cancer (Stages Ta, T1, and Tis): 2007 Update. *J Urol*. 2007;178(6):2314-2330. doi:10.1016/j.juro.2007.09.003
15. Morales A, Eidinger D, Bruce AW. Intracavitary Bacillus Calmette-Guerin in the treatment of superficial bladder tumors. *J Urol*. 1976;116(2):180-183. doi:10.1016/s0022-5347(17)58737-6
16. Sylvester RJ, van der MEIJDEN APM, Lamm DL. Intravesical bacillus Calmette-Guerin reduces the risk of progression in patients with superficial bladder cancer: a meta-analysis of the published results of randomized clinical trials. *J Urol*. 2002;168(5):1964-1970. doi:10.1097/01.ju.0000034450.80198.1c
17. Shelley MD, Kynaston H, Court J, et al. A systematic review of intravesical bacillus Calmette-Guérin plus transurethral resection vs transurethral resection alone in Ta and T1 bladder cancer. *BJU Int*. 2001;88(3):209-216. doi:10.1046/j.1464-410x.2001.02306.x
18. Han RF, Pan JG. Can intravesical bacillus Calmette-Guérin reduce recurrence in patients with superficial bladder cancer? A meta-analysis of randomized trials. *Urology*. 2006;67(6):1216-1223. doi:10.1016/j.urology.2005.12.014
19. Shelley MD, Wilt TJ, Court J, Coles B, Kynaston H, Mason MD. Intravesical bacillus Calmette-Guérin is superior to mitomycin C in reducing tumour recurrence in high-risk superficial bladder cancer: a meta-analysis of randomized trials. *BJU Int*. 2004;93(4):485-490. doi:10.1111/j.1464-410x.2003.04655.x
20. Shang PF, Kwong J, Wang ZP, et al. Intravesical Bacillus Calmette-Guérin versus epirubicin for Ta and T1 bladder cancer. *Cochrane Database Syst Rev*. 2011;(5). doi:10.1002/14651858.CD006885.pub2
21. Vale CL. Adjuvant Chemotherapy in Invasive Bladder Cancer: A Systematic Review and Meta-Analysis of Individual Patient Data: Advanced Bladder Cancer (ABC) Meta-analysis Collaboration. *Eur Urol*. 2005;48(2):189-201. doi:10.1016/J.EURURO.2005.04.005
22. Vale CL. Neoadjuvant Chemotherapy in Invasive Bladder Cancer: Update of a Systematic Review and Meta-Analysis of Individual Patient Data: Advanced Bladder Cancer (ABC) Meta-analysis Collaboration. *Eur Urol*. 2005;48(2):202-206. doi:10.1016/J.EURURO.2005.04.006
23. Grossman HB, Natale RB, Tangen CM, et al. Neoadjuvant Chemotherapy plus Cystectomy Compared with Cystectomy Alone for Locally Advanced Bladder Cancer. *N Engl J Med*. 2003;349(9):859-866. doi:10.1056/NEJMoa022148
24. Lyford-Pike S, Peng S, Young GD, et al. Evidence for a Role of the PD-1:PD-L1 Pathway in Immune Resistance of HPV-Associated Head and Neck Squamous Cell Carcinoma. *Cancer Res*. 2013;73(6):1733-1741. doi:10.1158/0008-5472.CAN-12-2384
25. Inman BA, Sebo TJ, Frigola X, et al. PD-L1 (B7-H1) expression by urothelial carcinoma of the bladder and BCG-induced granulomata. *Cancer*. 2007;109(8):1499-1505. doi:10.1002/cncr.22588
26. Chen BJ, Chapuy B, Ouyang J, et al. PD-L1 Expression Is Characteristic of a

Subset of Aggressive B-cell Lymphomas and Virus-Associated Malignancies. *Clin Cancer Res*. 2013;19(13):3462-3473. doi:10.1158/1078-0432.CCR-13-0855
27. Thompson RH, Gillett MD, Cheville JC, et al. Costimulatory B7-H1 in renal cell carcinoma patients: Indicator of tumor aggressiveness and potential therapeutic target. *Proc Natl Acad Sci*. 2004;101(49):17174-17179. doi:10.1073/pnas.0406351101
28. Alyea E, Weller E, Schlossman R, et al. T-cell--depleted allogeneic bone marrow transplantation followed by donor lymphocyte infusion in patients with multiple myeloma: induction of graft-versus-myeloma effect. *Blood*. 2001;98(4):934-939. doi:10.1182/blood.v98.4.934
29. Dong H, Strome SE, Salomao DR, et al. Tumor-associated B7-H1 promotes T-cell apoptosis: A potential mechanism of immune evasion. *Nat Med*. 2002;8(8):793-800. doi:10.1038/nm730
30. Freeman GJ, Long AJ, Iwai Y, et al. Engagement of the Pd-1 Immunoinhibitory Receptor by a Novel B7 Family Member Leads to Negative Regulation of Lymphocyte Activation. *J Exp Med*. 2000;192(7):1027-1034. doi:10.1084/jem.192.7.1027
31. Suzman DL, Agrawal S, Ning Y-M, et al. FDA Approval Summary: Atezolizumab or Pembrolizumab for the Treatment of Patients with Advanced Urothelial Carcinoma Ineligible for Cisplatin-Containing Chemotherapy. *Oncologist*. 2019;24(4):563-569. doi:10.1634/theoncologist.2018-0084
32. Loriot Y, Necchi A, Park SH, et al. Erdafitinib in Locally Advanced or Metastatic Urothelial Carcinoma. *N Engl J Med*. 2019;381(4):338-348. doi:10.1056/NEJMoa1817323
33. Turney A. FDA approves first targeted therapy for metastatic bladder cancer | FDA. US Food & Drug Administration. https://www.fda.gov/news-events/press-announcements/fda-approves-first-targeted-therapy-metastatic-bladder-cancer. Published 2019. Accessed October 3, 2019.
34. Robertson AG, Kim J, Al-Ahmadie H, et al. Comprehensive Molecular Characterization of Muscle-Invasive Bladder Cancer. *Cell*. 2017;171(3):540-556.e25. doi:10.1016/j.cell.2017.09.007
35. Cancer T, Atlas G. Comprehensive molecular characterization of urothelial bladder carcinoma. *Nature*. 2014;507(7492):315-322. doi:10.1038/nature12965
36. Holliday R. Epigenetics: A Historical Overview. *Epigenetics*. 2006;1(2):76-80. doi:10.4161/epi.1.2.2762
37. Waddington CH. An Introduction to Modern Genetics. *Proc R Entomol Soc London Ser A, Gen Entomol*. 1939;14(4-6):82-82. doi:10.1111/j.1365-3032.1939.tb00039.x
38. Holliday R, Pugh JE. DNA modification mechanisms and gene activity during development. *Science*. 1975;187(4173):226-232. http://www.ncbi.nlm.nih.gov/pubmed/1111098. Accessed October 9, 2019.
39. Riggs AD. X inactivation, differentiation, and DNA methylation. *Cytogenet Cell Genet*. 1975;14(1):9-25. doi:10.1159/000130315
40. GRIFFITH JS, MAHLER HR. DNA Ticketing Theory of Memory. *Nature*. 1969;223(5206):580-582. doi:10.1038/223580a0
41. Maynard Smith J. Models of a dual inheritance system. *J Theor Biol*.

1990;143(1):41-53. doi:10.1016/S0022-5193(05)80287-5
42. Kouzarides T. Chromatin modifications and their function. *Cell*. 2007;128(4):693-705. doi:10.1016/j.cell.2007.02.005
43. Jones JT, Akita RW, Sliwkowski MX. Binding specificities and affinities of egf domains for ErbB receptors. *FEBS Lett*. 1999;447(2-3):227-231. doi:10.1016/S0014-5793(99)00283-5
44. Yarden Y, Sliwkowski MX. Untangling the ErbB signalling network. *Nat Rev Mol Cell Biol*. 2001;2(2):127-137. doi:10.1038/35052073
45. Olayioye MA, Graus-Porta D, Beerli RR, Rohrer J, Gay B, Hynes NE. ErbB-1 and ErbB-2 acquire distinct signaling properties dependent upon their dimerization partner. *Mol Cell Biol*. 1998;18(9):5042-5051. http://www.pubmedcentral.nih.gov/articlerender.fcgi?artid=109089&tool=pmcentrez&rendertype=abstract. Accessed February 20, 2015.
46. Ward MD, Leahy DJ. Kinase Receiver-Activator Preference in ErbB Heterodimers Determined by Intracellular Regions and not Coupled to Extracellular Asymmetry. *J Biol Chem*. 2014;290(3):1570-1579. doi:10.1074/jbc.M114.612085
47. Yarden Y. The EGFR family and its ligands in human cancer. *Eur J Cancer*. 2001;37:3-8. doi:10.1016/S0959-8049(01)00230-1
48. Kolch W. Coordinating ERK/MAPK signalling through scaffolds and inhibitors. *Nat Rev Mol Cell Biol*. 2005;6(11):827-837. doi:10.1038/nrm1743
49. Schulze WX, Deng L, Mann M. Phosphotyrosine interactome of the ErbB-receptor kinase family. *Mol Syst Biol*. 2005;1:2005.0008. doi:10.1038/msb4100012
50. Citri A, Yarden Y. EGF-ERBB signalling: towards the systems level. *Nat Rev Mol Cell Biol*. 2006;7(7):505-516. doi:10.1038/nrm1962
51. Chang F, Steelman LS, Lee JT, et al. Signal transduction mediated by the Ras/Raf/MEK/ERK pathway from cytokine receptors to transcription factors: potential targeting for therapeutic intervention. *Leukemia*. 2003;17(7):1263-1293. doi:10.1038/sj.leu.2402945
52. Roux PP, Blenis J. ERK and p38 MAPK-activated protein kinases: a family of protein kinases with diverse biological functions. *Microbiol Mol Biol Rev*. 2004;68(2):320-344. doi:10.1128/MMBR.68.2.320-344.2004
53. Yang HY, Shao R, Hung MC, Lee MH. p27 Kip1 inhibits HER2/neu-mediated cell growth and tumorigenesis. *Oncogene*. 2001;20(28):3695-3702. doi:10.1038/sj.onc.1204472
54. Baselga J, Swain SM. Novel anticancer targets: revisiting ERBB2 and discovering ERBB3. *Nat Rev Cancer*. 2009;9(7):463-475. doi:10.1038/nrc2656
55. Song G, Ouyang G, Bao S. The activation of Akt/PKB signaling pathway and cell survival. *J Cell Mol Med*. 2005;9(1):59-71. doi:10.1111/j.1582-4934.2005.tb00337.x
56. Fresno Vara JA, Casado E, de Castro J, Cejas P, Belda-Iniesta C, González-Barón M. PI3K/Akt signalling pathway and cancer. *Cancer Treat Rev*. 2004;30(2):193-204. doi:10.1016/j.ctrv.2003.07.007
57. Huang J, Yan J, Zhang J, et al. SUMO1 modification of PTEN regulates tumorigenesis by controlling its association with the plasma membrane. *Nat Commun*. 2012;3:911. doi:10.1038/ncomms1919
58. Casalini P, Iorio M V, Galmozzi E, Ménard S. Role of HER receptors family in

development and differentiation. *J Cell Physiol*. 2004;200(3):343-350. doi:10.1002/jcp.20007
59. Schroeder JA, Lee DC. Dynamic expression and activation of ERBB receptors in the developing mouse mammary gland. *Cell Growth Differ*. 1998;9(6):451-464. http://www.ncbi.nlm.nih.gov/pubmed/9663464. Accessed March 18, 2015.
60. Sebastian J, Richards RG, Walker MP, et al. Activation and function of the epidermal growth factor receptor and erbB-2 during mammary gland morphogenesis. *Cell Growth Differ*. 1998;9(9):777-785. http://www.ncbi.nlm.nih.gov/pubmed/9751121. Accessed March 18, 2015.
61. Yang Y, Spitzer E, Meyer D, et al. Sequential requirement of hepatocyte growth factor and neuregulin in the morphogenesis and differentiation of the mammary gland. *J Cell Biol*. 1995;131(1):215-226. http://www.pubmedcentral.nih.gov/articlerender.fcgi?artid=2120590&tool=pmcentrez&rendertype=abstract. Accessed March 18, 2015.
62. Jones FE, Stern DF. Expression of dominant-negative ErbB2 in the mammary gland of transgenic mice reveals a role in lobuloalveolar development and lactation. *Oncogene*. 1999;18(23):3481-3490. doi:10.1038/sj.onc.1202698
63. Niemann C, Brinkmann V, Spitzer E, et al. Reconstitution of mammary gland development in vitro: requirement of c-met and c-erbB2 signaling for branching and alveolar morphogenesis. *J Cell Biol*. 1998;143(2):533-545. http://www.pubmedcentral.nih.gov/articlerender.fcgi?artid=2132838&tool=pmcentrez&rendertype=abstract. Accessed March 18, 2015.
64. Slamon DJ, Godolphin W, Jones LA, et al. Studies of the HER-2/neu proto-oncogene in human breast and ovarian cancer. *Science*. 1989;244(4905):707-712. http://www.ncbi.nlm.nih.gov/pubmed/2470152. Accessed October 9, 2014.
65. Hudziak RM, Schlessinger J, Ullrich A. Increased expression of the putative growth factor receptor p185HER2 causes transformation and tumorigenesis of NIH 3T3 cells. *Proc Natl Acad Sci*. 1987;84(20):7159-7163. doi:10.1073/pnas.84.20.7159
66. Kraus MH, Fedi P, Starks V, Muraro R, Aaronson SA. Demonstration of ligand-dependent signaling by the erbB-3 tyrosine kinase and its constitutive activation in human breast tumor cells. *Proc Natl Acad Sci U S A*. 1993;90(7):2900-2904. http://www.pubmedcentral.nih.gov/articlerender.fcgi?artid=46204&tool=pmcentrez&rendertype=abstract. Accessed March 18, 2015.
67. Holbro T, Beerli RR, Maurer F, Koziczak M, Barbas CF, Hynes NE. The ErbB2/ErbB3 heterodimer functions as an oncogenic unit: ErbB2 requires ErbB3 to drive breast tumor cell proliferation. *Proc Natl Acad Sci U S A*. 2003;100(15):8933-8938. doi:10.1073/pnas.1537685100
68. Lee-Hoeflich ST, Crocker L, Yao E, et al. A central role for HER3 in HER2-amplified breast cancer: implications for targeted therapy. *Cancer Res*. 2008;68(14):5878-5887. doi:10.1158/0008-5472.CAN-08-0380
69. Witton CJ, Reeves JR, Going JJ, Cooke TG, Bartlett JMS. Expression of the HER1-4 family of receptor tyrosine kinases in breast cancer. *J Pathol*. 2003;200(3):290-297. doi:10.1002/path.1370
70. Chow N-H, Chan S-H, Tzai T-S, Ho C-L, Liu H-S. Expression Profiles of ErbB Family Receptors and Prognosis in Primary Transitional Cell Carcinoma of the

Urinary Bladder. *Clin Cancer Res*. 2001;7(7):1957-1962. http://clincancerres.aacrjournals.org/content/7/7/1957.full. Accessed March 16, 2015.
71. Muller WJ, Sinn E, Pattengale PK, Wallace R, Leder P. Single-step induction of mammary adenocarcinoma in transgenic mice bearing the activated c-neu oncogene. *Cell*. 1988;54(1):105-115. doi:10.1016/0092-8674(88)90184-5
72. Moasser MM. The oncogene HER2: its signaling and transforming functions and its role in human cancer pathogenesis. *Oncogene*. 2007;26(45):6469-6487. doi:10.1038/sj.onc.1210477
73. Guy CT, Webster MA, Schaller M, Parsons TJ, Cardiff RD, Muller WJ. Expression of the neu protooncogene in the mammary epithelium of transgenic mice induces metastatic disease. *Proc Natl Acad Sci U S A*. 1992;89(22):10578-10582. http://www.pubmedcentral.nih.gov/articlerender.fcgi?artid=50384&tool=pmcentrez&rendertype=abstract. Accessed February 4, 2015.
74. Gao Y, Chang MT, McKay D, et al. Allele-Specific Mechanisms of Activation of MEK1 Mutants Determine Their Properties. *Cancer Discov*. 2018;8(5):648-661. doi:10.1158/2159-8290.CD-17-1452
75. Allen EM Van, Wagle N, Sucker A, et al. The Genetic Landscape of Clinical Resistance to RAF Inhibition in Metastatic Melanoma. *Cancer Discov*. 2014;4(1):94-109. doi:10.1158/2159-8290.CD-13-0617
76. Diamond EL, Durham BH, Haroche J, et al. Diverse and Targetable Kinase Alterations Drive Histiocytic Neoplasms. *Cancer Discov*. 2016;6(2):154-165. doi:10.1158/2159-8290.CD-15-0913
77. Slamon DJ, Clark GM, Wong SG, Levin WJ, Ullrich A, McGuire WL. Human breast cancer: correlation of relapse and survival with amplification of the HER-2/neu oncogene. *Science*. 1987;235(4785):177-182. http://www.ncbi.nlm.nih.gov/pubmed/3798106. Accessed November 8, 2014.
78. Geyer CE, Forster J, Lindquist D, et al. Lapatinib plus capecitabine for HER2-positive advanced breast cancer. *N Engl J Med*. 2006;355(26):2733-2743. doi:10.1056/NEJMoa064320
79. Cho H-S, Mason K, Ramyar KX, et al. Structure of the extracellular region of HER2 alone and in complex with the Herceptin Fab. *Nature*. 2003;421(6924):756-760. doi:10.1038/nature01392
80. Hudis CA. Trastuzumab--mechanism of action and use in clinical practice. *N Engl J Med*. 2007;357(1):39-51. doi:10.1056/NEJMra043186
81. Valabrega G, Montemurro F, Aglietta M. Trastuzumab: mechanism of action, resistance and future perspectives in HER2-overexpressing breast cancer. *Ann Oncol*. 2007;18(6):977-984. doi:10.1093/annonc/mdl475
82. Mota G, Manciulea M, Cosma E, et al. Human NK cells express Fc receptors for IgA which mediate signal transduction and target cell killing. *Eur J Immunol*. 2003;33(8):2197-2205. doi:10.1002/eji.200323534
83. Montemurro F, Valabrega G, Aglietta M. Lapatinib: a dual inhibitor of EGFR and HER2 tyrosine kinase activity. *Expert Opin Biol Ther*. 2007;7(2):257-268. doi:10.1517/14712598.7.2.257
84. Saura C, Garcia-Saenz JA, Xu B, et al. Safety and efficacy of neratinib in

combination with capecitabine in patients with metastatic human epidermal growth factor receptor 2-positive breast cancer. *J Clin Oncol*. 2014;32(32):3626-3633. doi:10.1200/JCO.2014.56.3809
85. Gounder MM, Solit DB, Tap WD. Trametinib in Histiocytic Sarcoma with an Activating MAP2K1 (MEK1) Mutation. *N Engl J Med*. 2018;378(20):1945-1947. doi:10.1056/NEJMc1511490
86. Wu P, Clausen MH, Nielsen TE. Allosteric small-molecule kinase inhibitors. *Pharmacol Ther*. 2015;156:59-68. doi:10.1016/J.PHARMTHERA.2015.10.002
87. Ishii N, Harada N, Joseph EW, et al. Enhanced inhibition of ERK signaling by a novel allosteric MEK inhibitor, CH5126766, that suppresses feedback reactivation of RAF activity. *Cancer Res*. 2013;73(13):4050-4060. doi:10.1158/0008-5472.CAN-12-3937
88. Ingham PW. Differential expression of bithorax complex genes in the absence of the extra sex combs and trithorax genes. *Nature*. 1983;306(5943):591-593. doi:10.1038/306591a0
89. Ingham PW. trithorax and the regulation of homeotic gene expression in Drosophila: a historical perspective. *Int J Dev Biol*. 1998;42(3):423-429. http://www.ncbi.nlm.nih.gov/pubmed/9654027. Accessed November 17, 2019.
90. Lewis EB. A gene complex controlling segmentation in Drosophila. *Nature*. 1978;276(5688):565-570. doi:10.1038/276565a0
91. Neigeborn L, Carlson M. Genes affecting the regulation of SUC2 gene expression by glucose repression in Saccharomyces cerevisiae. *Genetics*. 1984;108(4):845-858. http://www.ncbi.nlm.nih.gov/pubmed/6392017. Accessed October 11, 2019.
92. Stern M, Jensen R, Herskowitz I. Five SWI genes are required for expression of the HO gene in yeast. *J Mol Biol*. 1984;178(4):853-868. doi:10.1016/0022-2836(84)90315-2
93. Hirschhorn JN, Brown SA, Clark CD, Winston F. Evidence that SNF2/SWI2 and SNF5 activate transcription in yeast by altering chromatin structure. *Genes Dev*. 1992;6(12a):2288-2298. doi:10.1101/gad.6.12a.2288
94. Cote J, Quinn J, Workman J, Peterson C. Stimulation of GAL4 derivative binding to nucleosomal DNA by the yeast SWI/SNF complex. *Science (80-)*. 1994;265(5168):53-60. doi:10.1126/science.8016655
95. Cairns BR, Kim YJ, Sayre MH, Laurent BC, Kornberg RD. A multisubunit complex containing the SWI1/ADR6, SWI2/SNF2, SWI3, SNF5, and SNF6 gene products isolated from yeast. *Proc Natl Acad Sci*. 1994;91(5):1950-1954. doi:10.1073/pnas.91.5.1950
96. Khavari PA, Peterson CL, Tamkun JW, Mendel DB, Crabtree GR. BRG1 contains a conserved domain of the SWI2/SNF2 family necessary for normal mitotic growth and transcription. *Nature*. 1993;366(6451):170-174. doi:10.1038/366170a0
97. Kwon H, Imbalzano AN, Khavari PA, Kingston RE, Green MR. Nucleosome disruption and enhancement of activator binding by a human SW1/SNF complex. *Nature*. 1994;370(6489):477-481. doi:10.1038/370477a0
98. Imbalzano AN, Kwon H, Green MR, Kingston RE. Facilitated binding of TATA-binding protein to nucleosomal DNA. *Nature*. 1994;370(6489):481-485. doi:10.1038/370481a0
99. Wang W, Côté J, Xue Y, et al. Purification and biochemical heterogeneity of the

mammalian SWI-SNF complex. *EMBO J*. 1996;15(19):5370-5382. http://www.ncbi.nlm.nih.gov/pubmed/8895581. Accessed October 11, 2019.
100. Wang X, Nagl NG, Wilsker D, et al. Two related ARID family proteins are alternative subunits of human SWI/SNF complexes. *Biochem J*. 2004;383(Pt 2):319-325. doi:10.1042/BJ20040524
101. Phelan ML, Sif S, Narlikar GJ, Kingston RE. Reconstitution of a Core Chromatin Remodeling Complex from SWI/SNF Subunits. *Mol Cell*. 1999;3(2):247-253. doi:10.1016/S1097-2765(00)80315-9
102. Lickert H, Takeuchi JK, von Both I, et al. Baf60c is essential for function of BAF chromatin remodelling complexes in heart development. *Nature*. 2004;432(7013):107-112. doi:10.1038/nature03071
103. Yan Z, Wang Z, Sharova L, et al. BAF250B-associated SWI/SNF chromatin-remodeling complex is required to maintain undifferentiated mouse embryonic stem cells. *Stem Cells*. 2008;26(5):1155-1165. doi:10.1634/stemcells.2007-0846
104. Lessard J, Wu JI, Ranish JA, et al. An essential switch in subunit composition of a chromatin remodeling complex during neural development. *Neuron*. 2007;55(2):201-215. doi:10.1016/j.neuron.2007.06.019
105. Chi TH, Wan M, Zhao K, et al. Reciprocal regulation of CD4/CD8 expression by SWI/SNF-like BAF complexes. *Nature*. 2002;418(6894):195-199. doi:10.1038/nature00876
106. Wilsker D, Patsialou A, Zumbrun SD, et al. The DNA-binding properties of the ARID-containing subunits of yeast and mammalian SWI/SNF complexes. *Nucleic Acids Res*. 2004;32(4):1345-1353. doi:10.1093/nar/gkh277
107. Inoue H, Furukawa T, Giannakopoulos S, Zhou S, King DS, Tanese N. Largest Subunits of the Human SWI/SNF Chromatin-remodeling Complex Promote Transcriptional Activation by Steroid Hormone Receptors. *J Biol Chem*. 2002;277(44):41674-41685. doi:10.1074/jbc.M205961200
108. Wallberg AE, Neely KE, Gustafsson JA, Workman JL, Wright AP, Grant PA. Histone acetyltransferase complexes can mediate transcriptional activation by the major glucocorticoid receptor activation domain. *Mol Cell Biol*. 1999;19(9):5952-5959. doi:10.1128/mcb.19.9.5952
109. Muchardt C, Yaniv M. A human homologue of Saccharomyces cerevisiae SNF2/SWI2 and Drosophila brm genes potentiates transcriptional activation by the glucocorticoid receptor. *EMBO J*. 1993;12(11):4279-4290. doi:10.1002/j.1460-2075.1993.tb06112.x
110. Fryer CJ, Archer TK. Chromatin remodelling by the glucocorticoid receptor requires the BRG1 complex. *Nature*. 1998;393(6680):88-91. doi:10.1038/30032
111. Gao X, Tate P, Hu P, Tjian R, Skarnes WC, Wang Z. ES cell pluripotency and germ-layer formation require the SWI/SNF chromatin remodeling component BAF250a. *Proc Natl Acad Sci*. 2008;105(18):6656-6661. doi:10.1073/pnas.0801802105
112. Flores-Alcantar A, Gonzalez-Sandoval A, Escalante-Alcalde D, Lomelí H. Dynamics of expression of ARID1A and ARID1B subunits in mouse embryos and in cells during the cell cycle. *Cell Tissue Res*. 2011;345(1):137-148. doi:10.1007/s00441-011-1182-x
113. Raab JR, Resnick S, Magnuson T. Genome-Wide Transcriptional Regulation

Mediated by Biochemically Distinct SWI/SNF Complexes. Lieb JD, ed. *PLOS Genet*. 2015;11(12):e1005748. doi:10.1371/journal.pgen.1005748
114. Miller T, Krogan NJ, Dover J, et al. COMPASS: a complex of proteins associated with a trithorax-related SET domain protein. *Proc Natl Acad Sci U S A*. 2001;98(23):12902-12907. doi:10.1073/pnas.231473398
115. Agger K, Cloos PAC, Christensen J, et al. UTX and JMJD3 are histone H3K27 demethylases involved in HOX gene regulation and development. *Nature*. 2007;449(7163):731-734. doi:10.1038/nature06145
116. Yoo KH, Oh S, Kang K, et al. Histone Demethylase KDM6A Controls the Mammary Luminal Lineage through Enzyme-Independent Mechanisms. *Mol Cell Biol*. 2016;36(16):2108-2120. doi:10.1128/MCB.00089-16
117. Van Laarhoven PM, Neitzel LR, Quintana AM, et al. Kabuki syndrome genes *KMT2D* and *KDM6A* : functional analyses demonstrate critical roles in craniofacial, heart and brain development. *Hum Mol Genet*. 2015;24(15):4443-4453. doi:10.1093/hmg/ddv180
118. Hong S, Cho Y-W, Yu L-R, Yu H, Veenstra TD, Ge K. Identification of JmjC domain-containing UTX and JMJD3 as histone H3 lysine 27 demethylases. *Proc Natl Acad Sci U S A*. 2007;104(47):18439-18444. doi:10.1073/pnas.0707292104
119. Wu H, Goel V, Haluska FG. PTEN signaling pathways in melanoma. *Oncogene*. 2003;22(20):3113-3122. doi:10.1038/sj.onc.1206451
120. van Haaften G, Dalgliesh GL, Davies H, et al. Somatic mutations of the histone H3K27 demethylase gene UTX in human cancer. *Nat Genet*. 2009;41(5):521-523. doi:10.1038/ng.349
121. Schneider BJ, Kalemkerian GP, Bradley D, et al. Phase I study of vorinostat (suberoylanilide hydroxamic acid, NSC 701852) in combination with docetaxel in patients with advanced and relapsed solid malignancies. *Invest New Drugs*. 2012;30(1):249-257. doi:10.1007/s10637-010-9503-6
122. Li B, Dewey CN. RSEM: accurate transcript quantification from RNA-Seq data with or without a reference genome. *BMC Bioinformatics*. 2011;12(1):323. doi:10.1186/1471-2105-12-323
123. Love MI, Huber W, Anders S. Moderated estimation of fold change and dispersion for RNA-seq data with DESeq2. *Genome Biol*. 2014;15(12):550. doi:10.1186/s13059-014-0550-8
124. Subramanian A, Tamayo P, Mootha VK, et al. Gene set enrichment analysis: A knowledge-based approach for interpreting genome-wide expression profiles. *Proc Natl Acad Sci*. 2005;102(43):15545-15550. doi:10.1073/pnas.0506580102
125. Langmead B, Salzberg SL. Fast gapped-read alignment with Bowtie 2. *Nat Methods*. 2012;9(4):357-359. doi:10.1038/nmeth.1923
126. Zhang Y, Liu T, Meyer CA, et al. Model-based Analysis of ChIP-Seq (MACS). *Genome Biol*. 2008;9(9):R137. doi:10.1186/gb-2008-9-9-r137
127. Heinz S, Benner C, Spann N, et al. Simple combinations of lineage-determining transcription factors prime cis-regulatory elements required for macrophage and B cell identities. *Mol Cell*. 2010;38(4):576-589. doi:10.1016/j.molcel.2010.05.004
128. Robinson JT, Thorvaldsdóttir H, Wenger AM, Zehir A, Mesirov JP. Variant Review with the Integrative Genomics Viewer. *Cancer Res*. 2017;77(21):e31-e34. doi:10.1158/0008-5472.CAN-17-0337

129. Zehir A, Benayed R, Shah RH, et al. Mutational landscape of metastatic cancer revealed from prospective clinical sequencing of 10,000 patients. *Nat Med*. 2017;23(6):703-713. doi:10.1038/nm.4333
130. Chang MT, Asthana S, Gao SP, et al. Identifying recurrent mutations in cancer reveals widespread lineage diversity and mutational specificity. *Nat Biotechnol*. 2016;34(2):155-163. doi:10.1038/nbt.3391
131. Alexandrov LB, Nik-Zainal S, Wedge DC, et al. Signatures of mutational processes in human cancer. *Nature*. 2013;500(7463):415-421. doi:10.1038/nature12477
132. Sos ML, Koker M, Weir BA, et al. PTEN Loss Contributes to Erlotinib Resistance in EGFR-Mutant Lung Cancer by Activation of Akt and EGFR. *Cancer Res*. 2009;69(8):3256-3261. doi:10.1158/0008-5472.CAN-08-4055
133. Bose R, Kavuri SM, Searleman AC, et al. Activating HER2 mutations in HER2 gene amplification negative breast cancer. *Cancer Discov*. 2013;3(2):224-237. doi:10.1158/2159-8290.CD-12-0349
134. Greulich H, Kaplan B, Mertins P, et al. Functional analysis of receptor tyrosine kinase mutations in lung cancer identifies oncogenic extracellular domain mutations of ERBB2. *Proc Natl Acad Sci U S A*. 2012;109(36):14476-14481. doi:10.1073/pnas.1203201109
135. Di Fiore PP, Pierce JH, Fleming TP, et al. Overexpression of the human EGF receptor confers an EGF-dependent transformed phenotype to NIH 3T3 cells. *Cell*. 1987;51(6):1063-1070. doi:10.1016/0092-8674(87)90592-7
136. Macpherson I, Montagnier L. Agar suspension culture for the selective assay of cells transformed by polyoma virus. *Virology*. 1964;23(2):291-294. doi:10.1016/0042-6822(64)90301-0
137. Arcila ME, Drilon A, Sylvester BE, et al. MAP2K1 (MEK1) Mutations Define a Distinct Subset of Lung Adenocarcinoma Associated with Smoking. *Clin Cancer Res*. 2015;21(8):1935-1943. doi:10.1158/1078-0432.CCR-14-2124
138. Fischmann TO, Smith CK, Mayhood TW, et al. Crystal Structures of MEK1 Binary and Ternary Complexes with Nucleotides and Inhibitors. *Biochemistry*. 2009;48(12):2661-2674. doi:10.1021/bi801898e
139. Lee SH, Hu W, Matulay JT, et al. Tumor Evolution and Drug Response in Patient-Derived Organoid Models of Bladder Cancer. *Cell*. 2018;173(2):515-528.e17. doi:10.1016/j.cell.2018.03.017
140. LaFave LM, Béguelin W, Koche R, et al. Loss of BAP1 function leads to EZH2-dependent transformation. *Nat Med*. 2015;21(11):1344-1349. doi:10.1038/nm.3947
141. Puzio-Kuter AM, Castillo-Martin M, Kinkade CW, et al. Inactivation of p53 and Pten promotes invasive bladder cancer. *Genes Dev*. 2009;23(6):675-680. doi:10.1101/gad.1772909
142. Chen Z, Trotman LC, Shaffer D, et al. Crucial role of p53-dependent cellular senescence in suppression of Pten-deficient tumorigenesis. *Nature*. 2005;436(7051):725-730. doi:10.1038/nature03918
143. Soriano P. Generalized lacZ expression with the ROSA26 Cre reporter strain. *Nat Genet*. 1999;21(1):70-71. doi:10.1038/5007
144. Guijarro M V., Dahiya S, Danielson LS, et al. Dual Pten/Tp53 Suppression

Promotes Sarcoma Progression by Activating Notch Signaling. *Am J Pathol*. 2013;182(6):2015-2027. doi:10.1016/J.AJPATH.2013.02.035
145. Kawaguchi K, Oda Y, Saito T, et al. Genetic and epigenetic alterations of the PTEN gene in soft tissue sarcomas. *Hum Pathol*. 2005;36(4):357-363. doi:10.1016/J.HUMPATH.2005.01.017
146. Feil R, Wagner J, Metzger D, Chambon P. Regulation of Cre Recombinase Activity by Mutated Estrogen Receptor Ligand-Binding Domains. *Biochem Biophys Res Commun*. 1997;237(3):752-757. doi:10.1006/BBRC.1997.7124
147. Chu PG, Weiss LM. Expression of Cytokeratin 5/6 in Epithelial Neoplasms: An Immunohistochemical Study of 509 Cases. *Mod Pathol*. 2002;15(1):6-10. doi:10.1038/modpathol.3880483
148. Van Batavia J, Yamany T, Molotkov A, et al. Bladder cancers arise from distinct urothelial sub-populations. *Nat Cell Biol*. 2014;16(10):982-991. doi:10.1038/ncb3038
149. Shin K, Lim A, Odegaard JI, et al. Cellular origin of bladder neoplasia and tissue dynamics of its progression to invasive carcinoma. *Nat Cell Biol*. 2014;16(5):469-478. doi:10.1038/ncb2956
150. McCormick DL, Ronan SS, Becci PJ, Moon RC. Influence of total dose and dose schedule on induction of urinary bladder cancer in the mouse by N-butyl-N-(4-hydroxy-butyl)nitrosamine. *Carcinogenesis*. 1981;2(3):251-254. doi:10.1093/carcin/2.3.251
151. Fukushima S, Hirose M, Tsuda H, Shirai T, Hirao K. Histological classification of urinary bladder cancers in rats induced by N-butyl-n-(4-hydroxybutyl)nitrosamine. *Gan*. 1976;67(1):81-90. http://www.ncbi.nlm.nih.gov/pubmed/1269859. Accessed November 11, 2019.
152. Muzumdar MD, Tasic B, Miyamichi K, Li L, Luo L. A global double-fluorescent Cre reporter mouse. *genesis*. 2007;45(9):593-605. doi:10.1002/dvg.20335
153. Baeuerle PA, Gires O. EpCAM (CD326) finding its role in cancer. *Br J Cancer*. 2007;96(3):417-423. doi:10.1038/sj.bjc.6603494
154. Trzpis M, McLaughlin PMJ, de Leij LMFH, Harmsen MC. Epithelial cell adhesion molecule: more than a carcinoma marker and adhesion molecule. *Am J Pathol*. 2007;171(2):386-395. doi:10.2353/ajpath.2007.070152
155. Kaneko S, Li X. X chromosome protects against bladder cancer in females via a *KDM6A* -dependent epigenetic mechanism. *Sci Adv*. 2018;4(6):eaar5598. doi:10.1126/sciadv.aar5598
156. Chamie K, Litwin MS, Bassett JC, et al. Recurrence of high-risk bladder cancer: A population-based analysis. *Cancer*. 2013;119(17):3219-3227. doi:10.1002/cncr.28147
157. Garczyk S, Schneider U, Lurje I, et al. ARID1A-deficiency in urothelial bladder cancer: No predictive biomarker for EZH2-inhibitor treatment response? Real FX, ed. *PLoS One*. 2018;13(8):e0202965. doi:10.1371/journal.pone.0202965
158. Shen R, Seshan VE. FACETS: allele-specific copy number and clonal heterogeneity analysis tool for high-throughput DNA sequencing. *Nucleic Acids Res*. 2016;44(16):e131. doi:10.1093/NAR/GKW520
159. Ernst T, Chase AJ, Score J, et al. Inactivating mutations of the histone methyltransferase gene EZH2 in myeloid disorders. *Nat Genet*. 2010;42(8):722-

726. doi:10.1038/ng.621
160. Morin RD, Johnson NA, Severson TM, et al. Somatic mutations altering EZH2 (Tyr641) in follicular and diffuse large B-cell lymphomas of germinal-center origin. *Nat Genet*. 2010;42(2):181-185. doi:10.1038/ng.518
161. Mathur R. ARID1A loss in cancer: Towards a mechanistic understanding. *Pharmacol Ther*. 2018;190:15-23. doi:10.1016/J.PHARMTHERA.2018.05.001